Fall 2022

Arctic Ocean and Subarctic Seas Dynamics in a Changing Climate

Sarah B. Hall

ARCTIC OCEAN AND SUBARCTIC SEAS DYNAMICS IN A CHANGING CLIMATE

by

Sarah B. Hall

Bachelor of Science
Texas A&M University, 2018

Master of Ocean Science & Technology
Texas A&M University, 2019

Submitted in Partial Fulfillment of the Requirements

For the Degree of Doctor of Philosophy in

Marine Science

College of Arts and Sciences

University of South Carolina

2022

Accepted by:

Subrahmanyam Bulusu, Major Professor

Alexander Yankovsky, Committee Member

Gregory Carbone, Committee Member

Anthony Arguez, Outside Committee Member

Cheryl L. Addy, Interim Vice Provost and Interim Dean of the Graduate School

DEDICATION

This dissertation is dedicated to my family, Stephen, Karen, and Ryan Hall, whose endless love and support throughout my life have encouraged me to strive for achievements I would not have thought attainable otherwise.

ACKNOWLEDGEMENTS

Thank you to all those who helped to make this dissertation possible. Thank you to my committee: Dr. Subrahmanyam Bulusu, my major advisor, Dr. Alexander Yankovsky, Dr. Gregory Carbone, and Dr. Anthony Arguez. I would also like to acknowledge and thank my coauthors, Dr. Ebenezer S. Nyadjro, Dr. Annette Samuelsen, Dr. James H. Morison, and Dr. Michael Steele for their assistance and advice in preparing the bulk of this dissertation. Special thanks as well to Dr. Corinne Trott for her assistance through other projects and for the time spent troubleshooting coding problems with me. Truly, this would not have been possible without you all.

This research is supported through the United States Office of Naval Research Awarded #N00014-20-1-2680, awarded to my major professor, Dr. Subrahmanyam Bulusu. Additional funding was provided by the University of South Carolina's School of the Earth, Ocean and Environment (SEOE) through a Teaching Assistant for one semester. I would also like to thank SEOE for awarding me the 2022 Marine Science Award for Outstanding Publication.

As always, a special thank you to my family, Stephen, Karen, Ryan, and Kelsey Hall, for their unending encouragement, love, and guidance. I send appreciation to my nephew, Keelan John Hall, who was welcomed into this world during my program and whose smiles and inaudible mumbles through video chats have brought me happiness. Extended gratitude is sent to Tacey Hicks and Samuel Smith who encouraged this journey for me and whose endless support drives me to be the best I can be. Finally, I would like

to thank my friends and colleagues in the Satellite Oceanography Lab—Emily Eley, Lydia Duncan, Paul Ernst, Katherine Seikel, and Emma Hoffman— for their friendship and advice, scientifically and otherwise, through all of my endeavors. I have many other family members and friends to acknowledge who have planted positive inspirations along the way but I'm afraid the list might run longer than the pages of this dissertation, so thank you all.

ABSTRACT

Salinity is the primary determinant of the Arctic Ocean's vertical density stratification in the upper ocean, which has major implications on the ocean's physical dynamics alongside a period of rapidly declining sea ice. In recent decades, the Arctic's freshwater content (FWC) has increased as a result of the accumulation of freshwater source inputs. Additional freshwater exported to the North Atlantic may hinder overturning processes that are vital to the regulation of global climate. This dissertation employs *in situ* measurements, satellite observations, and ocean model simulations to better understand salinity and freshwater changes in the Arctic Ocean during this changing climate.

This work first explores surface freshwater flux through major Arctic straits with emphasis on years of high and low sea ice extent. The lowest sea ice extent on record occurred during September 2012 (~3.41 million km^2) and showed the greatest export to the Atlantic Ocean. Between 2010–2018, export through the Fram Strait strengthened. Next, this dissertation focuses on the Beaufort Gyre, a predominantly anticyclonic circulation system that contains roughly 25% of the Arctic's FWC, to delineate the discrepancies between salinity products. Most of the models and reanalysis products analyzed in this work overestimate salinity within the first 50 m when compared to *in situ* measurements, with the exception of ORAS5 (-0.052 bias at 5 m) and MIZMAS (0.105 bias at 5 m). This study reveals that the Russian Shelf makes up ~16% of total FWC in the Arctic Ocean with a trend of -15.63 km^3/year between 1979–2018, driven by Kara and Laptev sea negative trends. A notable regime shift occurred during the summer of 2007, where an anomalous

FWC decrease (increase) occurred over the Russian Shelf (Beaufort Gyre), which further suggests that neglecting the Russian Shelf creates an error of 25% in assessing Arctic Ocean FWC change during this 2007 regime transition. These results highlight the drawbacks and advantages of utilizing ocean model simulations for a comprehensive understanding of the Arctic Ocean's physical dynamics. This dissertation emphasizes the importance of continued observations and refining the accuracy of ocean models as polar regions become more susceptible to climate change.

TABLE OF CONTENTS

LIST OF TABLES

LIST OF FIGURES

LIST OF ABBREVIATIONS

AO ..... Arctic Oscillation

AMOC ..... Atlantic Meridional Overturning Circulation

BG ..... Beaufort Gyre

BGP ..... Beaufort Gyre Project

BS ..... Barents Sea

BSO ..... Barents Sea Opening

CAA ..... Canadian Arctic Archipelago

CTD ..... Conductivity–Temperature–Depth

ECCO ..... Estimating the Circulation and Climate of the Ocean

EGC ..... East Greenland Current

ESS ..... East Siberian Sea

EOF ..... Empirical Orthogonal Function

FW ..... Freshwater

FWC ..... Freshwater Content

FWV ..... Freshwater Volume

GLORYS12 ..... Global Ocean Reanalysis and Simulation version 12

HYCOM ..... Hybrid Coordinate Ocean Model

KS ..... Kara Sea

LS ..... Laptev Sea

MIZMAS ..... Marginal Ice Zone Modeling and Assimilation System

NABOS ..... Nansen and Amundsen Basins Observational System

NAO ..... North Atlantic Oscillation

NEMO ..... Nucleus for European Modeling of the Ocean

OISSS ..... Optimally Interpolated Sea Surface Salinity

ORAS5 ..... Ocean Reanalysis System version 5

RMSD ..... Root Mean Square Deviation

SMAP ..... Soil Moisture Active Passive

SMOS ..... Soil Moisture and Ocean Salinity

SIC ..... Sea Ice Concentration

SIE ..... Sea Ice Extent

SIZ ..... Seasonal Ice Zone

SIZRS ..... Seasonal Ice Zone Reconnaissance Surveys

SSS ..... Sea Surface Salinity

SST ..... Sea Surface Temperature

WS ..... White Sea

CHAPTER 1

INTRODUCTION

1.1 DESCRIPTION OF THE RESEARCH AREA

The Arctic Ocean is distinguished for its dynamically complex system of atmosphere, ocean, and cryosphere interactions. Despite its small size relative to the other oceans, alterations in the Arctic's climate can result in changes to the globe. The Arctic Ocean connects the relatively cooler and fresher North Pacific Ocean waters that flow in through the Bering Strait and the warm and more saline waters of the North Atlantic Ocean, originating from the Gulf Stream and passing through the eastern Fram Strait and the Barents Sea Opening. The flow of Arctic water is governed by its wind- and buoyancy-driven circulation patterns. The Arctic's two major ocean currents are the Beaufort Gyre (BG), a predominantly anticyclonic circulation system, and the Transpolar drift that leads from the Laptev and East Siberian Seas through the Fram Strait and into the North Atlantic Ocean (Figure 1.1). The export of Arctic water and sea ice occurs through the Canadian Arctic Archipelago and the western Fram Strait into the North Atlantic Ocean.

Salinity governs the Arctic Ocean's density structure as temperatures are relatively cool and homogeneous. Stratification plays a vital role in the formation of water masses, ocean convection, and the mixed layer depth, which drive circulation processes in high latitudes. The distribution and movement of low saline waters, or freshwater, is key to the understanding of how the climate is changing at regional and global scales.

Sources of freshwater include river and ice sheet discharge, net precipitation, sea ice melt, and low salinity waters inflowing from the Pacific (Aagaard and Woodgate, 2001; Serreze et al., 2006; Bamber et al., 2012). These processes vary locally and therefore, the Arctic's freshwater budget is also not uniform. Sources, circulation, and export are important when investigating the influences of freshwater distribution. The flow of Arctic water is governed by current circulation, the strength of the BG's anticyclonic mode, and atmospheric forcing. The Greenland Ice Sheet and other glaciers are releasing freshwater through their rapid melt in recent years (Solomon et al., 2021). Freshwater sinks or exports occur through the growth of sea ice, evaporation, and liquid and solid freshwater flux through major transport waterways (Rudels et al., 1994; Serreze et al., 2006; Haine et al., 2015).

1.2 Arctic Ocean and Atmosphere Changes

In the past few decades, the Arctic has undergone an ample amount of warming, at least twice the rate of the global average (Walsh, 2014). However, a recent study by Rantanen et al. (2022) suggests the Arctic could be warming 3.8 times as fast as the global average since 1979. This has escalated the concern for Arctic climate. rapid sea ice decline and the potential of "ice-free" summers in the near future, some studies suggest as early as 2035, and at least by 2050 (Docquier & Koenigk, 2021; Perovich et al., 2016). Sea ice melt causes the boundary layer to be exposed to more air-sea interactions, influencing the speed and direction of surface currents. An open sea surface can also induce a positive feedback mechanism where the dark sea surface absorbs more incoming solar radiation and in turn warms up more. Not only is the Arctic's sea ice extent declining, but the concentrations,

thickness and multi-year sea ice is diminishing as well. The melt (growth) of sea ice adds (removes) freshwater to (from) the immediate area.

The BG, its region is commonly regarded as the area between 130°W–150°W, 70.5°N–80.5°N (Regan et al., 2019), is authoritative to the Arctic Ocean's FW retention and release where strong geostrophic flow drives converging currents that induce a raised sea surface. Enhanced Ekman pumping (downwelling) deepens the freshwater layer within the BG results in freshwater accumulation. In during a cyclonic mode, the flow is weakened, and the vorticity relaxes resulting in the release of freshwater. By 2017 the BG storage accumulated $23x10^3$ km^3 of freshwater, a 40% increase in the past two decades. Therefore, there is concern for the possible rapid FW release from a near-future stabilizing gyre. This release of freshwater has been shown to reach lower latitudes with potential consequences of slowing the northern Atlantic Meridional Overturning Circulation (AMOC). The AMOC is a key component of the global ocean circulation (i.e., thermohaline circulation, global conveyor belt) which as regulated the warming climate by circulating warm lower latitude temperatures into the cooler deep water formation (Caesar et al., 2021). This overturning process has decreased since the 1930's further weakening the Gulf stream. Not only does this interrupt ocean circulation, but it also induces sea level rise on the northeast US coast, stronger storms in Britain with cooler climate in northern Europe. Therefore, the Arctic has much larger implications than just regional, but its release of FW could mean impeding effects to the regional and global climate (Rahmstorf et al. 2015). Therefore, the Arctic and its subpolar regions play a crucial role in the regulation of meridional heat transport through this thermohaline circulation (Zhang et al., 2021).

The Arctic Oscillation (AO) is a strong indicator of sea level pressure over the Arctic. The AO is a large scale climate index that is associated above 20°N and references the leading mode of sea level pressure. The positive AO phase is associated with lower than average pressure over the Arctic that gives intensified polar vortex and stronger westerly winds in the upper atmosphere. This process traps cooler temperatures in the north but also drives out older ice to the Atlantic. Negative AO impacts are in many ways opposite where higher pressure causes weaker westerlies. Cold air can thus seep out to adjacent continents and influence climate in the US and northern Europe.

In situ measurements allow for surface and depth measurements but are limited due to the harsh conditions of the Arctic and the expense of expeditions. Satellite radiometry is restricted to the top few centimeters of the ocean's surface, and even more so cannot penetrate sea ice in the Arctic Ocean for accurate observations. Therefore, physical dynamics of the Arctic Ocean have been reliant on ocean modeling simulations to estimate parameters in regions otherwise unobserved. The combination of *in situ*, remote sensing, and ocean modeling techniques in the Arctic Ocean during a changing climate has not been explored to the extent it deserves. Therefore, this dissertation has focused on the validity, comparisons, and discrepancies between these products.

This dissertation stresses the value of high spatiotemporal resolutions of ocean models in the Arctic Ocean region along with consistent validity to observations and improvement of their accuracy. The present thesis addresses the regional and overall freshwater changes that drive the Arctic Ocean’s physical dynamics in the changing climate. Special emphasis is placed on the combinational use of *in situ* data, satellite

observations, and ocean models' estimations to observe seasonal, interannual, and decadal changes in the Arctic Ocean.

1.3 Outline of the Dissertation

This dissertation consists of four additional chapters. Chapter 2, entitled "Surface Freshwater Fluxes in the Arctic and Subarctic Seas During Contrasting Years of High and Low Summer Sea Ice Extent", is published in *Remote Sensing*. This chapter combines modeled sea surface temperature, sea ice concentrations, wind speed and surface current speed as well as remote sensing-based salinity observations to investigate their spatiotemporal variations in the Arctic Ocean between 2010–2018. The study computes transect-averaged, sea surface freshwater flux through major Arctic pathways that connect to adjacent oceans between years that experienced anomalously high (2013/2014) and low (2012/2016) summer sea ice extent. It further explores an anomalous surface freshwater transport event that occurred over the subarctic and the North Atlantic regions during 2012.

Chapter 3 is entitled "Intercomparison of Salinity Products in the Beaufort Gyre and Arctic Ocean" and is published in *Remote Sensing*. This chapter compares salinity estimates from several ocean models and reanalysis products to salinity observations from remote sensing and *in situ* instruments, primarily in the BG region between 2012–2017. Freshwater content is computed in the BG region as well as the Arctic Basins (areas above 67°N and deeper than 500 m) from products where salinity at depth is available. This highlights the limitations of models and discrepancies of salinity from *in situ* measurements.

Chapter 4, entitled "The Role of the Russian Shelf in Seasonal and Interannual Variability of Arctic Sea Surface Salinity and Freshwater Content" has been submitted to

the *Journal of Geophysical Research: Oceans* and focuses on the Russian Shelf, a region in the Arctic Ocean where salinity and freshwater content has not been as well delineated or observed compared to the BG region. This chapter utilizes ORAS5 salinity over a four decadal period, 1979-2018, to quantify the contribution of freshwater volume from the Russian Shelf to the Arctic Ocean (above 66°N) and estimate the variability of salinity and freshwater content. The Arctic Ocean, Russian Shelf, and BG salinity and freshwater characteristics are computed with particular attention to the impact of a regime shift during the summer of 2007.

Finally, Chapter 5 summarizes the findings of Chapters 2–4 while presenting the major conclusions of this dissertation.

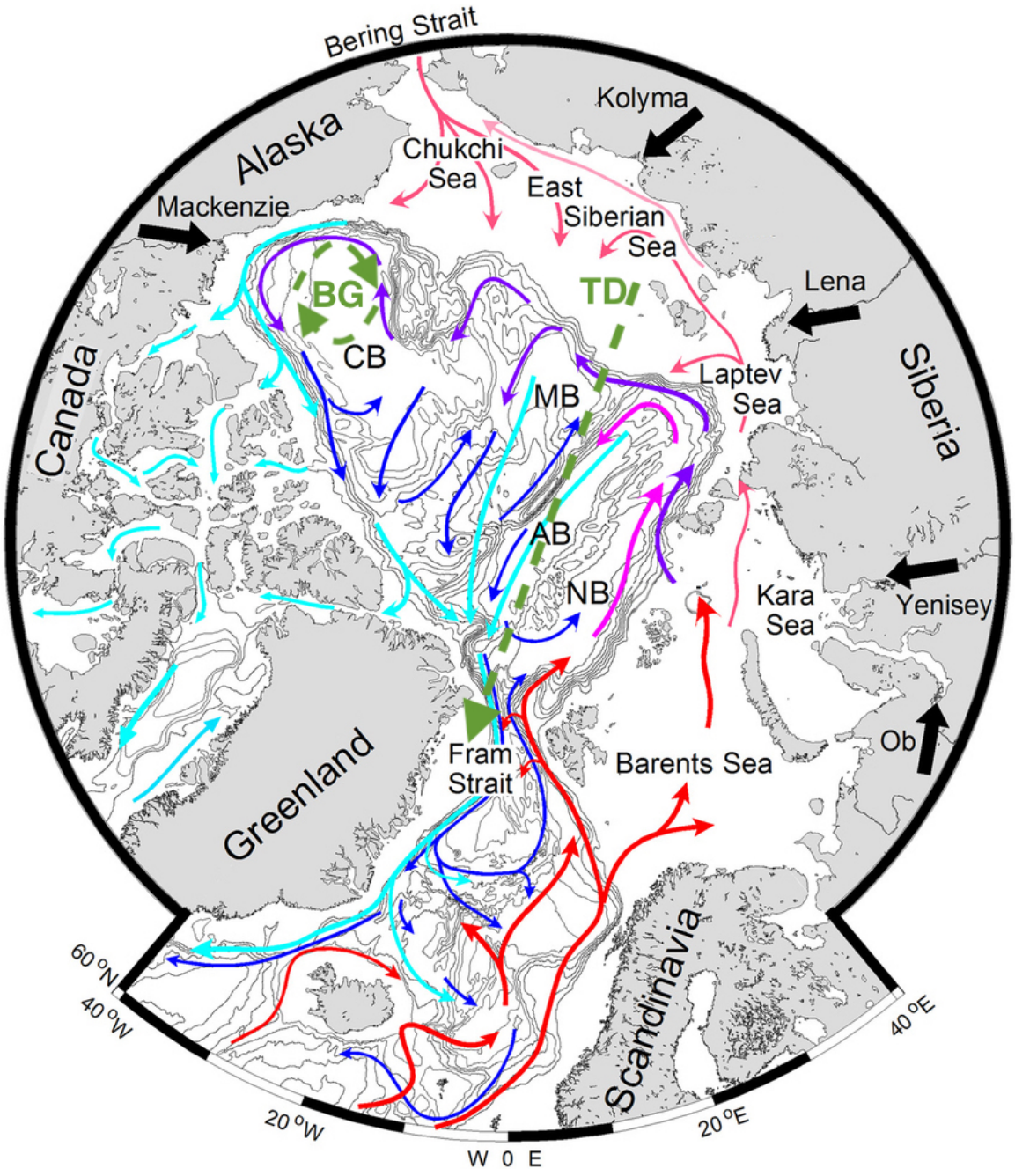

Figure 1.1 Dominating Arctic Ocean currents with inflowing relative warms surface currents (red) and colder surface currents (light blue) together with intermediate and deep currents (purple and dark blue). Major river discharge zones are indicated by black arrows with respective river names. Arctic Ocean Basins are abbreviated as follows: Canadian Basin (CB), Makarov Basin (MB), Amundsen Basin (AB), and Nansen Basin (NB). Simplistic circulation paths of the Beaufort Gyre (BG) and Transpolar Drift (TD) are illustrated by dashed, green arrows. [Figure adapted from Anderson & Macdonald, 2015].

CHAPTER 2

SURFACE FRESHWATER FLUXES IN THE ARCTIC AND SUBARCTIC SEAS DURING CONTRASTING YEARS OF HIGH AND LOW SUMMER SEA ICE EXTENT[1]

[1]Hall, S.B., B. Subrahmanyam, E.S. Nyadjro, and A. Samuelsen (2021). Surface Freshwater Fluxes in the Arctic and Subarctic Seas during Contrasting Years of High and Low Summer Sea Ice Extent. Journal of *Remote Sensing, 13*(8):1570, https://doi.org/10.3390/rs13081570.

ABSTRACT

Freshwater (FW) flux between the Arctic Ocean and adjacent waterways, predominantly driven by wind and oceanic currents, influences halocline stability and annual sea ice variability which further impacts global circulation and climate. The Arctic recently experienced anomalous years of high and low sea ice extent in the summers of 2013/2014 and 2012/2016, respectively. Here we investigate the interannual variability of oceanic surface FW flux in relation to spatial and temporal variability in sea ice concentration (SIC), sea surface salinity (SSS), and sea surface temperature (SST), focusing on years with summer sea–ice extremes. Our analysis between 2010–2018 illustrates high parameter variability, especially within the Laptev, Kara, and Barents seas, as well as an overall decreasing trend of FW flux through the Fram Strait. We find that in 2012, a maximum average FW flux of 0.32×10^3 ms^{-1} in October passed over a large portion of the Northeast Atlantic Ocean at 53°N. This study highlights recent changes in the Arctic and Subarctic Seas and the importance of continued monitoring of key variables through remote sensing to understand the dynamics behind these ongoing changes. Observations of FW fluxes through major Arctic routes will be increasingly important as the polar regions become more susceptible to warming, with major impacts on global climate.

2.1 INTRODUCTION

The Arctic Ocean serves as a dynamic link between the colder, fresher Pacific Ocean and the warmer, more saline Atlantic Ocean (Walsh et al., 2011). Despite covering only 3% of the Earth's total surface area, the Arctic and its subpolar regions play a crucial role in the regulation of meridional heat transport through thermohaline circulation (Serreze et al., 2011; Madhusoodanan et al., 2011). The Arctic has increasingly sustained warming at a rate that is at least twice the global average due to the accumulation of anthropogenic stressors including increased greenhouse gas emissions within the atmosphere in recent decades (Serreze et al., 2009). This phenomenon, referred to as Arctic amplification, has a major long-term influence on the Arctic's cryosphere and hydrosphere, including the decline of annual sea ice extent (SIE) and freshwater (FW) storage in the Arctic and its fluidity to adjacent subpolar seas and oceans. These interactions propagate further into the lower latitudes, consequently influencing the global circulation and climate.

Overturning caused by Arctic water deep convection is important for ocean ventilation. A slight increase in Arctic FW can contribute to stronger stratification, prohibiting advection and thus the regulation of global temperatures (Yang et al., 2016). Rabe et al. (2014) found an overall increase of 600 ± 300 km^3/year FW trend for the two decades leading up to 2012. On average, one-third of the Arctic FW input comes through the Bering Strait from the Pacific Ocean (Wang et al., 2019b). In contrast, the North Atlantic Ocean exchanges its warmer, more saline waters through the Norwegian and Barents Seas, for the Arctic's fresher waters that export through the Fram and Davis Straits (Woodgate & Aagaard, 2005; Tsubouchi et al., 2018). The Arctic's FW budget is also regulated by river discharge, sea ice melt, and net precipitation; values which have been

rising in conjunction with Arctic sea surface temperature (SST) and atmospheric wind stress (Timmermans & Marshall, 2020). McClelland et al. (2012) accounted FW river exports to the Arctic to be over 10% of the global discharge, which Brown et al. (2019) equates the largest source near Siberia at roughly $4.2x10^3$ km^3/year and precipitation at 2.2 $x10^3$ km^3/year during the first part of the 21st century. River runoff and net precipitation content can increase sea ice thickness as discussed by Weatherly and Walsh (1996). In this paper, we focus on the FW flux from marginal oceans and seas into and out of the Arctic ocean in relation to sea ice concentration (SIC). SIC refers to the amount of sea ice covering a specified area relative to the total area, given as a percentage in this study.

SIC growth (retreat) decreases (increases) the Arctic's FW content, making FW flux a good indicator for observing the distribution and intensity of Arctic sea ice on a regional and annual scale (Wang et al., 2018a; Haine et al., 2015). SIE, typically referenced as areas with a SIC above a 15% threshold, has declined at a rate of 4.7% per decade over the past four decades (Yadav et al., 2020) with more recent rates of about 10–13% per decade (Comiso et al., 2008; Serreze et al., 2016). Although commonly used, this threshold does have limitations when describing the annual thinning of sea ice or the depletion of multiyear sea ice (Matthews et al., 2020). Sea ice decline in the Arctic is regionally and temporally disproportionate, with a greater annual decrease shown within the Kara and Barents Seas compared to other Arctic seas (Parkinson et al., 2008), and years experiencing abnormally low (2012 and 2016) and relatively high (2013 and 2014) minimum summer SIE in the past decade. The lowest summer SIE occurred in 2012 and covered 3.41 million km^2 (Michon, 2020; Francis & Wu, 2020). A 48% increase in the following year of 2013 equated to roughly 5.35 million km^2 (Liu & Key, 2014). The lowest winter SIE occurred

in March of 2016 which contributed to its low sea ice coverage of 4.14 million km^2 in the summer (Perovich et al., 2016). The alarming minimum SIE in 2012 followed by two consecutive high summer SIEs and then another low raised further concerns for the lack of predictability in Arctic sea ice trends; therefore, we observe significant variations of related, climatic parameters between these four years and within the past decade to better understand past causes, current trajectories, and future implications.

SST and sea surface salinity (SSS) influence SIC. The combination of solar radiation with atmospheric-to-ocean heat flux drives the strong seasonality of SST, influencing the conditions for sea ice to form or melt (Praetorius et al., 2018). Higher SST limits the capacity of multi-year sea ice to form in the Arctic; an important feature describing the preservation of sea ice throughout the summer (Perovich & Richter-Menge, 2009). Sea ice formation (melt) causes local salinity to increase (decrease). SSS is also a reliable proxy for measuring the Arctic's FW flux between sources and exports (Fournier et al., 2020). Declining sea ice provides positive feedback by decreasing albedo and allowing more upward surface heat flux and increased SST that will continue to lessen ice accumulation (Kim et al., 2016). SST is regionally important for sea ice patterns but tends to be generally uniform at near-freezing temperatures over the Arctic, making SSS and FW transport the main parameters that govern the convection and overturning dynamics of surface water masses to the deep ocean (Yang et al., 2016). The lack of SIC allows for the fresher surface waters to endure oceanic stress between the atmospheric and surface water boundary (Harms & Karcher, 2005; Kodaira et al., 2020). Davis et al. (2016) showed that even with a net increase of FW, the Arctic's halocline instability and vertical mixing are still determined by wind-driven motion on ice free ocean surfaces, which drive currents

and could weaken the SIC in the Arctic. The direction and magnitude of wind and oceanic currents control FW variability through anticyclonic (cyclonic) tendencies that cause converging (diverging) interactions, leading to a build-up (release) of FW (Giles et al., 2012; Wang et al., 2017, Morison et al., 2012). Ice drift speed increase poses a threat to perennial ice, leaving an Arctic dominated by the more vulnerable seasonal ice (Kwok et al., 2013). As Arctic conditions continue to change and the declination of annual sea ice becomes more apparent, winds will continually hinder the stability of sea ice formation and oceanic drifts will intensify (Wang et al., 2021a).

The paucity of *in situ* data within the Arctic is due to limited accessibility in its harsh environmental conditions. Satellite passive-microwave measurements within the Arctic and subarctic regions since 1979 have helped mitigate these uncertainties (Stroh et al., 2015). Although satellite data has bias, specifically with temperature sensitivity of L-band radiometry, research has shown its data to be accurate in communicating general Arctic trends and thus is a key component to observe the spatial and temporal scales where *in situ* data are lacking (Lang et al., 2016). In this study we use satellite-derived salinity from the European Space Agency's (ESA) Soil Moisture and Ocean Salinity (SMOS) and the National Aeronautics and Space Administration's (NASA) Soil Moisture Active Passive (SMAP) missions, for their spatial resolution and available timeframes (Fournier et al., 2019; Tang et al., 2018). SMAP retrieves 2- to 3-day temporal repetitions with 40 km spatial resolutions compared to the 3-day and 45–50 km temporal and spatial resolutions from SMOS (Lind et al., 2018). For areas that both *in situ* instruments and satellites cannot reach, i.e., sea surface areas covered by ice, ocean models provide an approximation of regional indices.

The main objective for this study is to analyze the influence of the polar region's FW flux impacted by related parameters during anomalous summer low (2012/2016) and relatively high (2013/2014) minimum SIEs. This study builds from the need to further understand FW flux processes affected by atmospheric and oceanic interrelations (Haine et al., 2015; Serreze et al., 2016). FW flux within the northern latitudes is important for the generation of the Arctic's strong stratification, marine biological production (Kędra et al., 2015), mid-latitude weather patterns, and global circulation and climate (Wang et al., 2018a; Ricker et al., 2017). Properties of SST, SSS, wind, and oceanic currents have been shown to fundamentally influence the annual variations of sea ice within the Arctic (Polyakov et al., 2018). We divide the Arctic into three regions oriented around areas influenced by the Pacific Ocean, Atlantic Ocean, and the Canadian Arctic Archipelago (CAA). Results from this paper will help better understand the driving forces for and consequences of Arctic sea ice declination or growth, with supplementary influences on local wildlife, regional maritime advancements, oceanic circulation, and global climate change. The rest of this paper is ordered as follows: Section 2 describes data and methods, Section 3 illustrates research results, Section 4 deliberates discussion, and Section 5 summarizes conclusions of our study.

2.2 Materials and Methods

A. Data

We use the Group for High-Resolution Sea Surface Temperature (GHRSST) Level-4 Canadian Meteorological Center (CMC) SST product (Chao et al., 2009). This 0.2° × 0.2° gridded product combines data from a variety of satellite sensors including the National Oceanic and Atmospheric Administration's (NOAA) Advanced Very High-

Resolution Radiometer (AVHRR) and ESA's Along Track Scanning Radiometer (ATSR) series from ERS-1, ERS-2, and Envisat, as well as *in situ* observations and buoys. SIC data for this study is produced as part of the U.K. Meteorological Office (UKMO) Operational Sea Surface Temperature and Sea Ice Analysis (OSTIA) product (Prange & Gerdes, 2006). The 0.05° × 0.05° gridded OSTIA ice concentration data is sourced from the EUMETSAT Ocean and Sea Ice Satellite Application Facility (OSI-SAF).

SMOS version 5 data for this study was obtained from L'OCEAN Centre Aval de Traitement des Données SMOS (CATDS) as a Level-3 monthly 0.25° × 0.25° gridded product (Boutin et al., 2018). We also use SMAP Level-3 SSS Combined Active Passive (CAP) V5.0 data obtained from NASA's Jet Propulsion Laboratory (JPL) via the Physical Oceanography Distributed Active Archive Center (PO.DAAC) (Fore et al., 2016). This 0.25° × 0.25° gridded product is based on the newly released SMAP V5 Level-1 Brightness Temperatures. It uses an enhanced calibration methodology which improves absolute radiometric calibration and reduces the biases between ascending and descending passes. The SMOS mission has provided satellite SSS data since 2009 while the more recent launch of SMAP supplies data since mid-2015 (Fournier et al., 2019; Tang et al., 2018).

Surface wind data for this study are from Remote Sensing Systems' (RSS) Cross-Calibrated Multi-Platform (CCMP) version 2.0, 6-hourly ocean vector wind analysis product on a 0.25° × 0.25° grid (Wentz et al., 2015). The CCMP dataset is produced by combining cross-calibrated satellite microwave winds and instrument observations using a Variational Analysis Method (VAM).

Due to limited coverage of satellite-derived ocean currents data in the Arctic, we use the Ocean Reanalysis System 5 (ORAS5) ocean current data from the European Centre

for Medium-Range Weather Forecasts (ECMWF) (Zuo et al., 2019). ORAS5 has 75 vertically stratified layers and uses the Nucleus for European Modeling of the Ocean (NEMOv3.4) for its ocean model with a coupled sea ice model, and ERA-Interim and WAVE forcing with observational data assimilation. ORAS5 is available on a 0.25° × 0.25° horizontal grid and is obtained from Integrated Climate Data Center (ICDC) at the University of Hamburg (http://icdc.cen.unihamburg.de/projekte/easy-init/easy-init-ocean.html).

B. Methods

B.1. Arctic Sectors for Time Series Analysis

We compute monthly mean fields from daily mean fields. In addition, we compute interannual anomalies by subtracting the monthly climatologies from the monthly time series. We then define low (2012 and 2016), and high (2013 and 2014) sea ice years based on the ice index from Fetterer et al. (2017). In order to analyze regional variations, we divide the Arctic Ocean into the following sectors (Figure 2.1):

Atlantic sector: 90°E–45°W and 65°N–90°N.

Canadian sector: 45°W–140°W and 65°N–90°N.

Pacific sector: 140°W–90°E and 65°N–90°N.

This study examines FW flux within three major parts: the Atlantic, Pacific, and Canadian sectors, associated by their distinct characteristics with adjacent water masses, fluid dynamics, and climatic parameters (Figure 2.1). The Atlantic sector is influenced by the inflow of warm, saline North Atlantic water through the eastern Fram Strait and the export of cold, Arctic FW through the Western Fram Strait. In contrast to the Atlantic, the

Pacific Ocean provides fresher water to the Arctic through the Bering Strait inflow. Finally, the Canadian sector encompasses exchange between the CAA and the North Atlantic Ocean by the import (export) of water through the eastern (western) portion of the Davis Strait (Peterson, 2006). Past studies have described the complex and dynamic transports within the Arctic and connected water pathways (Haine et al., 2015; Aune et al., 2018). Time series of FW flux, SST, SSS, SIC, surface wind, and oceanic currents are analyzed in these regions. Transects at 70°N were selected for all three sectors to measure the flux of major ocean current passageways connecting to the Arctic.

B.2 FRESHWATER FLUX ESTIMATION

We compute surface FW flux (FW, units m^2s^{-1}) as Nichols and Subrahmanyam (2019):

$$FW_{zonal} = S_{fw} \times U \times lat_{dist} \quad (2.1)$$

$$FW_{meridional} = S_{fw} \times V \times lon_{dist} \quad (2.2)$$

where the standardized (unitless) freshwater anomaly (S_{fw}) from salinity,

$$S_{fw} = \frac{S_{ref} - SSS}{S_{ref}} \quad (2.3)$$

S_{ref} is the reference salinity 34.8 psu, the mean salinity in the Arctic region (Haine et al., 2015, Mazloff et al., 2010). SSS is sea surface salinity, U is zonal surface velocity (ms^{-1}), V is meridional surface velocity (ms^{-1}), and lat_{dist} and lon_{dist} are the horizontal expanse of the data grid cells (m).

2.3 RESULTS

A. ARCTIC'S MEAN STATE (2016-2018)

The Arctic's surface waters are influenced by complex atmospheric and oceanic interactions, of which the cryosphere plays an important role. Differences in SST, SSS, and SIC provide valuable insight into trends of Arctic FW flux and its connection to lower latitudes (Kawai et al., 2018) (Figure 2.2). The warm inflow of water in the Atlantic region restricts the extent of sea ice formation as seen in Figure 2.2a,b. In contrast, the Pacific and Canadian sectors are colder with less saline waters, which allow sea ice to extend much further south in those regions. Regional SSS variability is pronounced by the localized increase of river discharge and net precipitation (Figure 2.2c,d).

Since FW input on smaller scales is more detailed, we compare the SSS observations from SMAP and SMOS satellite data to detect the lower saline areas within the Arctic. From 2016–2018, SMAP details lower salinity gradients in Northeast Greenland, part of the CAA, and to a larger extent in the Pacific sector. SMAP also shows higher SSS extending north across Eurasia. Both satellite missions overlap during the 2016–2018 time period and are therefore used for comparison in Figure 2.2. The coarser resolution of SMAP seen in Figure 2.2c is favored when observing mesoscale and coastal regions such as the Laptev, Kara, and Beaufort seas in the Pacific sector, the finite differences within the CAA in the Canadian sector, and along the west coast of Greenland in the Atlantic sector (Lind et al., 2018). These areas incorporate major river mouths and edges of sea ice, which SMAP computes lower salinity gradients and contribute to the FW budget; details of which are not as well defined in SMOS. Although SMAP depicts more fine-scale changes occurring in the Arctic (Tang et al., 2018), SMOS has collected data for

a longer period of time (Olmedo et al., 2018); therefore, we will analyze SMOS salinity for the rest of the paper, as it contains salinity observations covering the 2010–2018 study period and has been previously used successfully in the Arctic region (Supply et al., 2020).

Ocean advection and the momentum of wind-driven circulation (Figure 2.3) influence the movement of these parameters and the transport of FW throughout the Arctic (Timmermans & Marshal, 2020). Atmospheric winds are weaker in the central Arctic and generally stronger near coastal regions and over major water pathways (Figure 2.3a–c). The strongest averaged winds between 2016–2018 occur in the southwestward movement over the Fram Strait, Bering Strait, and CAA. Currents flow with more distinct patterns especially around land masses and their adjacent ocean shelves (Figure 2.3d–f). The major pathways are illustrated by overall movements in Figure 2.3f. There is a noticeably strong current in the Laptev Sea with an average northeastward flow and another in the Beaufort Sea where the predominantly anticyclonic flow of the Beaufort Gyre occurs. Understanding the variability of SSS, SST, and SIC to the forcing of wind and currents is important when estimating the FW accumulation and pathways within the Arctic.

B. Interannual Variability Time Series

We construct monthly timeseries of these parameters to examine irregularities on an interannual scale between 2010 and 2018: years encompassing the low (2012/2016) and high (2013/2014) SIEs (Figure 2.4). We analyze the 2010–2018 monthly interannual anomalies of SST, SIC, and SSS in Figure 2.5 to observe the extent of irregularities especially within the focus years. The interannual anomalies are computed by subtracting the monthly climatologies from the monthly time series. The unavailability of SSS data,

specifically in the Pacific sector, result from the limitation of satellite observations due to sea ice obstruction.

Surface waters in the Atlantic sector are overall warmer than the Pacific and Canadian sectors because of the warm Gulf stream flow brought to the high latitudes from the North Atlantic Current (Houpert et al., 2018). Low SIE years of 2012/2016 had SICs lower than 60% in all sectors (Figure 2.4b). The largest SIC change was more than a 20% increase between 2012 to 2013 summers in the Pacific sector. The SIC was particularly low in the Atlantic sector the same year, whereas the Canadian and Pacific sectors show greater than 5% and 10% SIC anomalies, respectively (Figure 2.5b). 2013 also experienced the lowest SST anomalies and higher SSS anomalies (Figure 2.5a,g) in the Pacific and Canadian sectors. The Canadian sector's sea ice retained roughly the same minimum concentration through 2014. The SIC in the Atlantic sector did not decrease nearly as much in 2014, whereas the Pacific sector's SIC decreased and SST increased more than the prior year. The SSS in that sector remained higher than average in 2014 than any other year during this time period. All sectors experienced positive and negative SIC anomalies in 2014 and 2016, respectively, unlike in earlier corresponding years where the Atlantic sectors did not align with a similar magnitude as the Pacific and Canadian regions (Figure 2.5d). By 2016 the Atlantic sector also experienced higher than average SST and SSS. There was a 10% difference in SIC in the Canadian sector between high and low SIE years.

The winds (Figure 2.4c,d) and currents (Figure 2.4e,f) are quite variable on an interannual scale. General observations show that Atlantic winds are slightly stronger in the southward direction, as shown in Figure 2.3c, except for 2016 where there is a strong increase in northward wind flow over the summer months. Currents had the strongest

eastward flow in the Pacific and Canadian sectors during the summer of 2016. Meridional currents in Figure 2.3f are distinguishable between sectors because of their associated inflow and outflow patterns, as discussed earlier.

C. Multiparameter Composite Mean Analysis

Next, we observe the geographical distributions of the interannual fluctuations between the high/low SIE years. We analyze the means of SST, SIC, and SSS between August and October to encompass the annual sea ice low that occurs in the month of September (Figure 2.6).

In 2012, the largest warm water anomaly of more than 2°C was found close to the coast north of Alaska/Western Canada, while in 2016, a warm anomaly of similar magnitude was found in the eastern Barents Sea/Kara Sea. Overall, positive SST covers more surface area during 2012/2016. The Kara and Laptev Seas show great differences in SST magnitude and dispersal within all four years. SIE anomalies within the autumn months (Figure 2.6g) display the highest concentrations near the northern pole, especially north of Greenland in the Canadian sector.

To understand these parameters more precisely, the individual monthly data is also shown in Figures 2.7–2.9. SST variability is primarily strongest near the coastal regions, but the degree and spatial coverage are not as anticipated for each year (Figure 2.7). SST mapped in Figure 2.7a, and consistent with a study by Tsubouchi et al. (2018), is higher near the Barents Sea (up to ~9 ℃) and the Eastern Fram Strait (~7 ℃). The SST in the Bering Sea shows the high variability (~−2 ℃ to 8 ℃). The CAA and Beaufort Sea are dominated by high SST in 2012/16 and cooler SST in 2013/2014. The Pacific sector underwent a large low SST anomaly in 2013, allowing for the recovery and retention of

SIC. Overall, 2016 experienced the highest summer SST in the Bering Strait and northern Canadian regions (Carvalho & Wang, 2020). Overall, positive SST anomaly differences are shown near the Bering Strait and Laptev Sea within the Pacific sector. In contrast, the Kara Sea in the Arctic sector and CAA in the Canadian Sector have a negative SST anomaly difference, meaning that the low-sea ice years were warmer overall in those areas.

While the averaged SICs of each section were lower in 2012/2016 than 2013/2014 as seen in Figure 2.5b, the spatial distribution of the sea ice varied between years where differences were most prominent north of the Bering Strait. Overall, the SIE area difference (Figure 2.6l) has a higher anomaly concentrated within the Pacific sector compared to the Arctic or Canadian sector.

Next, we analyze monthly SIC discrepancies between the summer months of the high/low SIE years in Figure 2.8. Large variability occurs between August and September as the melt season peaks. SICs are highest north of Greenland and the CAA. Stronger anomalies occur in the Pacific sector between the focused years. SICs in 2012 were abnormally low along the sea ice perimeter, but higher near the northern pole, whereas 2016 showed slightly lower concentrations overall but higher than average concentrations north of the Laptev sea.

Since sea ice accumulates less in the Atlantic sector due to its higher SST and SSS characteristics, the retention of sea ice within the Pacific sector during the later melt months of August through October are important in determining the overall annual minimum SIE.

Areas of sea ice growth (melt) tend to decrease (increase) local SSS, making it an important parameter when observing the deduction (addition) to the FW budget (Figure 2.9). Adjacent oceans contribute different concentrations of salinity, showing fresher

waters in the Pacific as opposed to a more saline Atlantic sector from Atlantic Ocean inflow. Since the CAA primarily experiences outflow of Arctic water, salinities vary interannually. In 2013 and 2014, more saline conditions were concentrated around Greenland in the Canadian/Atlantic sectors. This compares well with Figure 2.5, which shows the Canadian sector having the highest SSS in the years of high SIE.

FW flux between the Arctic and the sector transects primarily travel north, into the Arctic or south, away from the Arctic; therefore, we compute the meridional transport instead across these sections (Figure 2.10). Due to the Bering Strait inflow, the Pacific sector experiences a higher FW flux compared to the Atlantic sector's balanced transports and the Canadian sectors' outflow (Woodgate & Aagaard, 2005). The largest export of FW in the Atlantic sector occurs in 2012 (Figure 2.10a), a time when the Pacific sector experiences an anomalously low import of FW (Figure 2.10b).

D. Atlantic Freshwater Pathways

The FW outflow from the Arctic Ocean into the North Atlantic incorporates numerous pathways, many of which oppose each other, i.e., the northeast Barents Sea Opening (BSO) flow and the southwest Fram Strait current. Therefore, we analyze the dominant flux pathways in the Arctic sector separately (Figure 2.11). Two pathways connecting the Atlantic and Arctic Ocean are the BSO and the Fram Strait (Figure 2.11a). A third transect is computed to capture the low anomalous salinity event in the summer to fall of 2012, hereafter referred to as the northeast Atlantic section (NEA) (Figure 2.11a).

Dominant movement through the BSO flows in the zonal direction, while the Fram Strait and the NEA experience predominantly meridional flows; therefore, we computed FW flux in the transects to their respective directional transport (Figure 2.11b,c).

Fluctuations in transport depend on atmospheric processes driving currents through these sectors, with no obvious seasonal oscillations over the regional areas. As seen in Figure 2.11, October 2012 has a high FW flux through the NEA transect equating to 0.32×10^3 m^2s^{-1} which has a positive anomalous FW flux of 0.47×10^3 m^2s^{-1}. In the summer of 2012, the Fram Strait and BSO have their highest FW flux at 0.12×10^3 m^2s^{-1} and 0.10×10^3 m^2s^{-1} respectively.

The general trend of the FW flux through the Fram Strait decreases at a monthly rate of -6.0 m^2s^{-1} from 2010–2018, with a more recent declining monthly trend of -10 m^2s^{-1} from 2015–2018. This is especially true during 2017 and 2018 where a drastic negative FW flux occurs, as opposed to the positive flux through the NEA transect (Figure 2.11b,c). Higher SSS are alongside the eastern Greenland coast in 2013, causing its lower FW flux anomalies through the Fram Strait. A larger salinity gradient passes through the NEA transect in the summer of 2014 as shown in Figure 2.9j and computed in Figure 2.11c. Quantifying the FW flow specifically within these three transects distinguishes the Arctic's contribution to the North Atlantic and vice versa; especially as annual conditions change towards a warmer, northern climate regime.

2.4 Discussion

A. Multiparameter Variability in Extreme SIE Years

A.1 SST, SSS, SIC

SIE retains its highest extent between March and April, while retreating to its lowest extent by September or August depending on the threshold of SIC used, typically greater than or equal to 15% (Matthews et al., 2020). We observe climatic trends through

years of low (2012/2016) and high (2013/2014) SIE and associations between parameters of SST and SSS that attribute to their SIC extremes. We also delineate monthly patterns in the summers of those years which influence the transport of FW between the Arctic and subarctic regions. Brown et al. (2019) describes precipitation to have less of an input to the Arctic's FW storage, but more complexity when quantifying. This study features the recent SSS Arctic state through SMOS satellite data in relation to other parameters between 2010 and 2018. SSS was greater in the high SIE years, especially in the Canadian sector where higher concentrations of sea ice retained the fresher waters.

Interannual variability of SST influenced the low SIE of 2012/2016 as warmer areas intensified throughout the Arctic while 2013/2014 showed overall cooling through each month observed. SST varied within different Arctic seas, governing the conditions for sea ice formation. Although low on average, regional Arctic SST is increasing annually which can obstruct the formation of winter sea ice and the retention of multi-year sea ice during the summer. Anomalous warm SST in 2012 and 2016 occurred especially in the Barents and Kara seas, which Jung et al. (2017) credited to the influence of eddy transport and retention.

The Atlantic sector experienced the lowest SIC during 2013, while the Pacific and Canadian sectors remained high. This has been attributed to a strong warm temperature anomaly in the Barents Sea as well as an overall negative sea level pressure, which suggests the lower sea ice melt and higher SSS compared to the other sectors (Francis & Wu, 2020). 2014 showed anomalously high SST during the early summer despite its retention of SIC in all sectors, especially the Atlantic, which was lower than normal the year prior. Di Lorenzo et al. (2016) examined a marine heatwave in 2014 in the North Pacific that created

the anomalous high SST entering the Arctic through the Bering Strait mainly fed by atmospheric forcing. High SSTA from the Pacific sector in 2016 matches the studies from Hu et al. (2017) and Hartmann (2015) that investigated the influentially strong, warm phase of the El Niño Southern Oscillation (ENSO) of that year. This induced warmer SSTs in the northeast Pacific Ocean, curating warmer surface temperatures through the Bering Strait from oceanic heat loss and weak, cold water advection to the upper ocean during 2016.

The summer of 2014 also experienced a higher than normal SIC, shown by late melting and early freeze onset days (Petty et al., 2018). Sea ice accumulates highest North of Greenland and the CAA aided by anticyclonic wind from the Beaufort Sea; however, Petty et al. (2018) describes melt and freeze onset days throughout this time period that could contribute to the levels of SIC seen in this study. Earlier melt onset days in 2012/2016 hindered the chance for sea ice to accumulate over the fall months. Faster sea ice melt quickens the pace of FW release back to the ocean surface and the interaction to the atmosphere or oceanic fluid dynamics. Melt onset days started at consistent times in 2013/2014; however, in 2013, an early freeze onset was recorded in the Eastern Arctic, comparing well to that of high concentrations that October. There was a later freeze onset in 2016, restricting its ability to store as much ice, which correlates well to the total lower sea ice anomalies spread throughout the sea ice area of that year. Ricker et al. (2017) also pointed that the inability to sustain multiyear sea ice caused unfavorable conditions for the increase of SIC in 2016, matching our observations of lower SIC overall. The preservation of thick sea ice over winter months, specifically from the northwest part of Greenland, permitted a higher minimum SIE for 2013 and 2014 (Tilling et al., 2015). Comiso et al. (2008) expresses the implications that pre-conditioning warming has on the following

years' SIE. Increased present and near-future atmospheric warming will impede the ability for sea ice to remain throughout the summer months.

A.2 Winds and Currents

Atmospheric forcing plays a significant role on the direct contact with the ocean surface interface and governs the intensity of water transport. Winds also influence deep convection, especially in the North Atlantic Meridional Overturning Circulation (AMOC). Ocean current direction and magnitude are driven by atmospheric wind forcing, both of which modify sea ice content and drift (Francis et al., 2009). For example, storm forcings in 2012 caused prominent variations, leading towards changes in the Beaufort Sea where the spatial distribution of SIC varies (Vihma, 2014). Summer sea ice especially increased in the Beaufort Sea from 2012 to 2013 (Figure 2.6j), which Liu and Key (2014) attributed to the decrease in winter cloud cover. Future research can incorporate the effects of higher atmospheric conditions to SIC and subsequently the relationship to FW flux. The 33% SIE increase from September of 2013 to 2012 was mainly attributed to the retention of sea ice and accumulation driven by atmospheric forcing (Tilling et al., 2015).

Meridional currents in each sector are most distinguishable between the Arctic and subarctic regions where the Pacific sector has a constant northward current that flows into the Arctic while the dominant current in the Canadian sector is southward, out of the Arctic. The meridional current in the Atlantic sector is balanced by the inflow of water to the Arctic through the Barents Sea and the east side of the Fram Strait with a substantial southward flow out of the Arctic on the west side of the Fram Strait (Tsubouchi et al., 2018). A strong, wide current is also observed within the Arctic in the north Laptev sea, one of the first areas to begin the growth of winter sea ice every year (Kim et al., 2016). The extent of this study

observes currents flowing into the Arctic from subarctic regions; future studies can incorporate the movement of water flow solely within the Arctic. Currents in 2016 had a greater southwestward movement in the Pacific and Canadian sectors than usual. Overland et al. (2016) suggests an eastern shift of winds driven by the midlatitudes caused the lowest February temperatures in 2016, with a 2℃ warmer anomaly, preconditioning thinner and more mobile ice compared to the earlier years of the 2010s (Kwok et al., 2013). Increased winds and current drift speeds could result in a higher sea ice or liquid FW transport out of the Arctic.

A.3 Freshwater Fluxes

An averaged negative FW flux occurs in the Atlantic and Canadian Sectors while a positive FW flux is prominent in the Pacific Sector. However, there are large variations in the interannual anomalies of meridional FW flux throughout the Arctic. Years of low SIE seem to vary primarily in the Pacific Sector which can be attributed to the predominant, anticyclonic movement of the Beaufort Gyre circulating FW to diverging regions (Wang et al., 2019a). With an earlier melt season, outflow of FW in 2016 occurred at a higher magnitude in the Canadian Sector as opposed to an export through the Eastern Greenland Current (EGC). Dodd et al. (2009) assigns the EGC responsible for exporting between ½ to ¾ of the Arctic's sea ice and liquid FW to the North Atlantic, where interaction with the Nordic seas can impact the overturning of North Atlantic surface waters important for the AMOC. Jahn et al. (2012) observed FW in sea ice is exported primarily through the Fram Strait in the Atlantic sector while larger liquid FW is generally expelled through the CAA.

A significantly notable surface FW anomaly in 2012 passed in the East Greenland Current (EGC) through the Denmark Strait, of which explanations are still not well

illustrated (de Steur et al., 2018). Therefore, we observed the implications of subpolar FW transport in the North Atlantic Ocean.

A.4 Atlantic Freshwater Pathways

Compared to the Pacific and Canadian sectors, the Atlantic sector incorporates various flow directions and cannot be accurately characterized by one transect. Skliris et al. (2020) observed up to a 20% increase within the last 40 years of average meridional FW export from the Arctic to the North Atlantic Ocean, an area that depends on weaker stratification for thermohaline circulation. In order to understand the contribution of FW inflow and dispersion of outflow, we observed freshwater fluxes through three separate transects in the Atlantic region.

A low salinity anomaly occurred in 2012 where about a 75% larger FW transport was exported into the Atlantic Sector unlike that of its shared low SIE year of 2016 (de Steur et al., 2018). De Steur et al. (2017) described high FW transport anomalies within July 2012, most likely continuing FW export through the EGC as seen in Figure 2.9. Nghiem et al. (2012) attributed the decrease in adjacent surface salinity of Greenland to the anomalously large melt across 98% of the ice sheet most likely due to a warm ridged air interaction. However, it is still uncertain to what parameters or their contribution to the abnormal FW outflow away from Greenland. We explore this unusual surface FW event further in Figure 2.11.

Sea ice export through the Fram Strait declined between 1991 and 2010, whereas southward FW flux has increased about 49% from the 1959–1990 average in the southeast of Greenland (Bamber et al., 2012). Josey et al. (2005) suggests that other contributions to the fresher NEA region is from net precipitation and pressure gradient of the North Atlantic

Oscillation (NAO). The more likely factor is a change in the East Atlantic Pattern, which is similar to the NAO but with a southward shift. FW flux through the NEA is higher in both years of low SIE, suggesting FW export effects from the Arctic on mid-latitudes. As low SIE years become more dominant, FW flux into the North Atlantic could change the AMOC drastically if prompted by enough Arctic FW, changing the global thermohaline circulation. Therefore, incorporating FW observations from precipitation and river input with Arctic FW export when observing changing SSS will improve the knowledge of polar region influence on the global circulation.

2.5 CONCLUSION

The Arctic's cold, FW budget is a driving factor to the strength of the polar halocline and the slowdown of the overturning advection in the north AMOC, despite its relatively small surface area. A seasonal contributor for increased FW is Arctic sea ice with lowest extents at the end of the melt season in September. In the last decade, there is a general decreasing trend of annual SIE due to Arctic Amplification as a consequence of anthropogenic induced climate change primarily induced by greenhouse gas emissions (2016); however, the yearly variations of these extents are still unknown. From this study, we utilize remote sensing data and model outputs to examine the transport and variability of climactic parameters in the Arctic and interconnected spatiotemporal ranges.

With box-averages of each sector, we described the major contributions of adjacent seas and Arctic characteristics, then focused on the multiparameter variations within the individual years of low and high sea ice extent. There, we specified trends in different regions through the scope of the summer seasons where large fluctuation occurred in the Laptev, Kara, and Barents seas. We observed an anomalous surface FW transport event in

the subarctic and the North Atlantic regions in 2012. Past studies mention the possible contribution of the increasing annual declination of the southeastern Greenland ice sheet (Morison et al., 2012, Prange & Gerdes, 2006, Peterson, 2006).

Models and satellites allow us to estimate parameters where *in situ* instruments lack, especially in harsh conditions that polar climates bring. However, there are limitations within validity of model estimations and satellite radiometer's sensitivity to colder temperatures (Lang et al., 2016). Future work should focus on the contribution of FW through precipitation and river input and the possible implications that the Greenland Ice sheet melt has on the FW exchange with the Arctic and subarctic regions, especially on the impacts of SIE. Annual sea ice declination and FW increase within the Arctic are of major importance to understanding and predicting the polar regime.

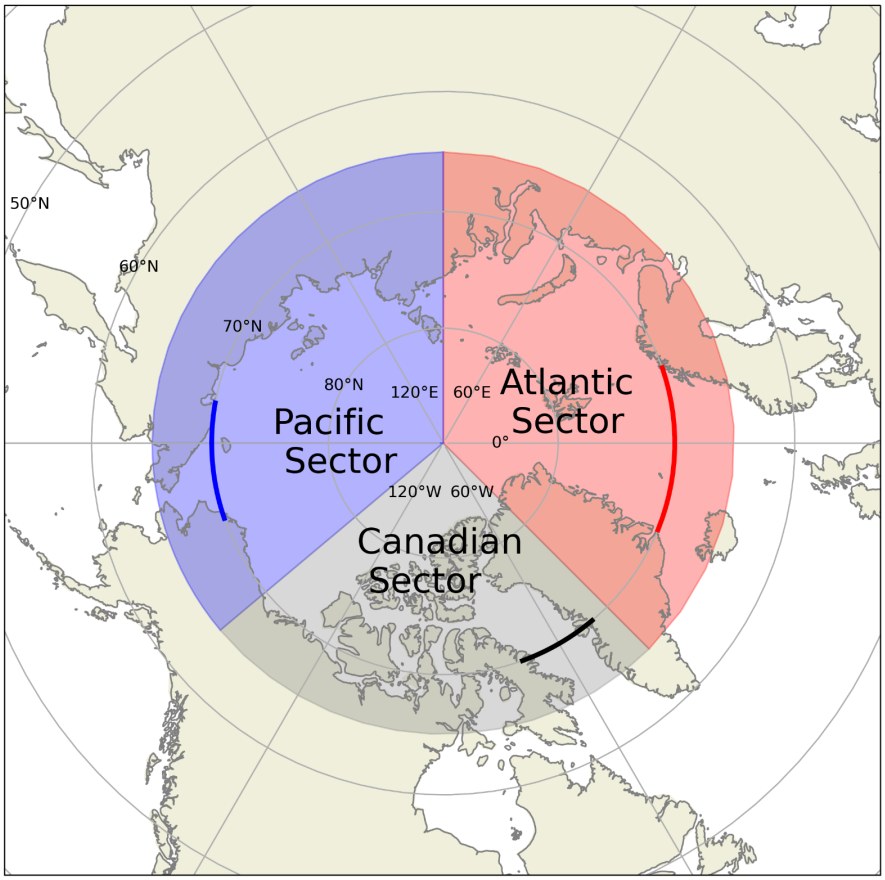

Figure 2.1 Schematic of the Arctic Ocean showing Pacific, Canadian, and Atlantic sectors used for box averaging. Highlighted lines show transects used to compute net freshwater fluxes across the respective sectors.

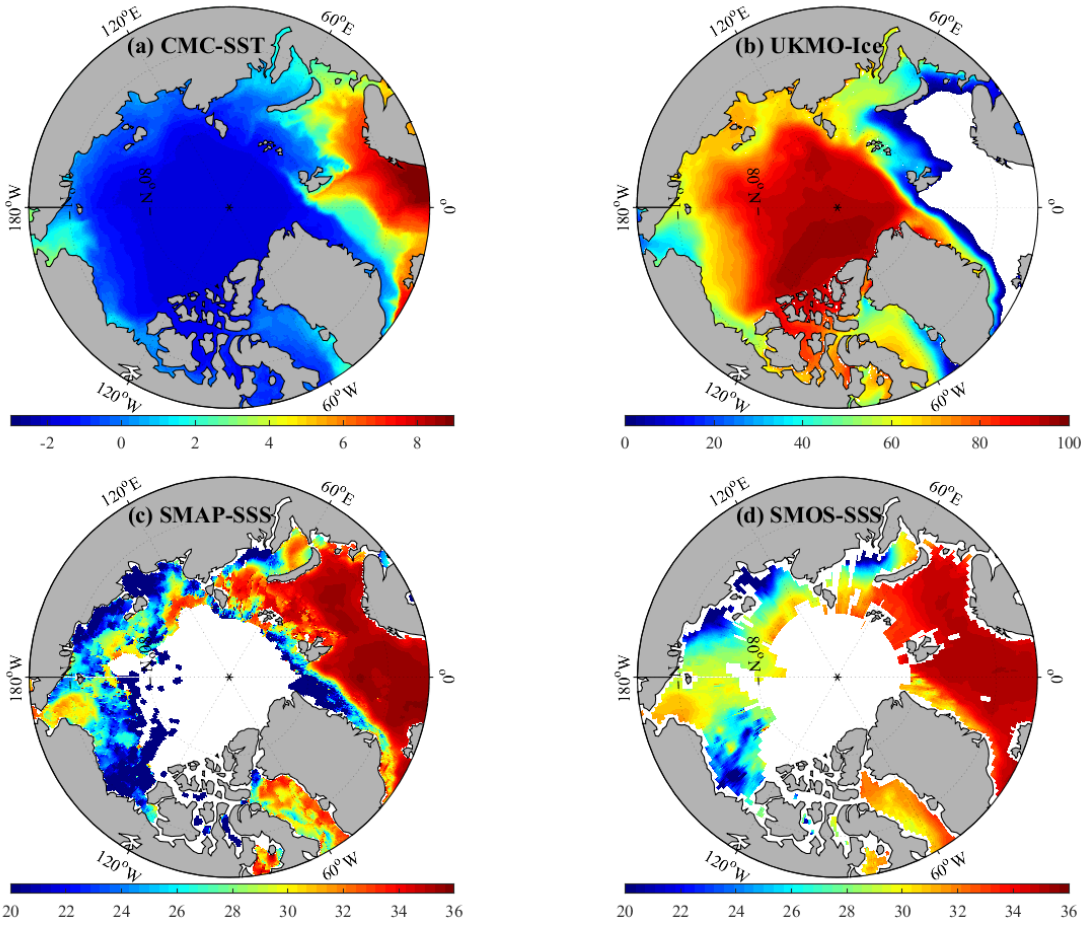

Figure 2.2 Annual mean (covering 2016–2018) for (a) CMC SST (°C), (b) UKMO Ice concentration (%), (c) SMAP SSS (psu), and (d) SMOS SSS (psu).

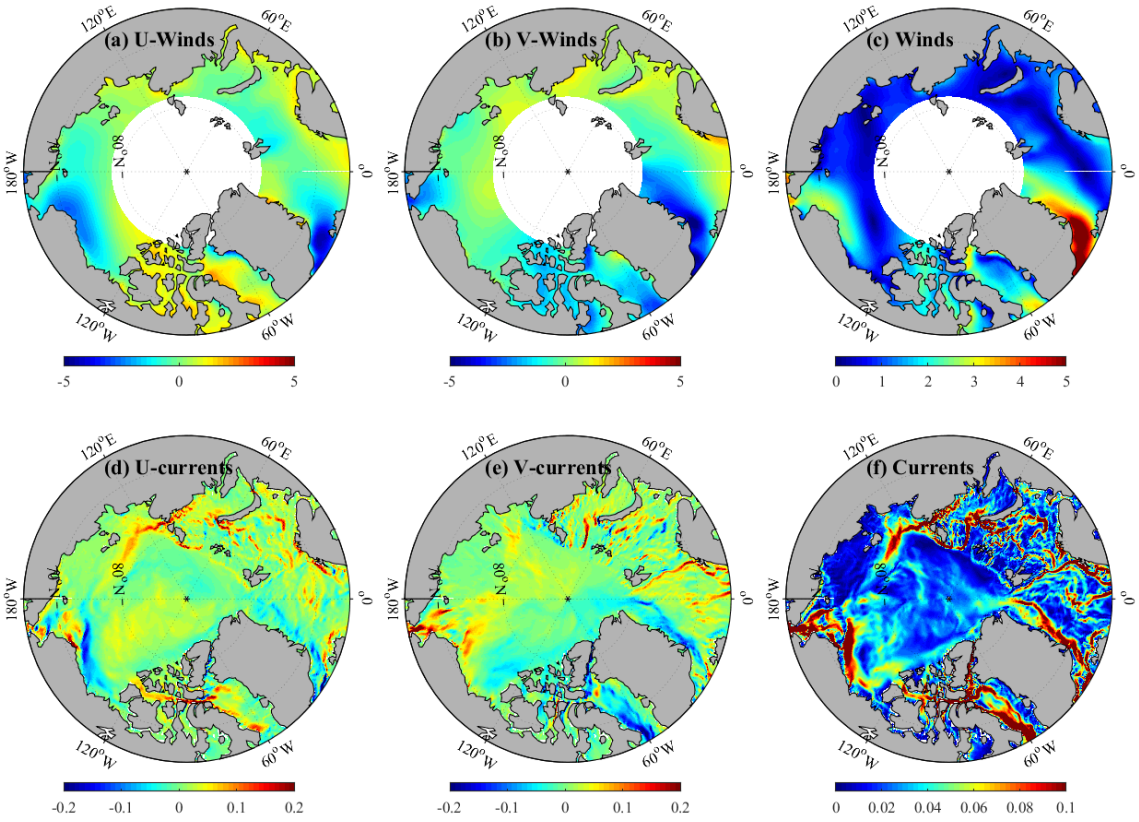

Figure 2.3 Annual mean (covering 2016–2018) for (a) CCMP zonal wind speed (ms^{-1}), (b) CCMP meridional wind speed (ms^{-1}), (c) CCMP wind speed magnitude (ms^{-1}) (d) ORAS5 zonal surface current speed (ms^{-1}), (e) ORAS5 meridional surface current speed (ms^{-1}) and (f) ORAS5 surface current magnitude (ms^{-1}).

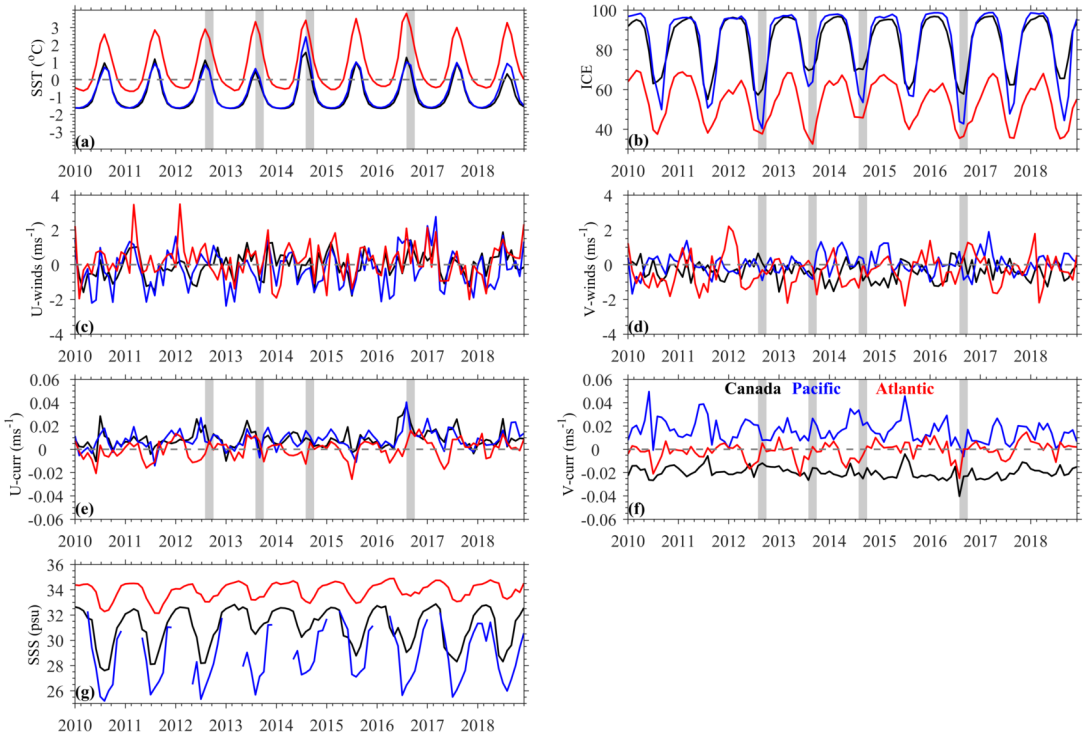

Figure 2.4 Box-averaged monthly time series for the Canadian (black), Pacific (blue) and Atlantic (red) sectors for (a) CMC SST (°C), (b) UKMO ice concentration (%), (c) zonal winds speed (ms^{-1}), (d) meridional wind speed (ms^{-1}), (e) zonal currents (ms^{-1}), (f) meridional currents (ms^{-1}), and (g) SMOS SSS (psu). The gray-colored bands show the periods of minimum (2012/2016) and maximum (2013/2014) September sea ice extent.

Figure 2.5 Box-averaged interannual anomalies time series for the Canadian (black), Pacific (blue) and Atlantic (red) sectors for (a) CMC SST (°C), (b) UKMO Ice concentration (%), (c) zonal winds speed (ms^{-1}), (d) meridional wind speed (ms^{-1}), (e) zonal currents (ms^{-1}), (f) meridional currents (ms^{-1}), and (g) SMOS SSS (psu). The gray-colored bands show the periods of minimum (2012/2016) and maximum (2013/2014) September sea ice extent.

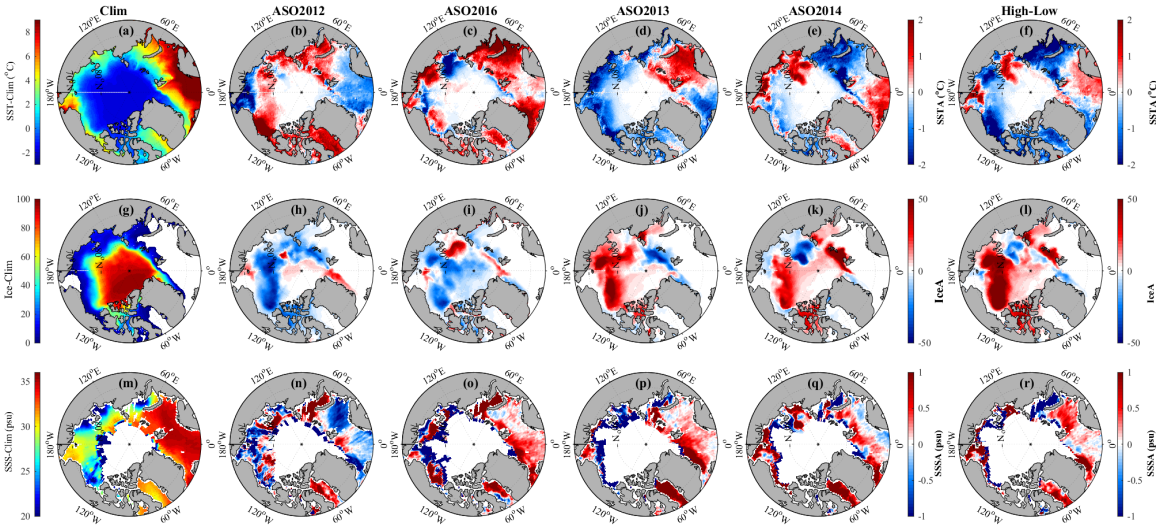

Figure 2.6 Composite means of August to October. First row (a–f): (a) 2010–2018 climatology of CMC SST (°C). Composite means of August to October SST interannual anomalies (°C) for (b) 2012, (c) 2016, (d) 2013 and (e) 2014. (f) shows the SST interannual anomalous difference between high/low SIE years (i.e., mean of (d) and (e) minus mean of (b) and (c). Second row (g–l): as in first row but for ice concentration (%). Third row(m–r): as in first row but for SSS (psu).

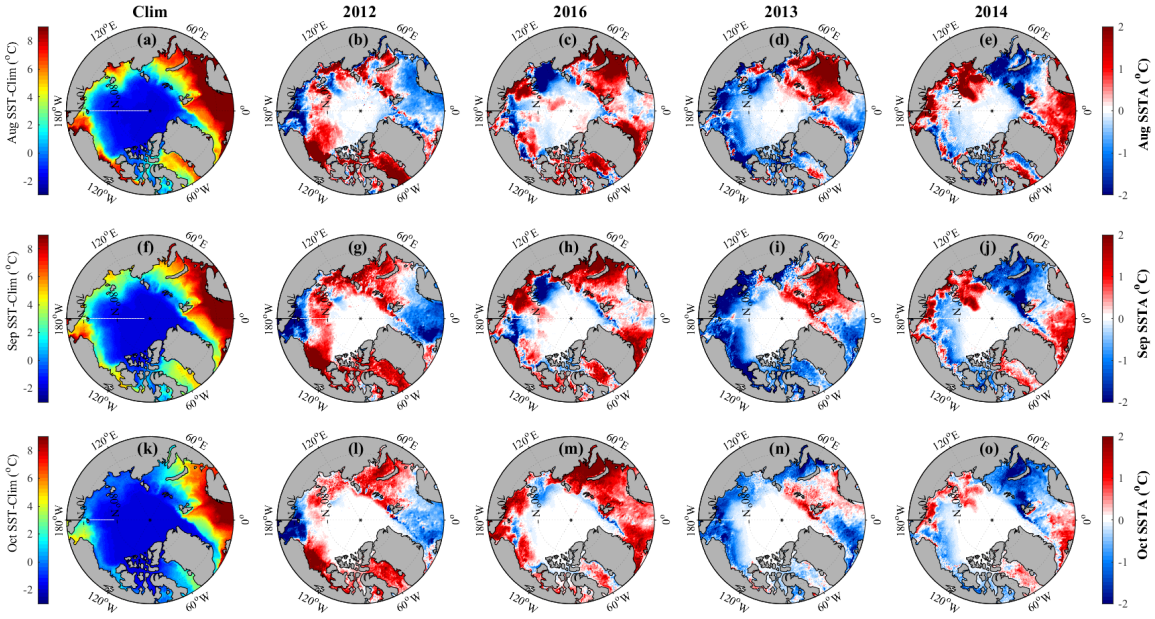

Figure 2.7 First row: (a) August climatology of CMC SST (°C). August interannual SST anomalies (°C) for (b) 2012, (c) 2016, (d) 2013 and (e) 2014. Second row: as in first row but for September. Third row: as in first row but for October.

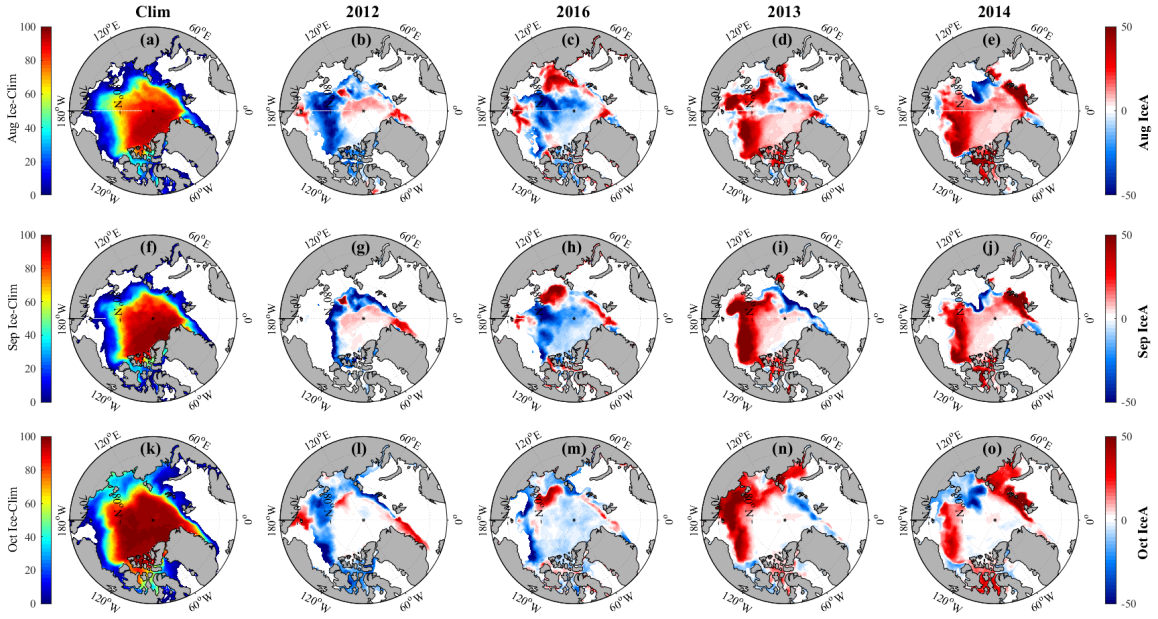

Figure 2.8 First row: (a) August climatology of UKMO Ice concentration (%). August interannual SIC anomalies (%) for (b) 2012, (c) 2016, (d) 2013 and (e) 2014. Second row: as in first row but for September. Third row: as in first row but for October.

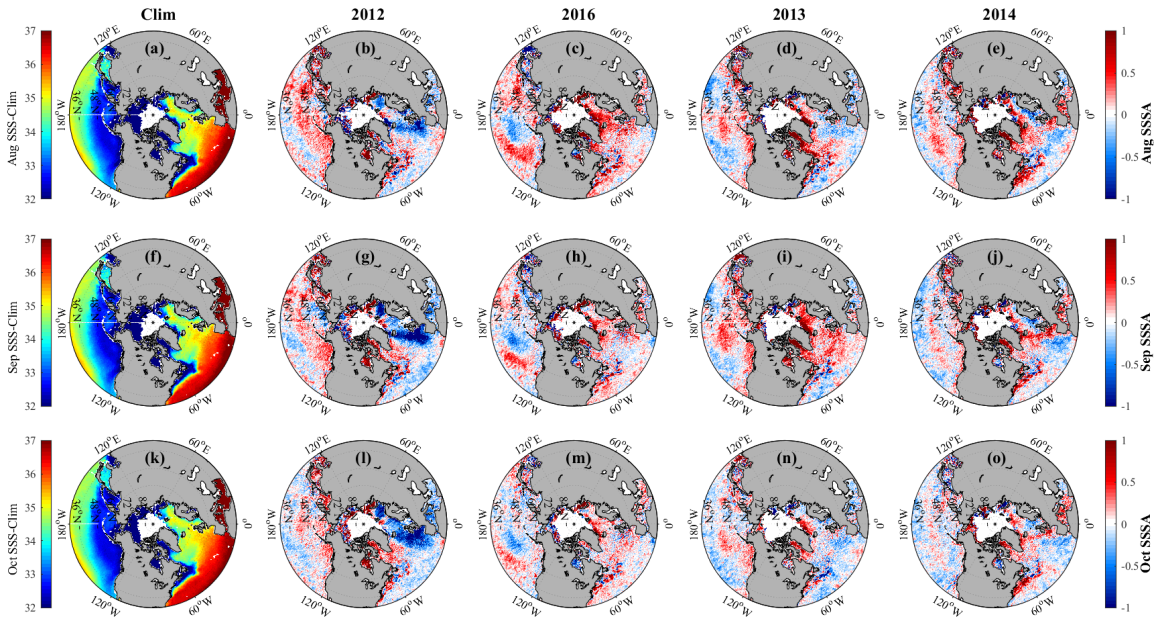

Figure 2.9 First row: (a) August climatology of SMOS SSS (psu). August SSS interannual anomalies (psu) for (b) 2012, (c) 2016, (d) 2013 and (e) 2014. Second row (f–j): as in first row but for September. Third row (k–o): as in first row but for October.

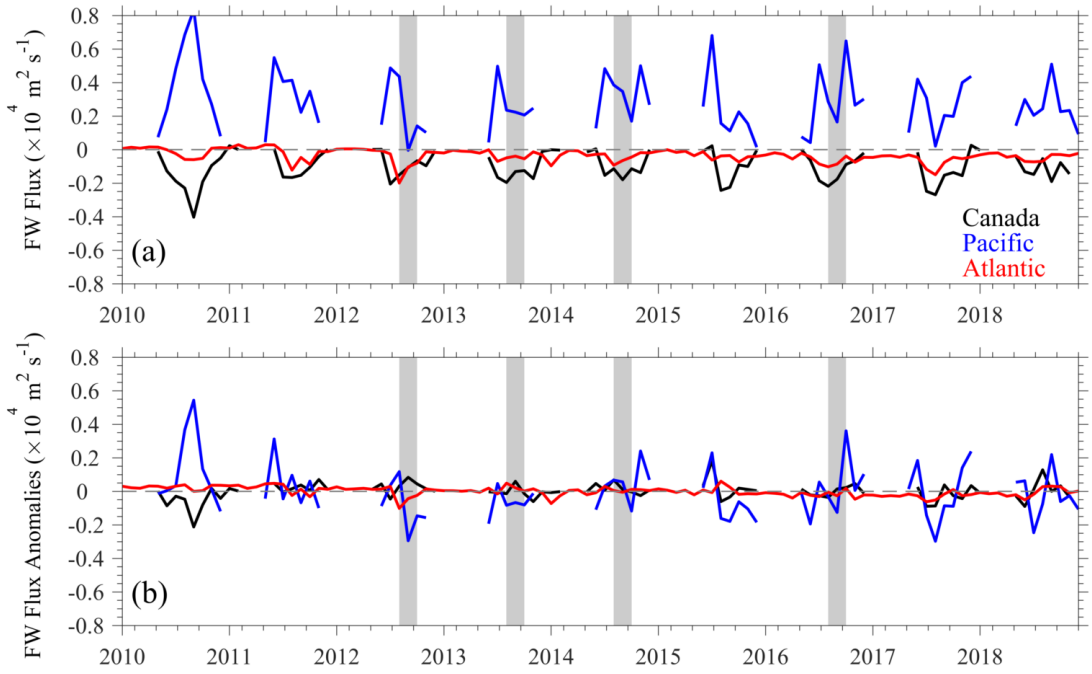

Figure 2.10 (a) Monthly net meridional FW fluxes (m^2s^{-1}), and (b) interannual anomalies of net meridional FW fluxes (m^2s^{-1}) across 70°N in the Canadian (black), Pacific (blue), and Atlantic (red) sectors. The gray-colored bands show the periods of minimum (2012/2016) and maximum (2013/2014) sea ice extent.

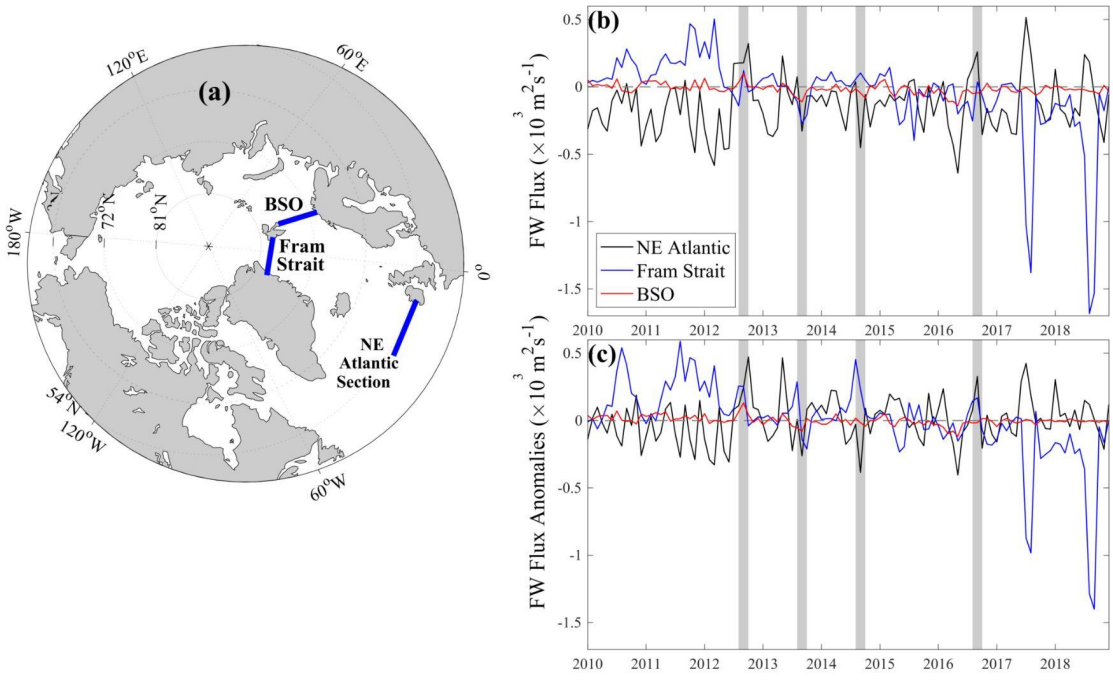

Figure 2.11 (a) A schematic of the Arctic Ocean showing the Northeast (NE) Atlantic Section (53°N, 10°W to 25°W), Fram Strait (79°N, 11°E to 19°W), Barents Sea Opening (BSO) (71°N to 77°N, 23°E) with corresponding (b) FW Flux and (c) FW Flux interannual anomalies (m^2s^{-1}) during 2010–2018. Meridional flux was computed for NE Atlantic and Fram Strait sections, while zonal flux was computed for the BSO as the dominant movements. The gray-colored bands show the periods of minimum (2012/2016) and maximum (2013/2014) September sea ice extent.

CHAPTER 3

INTERCOMPARISON OF SALINITY PRODUCTS IN THE BEAUFORT GYRE AND ARCTIC OCEAN[2]

[2]Hall, S.B., B. Subrahmanyam, and J.H. Morison (2022). Intercomparison of Salinity Products in the Beaufort Gyre and Arctic Ocean. *Remote Sensing 14*(1): 71, https://doi.org/10.3390/rs14010071.

ABSTRACT

Salinity is the primary determinant of the Arctic Ocean's density structure. Freshwater accumulation and distribution in the Arctic Ocean have varied significantly in recent decades and certainly in the Beaufort Gyre (BG). In this study, we analyze salinity variations in the BG region between 2012 and 2017. We use *in situ* salinity observations from the Seasonal Ice Zone Reconnaissance Surveys (SIZRS), CTD casts from the Beaufort Gyre Exploration Project (BGP), and the EN4 data to validate and compare with satellite observations from Soil Moisture Active Passive (SMAP), Soil Moisture and Ocean Salinity (SMOS), and Aquarius Optimally Interpolated Sea Surface Salinity (OISSS), and Arctic Ocean models: ECCO, MIZMAS, HYCOM, ORAS5, and GLORYS12. Overall, satellite observations are restricted to ice-free regions in the BG area, and models tend to overestimate sea surface salinity (SSS). Freshwater Content (FWC), an important component of the BG, is computed for EN4 and most models. ORAS5 provides the strongest positive SSS correlation coefficient (0.612) and lowest bias to *in situ* observations compared to the other products. ORAS5 subsurface salinity and FWC compare well with the EN4 data. Discrepancies between models and SIZRS data are highest in GLORYS12 and ECCO. These comparisons identify dissimilarities between salinity products and extend challenges to observations applicable to other areas of the Arctic Ocean.

3.1 INTRODUCTION

Arctic Ocean salinity is a key element of seasonal and interannual variability (Fournier et al., 2020). In this paper, we provide a comparison regarding modeled, remotely sensed, and directly observed salinity in the Arctic Ocean. We had two objectives. First, we wished to learn the validity of remotely sensed and modeled salinity compared to *in situ* observations. Low water temperatures and the consequently low thermal expansion coefficient make Arctic Ocean salinity the primary determinant of stratification and the density distribution controlling geostrophic circulation. This, combined with the facts that surface buoyancy fluxes resulting from sea ice formation and melt are due overwhelmingly to salt flux, and that the inflows to the Arctic Ocean are characterized by large differences in salinity, results in the Arctic Ocean being a salt-stratified sea. Furthermore, the Arctic Ocean is a critical link in the global freshwater–thermohaline chain, where the high salinity Atlantic Water combines with less saline Pacific Water and runoff from drainage basins extends south beyond the Arctic Circle. While salinity is important, owing to the ice cover and remoteness, it is extremely difficult to make *in situ* observations of salinity in critical areas of the Arctic Ocean. Ultimately, we must rely on remote sensing and models to infer salinity changes in these areas.

Second, we sought a better understanding of Arctic Ocean salinity and freshwater content (FWC) changes, with special emphasis on the Beaufort Sea. The mean density structure and wind-driven surface circulation of the Arctic Ocean are largely dominated by the anticyclonic Beaufort Gyre in the Canadian Basin, along with the Transpolar Drift from the Pacific side of the Arctic Basin, over the Pole to the Fram Strait gateway to the North Atlantic. Consequently, changes in the Beaufort Gyre circulation and freshwater storage

have been studied extensively in recent decades (Krishfield et al., 2014; Proshutinsky & Johnson, 1997; Proshutinsky et al., 2009) and are of current interest in their own right.

However, analysis of changes relative to the time-averaged Arctic Ocean circulation and freshwater distribution over the last 70 years reveal that the leading pattern of variability is centered not in the Beaufort Sea, but on the Russian side of the Arctic Ocean. In its positive phase, this pattern is dominated by a sea surface trough with cyclonic circulation roughly around in the Makarov Basin (Morison et al., 2021). The positive (or Cyclonic Mode) phase became more dominant, along with an increase in area-average Arctic Ocean vorticity, beginning in 1990 and associated with a one standard deviation increase in the average winter Arctic Oscillation index. As part of this regime shift, the dominant mode tends to include an increase in the intensity, but not the size, of the anticyclonic Beaufort Gyre adjacent to the dominant growing and intensifying cyclonic circulation centered on the Makarov Basin.

As a consequence of these findings, we need to see increased observations on the Russian margins of the Arctic Basin. Without them, we are blind to the dominant mode of variability in circulation and freshwater pathways (Morison et al., 2012). The extreme remoteness of this region has resulted in there being virtually no modern repeat *in situ* observations there. Therefore, we looked to this study to not only explore salinity in the observation-rich Beaufort Sea for its own sake but to validate modeled salinities and remotely sensed sea surface salinity (SSS) with which to infer salinity on the observation-poor Russian side of the Arctic Ocean in future studies.

This paper is structured as follows. Section 2 will detail the data used from each product: satellite observations, ocean model simulations, and *in situ* measurements. Section

3 provides research results followed by a related discussion in Section 4. Section 5 will summarize our conclusions of this study.

3.2 Observations and Models

We used a multiple-product analysis to evaluate salinity comparisons between *in situ* observations, satellite missions, and ocean models. Our study covers January 2012 to December 2017 and matches the availability of all salinity products used in this study. There are inherent differences between products on temporal and spatial scales. While satellites can only observe the top few centimeters of the ocean, measurements from profiling instruments stabilize between a depth of 2 m, and ocean models typically start estimations at a 5 m depth. Vertical layers varied between ocean models and were therefore linearly interpolated to the depths of *in situ* observations.

The liquid FWC calculation quantifies the vertically integrated salinity anomaly from a particular reference salinity (S_{ref}), which in this case is 34.8 psu indicated by the mean of the Arctic Ocean and commonly used in other studies (Haine et al., 2015, de Steur et al., 2013; Aagaard & Carmack, 1989). Following Carmack et al. (2008), Fuentes-Franco & Koenigk (2019), and Dewey et al. (2017), we calculate integrated liquid FWC (m) from salinity measurements and estimations using the equation:

$$\text{FWC} = \int_{z=500m}^{z=5m} \frac{S_{ref} - S(z)}{S_{ref}} dz \qquad (3.1)$$

where S(z) indicates the salinity (psu) versus depth z. We integrate FWC from 5 m, based on the initial depth available from all models to 500 m depth to encompass the important components of the upper Arctic Ocean.

A. Observations

A.1 Satellite Data

We use three sensor products that rely on passive microwave radiometry to observe oceanic parameters on the sea surface. The Soil Moisture and Ocean Salinity (SMOS) Version 3.1 SSS product produced at the Barcelona Expert Center (BEC) is especially useful in that it was specifically designed to measure ocean surface salinity in the Arctic region. The product has a spatial resolution of 25 km and uses an Equal-Area Scalable Earth (EASE)–Grid 2.0 with a temporal resolution of 3 days spanning from 2011–2019. A later mission, the Soil Moisture Active Passive (SMAP), has provided data since 2015 and is available via the Physical Oceanography Distributed Active Archive (PO.DAAC). This 0.25° × 0.25° gridded product is based on the latest version 4.0 data from Remote Sensing Systems (RSS) Level 3 SSS, including 8-day running means (Meissner et al., 2021; Meissner et al., 2018). The latest version includes higher coastal resolutions and a sea-ice mask algorithm reliant on RSS AMSR– 2–sea–maps. The third satellite-based product used in this research is the Multi-Mission Optimally Interpolated Sea Surface Salinity (OISSS) Level 4 V1.0 (Melnichenko et al., 2021). This dataset was produced by the International Pacific Research Center (IPRC), University of Hawaii at Manoa, in association with RSS, Santa Rosa, California. Data combines SMOS, SMAP, and Aquarius/SAC-D mission observations on a 0.25° × 0.25° spatial grid with a 4-day temporal resolution using optimal interpolation and is available on the PO.DAAC data portal from 28 August 2011 to present (Melnichenko et al., 2014; Melnichenko et al., 2016).

A.2 IN SITU MEASUREMENTS

The Office of Naval Research sponsored Seasonal Ice Zone Reconnaissance Surveys (SIZRS) have been conducted since 2012 by the University of Washington Polar Science Center onboard US Coast Guard C–130 aircraft to create ocean and atmosphere sections across the Beaufort Sea seasonal ice zone (SIZ) (Morison et al., 2012). The sections are created once a month during the summer melt season, typically June—October. Ocean stations are located at each degree of latitude along the 150°W longitude line from 72°N to 76°N or beyond the ice edge, whichever is farther north. Conductivity–Temperature–Depth (CTD) and current profiles are made using Sippican/Tsurumi–Seiki (TSK) Aircraft eXpendable CTDs (AXCTD) and Sippican Aircraft eXpendable Current Profilers (AXCP) that are dropped in open water or through leads in the sea ice and transmit profile data in real time to the aircraft's antenna for recording onboard.

The Beaufort Gyre Exploration Project (BGP) is based at the WHOI in collaboration with researchers from Fisheries and Oceans Canada at the Institute of Ocean Sciences. Data have been collected using buoys and moorings since 2003. For this study, we use hydrographic profiles collected by annual CTD surveys in the BG region (Figure 3.1). Locations of the CTD casts were not uniform in the BG boundary but were consistently taken along the 150°W longitude (purple line), which we use for transect average comparisons.

The Met Office Hadley Center "EN" series global objective analysis product's most recent version 4.2.1 (EN4) provides monthly ocean temperature and salinity profiles with objective analyses and uncertainty estimates since 1900 (Good et al., 2013). EN4 salinity data relies on observations from Argo floats, Arctic Synoptic Basinwide Oceanography,

Global temperature and salinity profile program, and the world ocean database. Salinity profiles are available on uniform 1° horizontal resolutions with 42 depth levels beginning at a 5 m depth.

B. Ocean Model Simulations and Reanalysis Products

We used numerous ocean model simulations and reanalysis products to compare among their different base models, spatiotemporal resolutions, and assimilation methods, of which summaries are provided in Table 3.1.

The first model used in this study was the National Aeronautics and Space Administration's (NASA) Estimating the Circulation and Climate of the Ocean (ECCO): version 4, release 4 (v4r4) modeling system (Fukumori et al. 2021; Forget et al 2015). ECCOv4r4 uses a Lat–Lon–Cap 90 (LLC90) grid with varying horizontal resolutions between 110-km at mid-latitudes and 22-km in polar regions. ECCOv4r4 provided daily salinity data from January 1992 to December 2017 (*ECCO Consortium; accessed on 22 Feb 2021*).

The Marginal Ice Zone Modeling and Assimilation System (MIZMAS) developed by the Applied Physics Laboratory Polar Science Center (APL/PSC) produces 3–D daily salinity estimates starting at a 2.5 m depth and horizontal resolutions to about 20 km (Zhang & Rothrock, 2003). Reanalysis data from NCEP/NCAR is incorporated into the atmospheric forcing, to drive the seven ensemble predictions (Zhang et al., 2013; Kalnay et al., 1996). Further information regarding the MIZMAS ice- ocean model is detailed by Zhang et al. (2016) in conjunction with other product analyses. We obtained MIZMAS data from PSC for 2012–2017 for the Pacific Arctic Ocean region.

The Hybrid Coordinate Ocean Model (HYCOM) sponsored by the National Ocean Partnership Program (NOPP) is coupled with the Los Alamos Sea Ice model (CICE), which provides SSS simulations at a 1/12° global spatial resolution (Hunke & Lipscomb, 2008; Chassignet et al., 2009). Daily data is processed by averaging 12-hourly data and computes real-time simulations and forecast verification statistics of oceanic, sea ice, and atmospheric conditions. Atmospheric forcing is provided by the Fleet Numerical Meteorology and Oceanography Center 3-hourly 0.281° Navy Global Environmental Model.

We use monthly salinity data provided by the European Centre for Medium-Range Weather Forecasts (ECMWF) through the Ocean Reanalysis System's version 5 (ORAS5), which uses the Nucleus for European Modeling of the Ocean (NEMOv3.4) for its ocean model coupled with a sea ice model (Zuo et al., 2019). This version consists of eddy-permitting 1/4° horizontal resolution with 75 vertically stratified layers and is available via the Integrated Climate Data Center (ICDC) at the University of Hamburg. ORAS5 derived its forcing fields from ERA–Interim, an atmospheric reanalysis, until 2015 (Zuo et al., 2019). The post–2015 reanalysis product uses revised CORE bulk formulas and wave forcing from the ECMWF Numerical Weather Prediction (NWP) model (Breivik et al., 2015; Large & Yeager, 2019).

GLORYS12 Version 1 is a global ocean eddy-resolving reanalysis product produced by Mercator Ocean International and based on the Copernicus Marine Service (CMEMS) forecasting system. Like ORAS5, the model constituent of GLORYS12 uses the NEMO platform driven at the surface by ECMWF ERA–Interim atmospheric

reanalysis. Salinity data was provided daily from 1993–2019 at a 1/12° spatial resolution with 50 standard vertical layers starting at 0.5 m (Verezemskaya et al., 2021).

3.3 *RESULTS*

A. SEA SURFACE SALINITY

The Arctic Ocean serves as a connection between the less saline North Pacific Ocean and the more saline North Atlantic Ocean, and these contrasting salinity characteristics determine the dominant structure of the Arctic Ocean FWC. To examine all products, including the open–water surface restricted remote sensing observations, we first assessed SSS averaged over September 2015 (Figure 3.2), the month when minimum sea ice extent typically occurs (Boé et al., 2009). The BG region, as an area of interest for this study, was outlined in a black box. Overall, the salinity values between observations and estimations agree on large spatial scales. For example, high salinities are prominent on the North Atlantic side of the Arctic Ocean extending from the Nordic Sea, compared to the lower salinities on the North Pacific side owing to the relatively fresh inflow of Pacific Water through the Bering Strait. Fresher waters observed over the Russian continental shelf are near the discharge regions of major Russian rivers, i.e., the Ob, Yenisey, and Lena rivers. However, the local salinity details can be quite different among the products. In particular, local salinity variances between models are apparent in the western part of the Kara Sea, the Canadian Archipelago, the coastal edges of Greenland, and notably in the BG.

While all satellite SSS measurements are restricted to the open-water regions between the coast and ice edge, SMOS provides higher coverage of data in the Arctic

Ocean com- pared to SMAP or OISSS, especially in the Amerasian Basin (Figure 3.2a–c). The EN4 data and models resolve salinities close to Arctic Ocean coastlines, and with the exception of ECCO and MIZMAS, extend even into the Ob River channel. MIZMAS data provided is tuned for and restricted to the Canadian Basin. Low salinity in MIZMAS extends throughout the BG region and across the northern Chukchi Sea to the East Siberian Sea, which is not as pronounced in other products. The lower salinity observed in MIZMAS can potentially be attributed to calibration with SIZ hydrographic data and incorporation of floe size distributions in the model. EN4 has the largest horizontal resolution gridded at 1 degree. Therefore, the interpolation of SSS is not as refined as the salinity in the ocean models. Modeling constituents are similar between ORAS5 and GLORYS12 reanalysis products, but GLORYS12 illustrates more saline waters than ORAS5 near the pole, in the Canadian Archipelago, and in the Canadian Basin.

While all satellite SSS measurements are restricted to the open-water regions between the coast and ice edge, SMOS provides higher coverage of data in the Arctic Ocean compared to SMAP or OISSS, especially in the Amerasian Basin (Figure 3.2a–c). The EN4 data and models resolve salinities close to Arctic Ocean coastlines, and with the exception of ECCO and MIZMAS, extend even into the Ob River channel. MIZMAS data provided is tuned for and restricted to the Canadian Basin. Low salinity in MIZMAS extends throughout the BG region and across the northern Chukchi Sea to the East Siberian Sea, which is not as pronounced in other products. The lower salinity observed in MIZMAS can potentially be attributed to calibration with SIZ hydrographic data and incorporation of floe size distributions in the model. EN4 has the largest horizontal resolution gridded at 1 degree. Therefore, the interpolation of SSS is not as refined as the salinity in the ocean

models. Modeling constituents are similar between ORAS5 and GLORYS12 reanalysis products, but GLORYS12 illustrates more saline waters than ORAS5 near the pole, in the Canadian Archipelago, and in the Canadian Basin.

SSS in the BG Region is further emphasized in Figure 3.3, which provides evidence of distinctive regional salinity differences between the products. Overall, the products show relatively lower salinity in the central and eastern portions of the outlined BG region and more saline waters near the southwest portion, where the North Pacific inflow is near the surface. Satellite observations are especially limited in the northeast BG region (Figure 3.2a–c). HYCOM and MIZMAS illustrate band-type patterns of alternating lower and higher salinity values between latitudes, in contrast to other products that show gradual freshening towards the center of the BG. Compared with other models, MIZMAS has the lowest salinity at the mouth of the Mackenzie River and along the Alaskan coast. Interpolation of EN4 produces a more homogeneous appearance of lower salinity throughout the BG area. As with EN4, ORAS5 contains a large span of low salinity in the BG, but with more variations at smaller spatial scales. The GLORYS12 product had the highest salinity in September 2015 throughout the BG region.

SIZRS and BGP have examined salinity and freshwater conditions in the BG using a multitude of *in situ* techniques, with the most persistent repeat sections conducted along 150°W longitude. Therefore, to further compare the salinity in the BG, we refined our analysis to a transect average at the BG region's center longitude (150°W, 70.5°N–80.5°N) (Figure 3.4). Transect averages of SIZRS salinity show consistent annual patterns in which peaks occur around May and decrease to a minimum during July or August. SIZRS contains a few points that are much lower than in other years, such as July of 2012 and

2015. In Figure 3.4, SSS provided by BGP CTD casts denote the average date that data were collected along the transect during each annual expedition. BGP closely matched SIZRS, with the exception of 2014 and 2015, where differences were greater than 1, perhaps due to differences in the timing of the transects. Satellite-derived salinities below 15 psu were excluded due to possible sea ice contamination that could confuse product comparisons. Satellites showed the most drastic variations in salinity, likely due to variation of data coverage along 150°W. In general, SMOS and SMAP related to averaged SSS of the *in situ* and EN4 product, with most values within 1 psu while OISSS was more variable on shorter timescales.

Transect averages of SSS from the ocean models were comparable to the EN4 data in the sense that peaks occur before summer, around April, and the SSS minimum occurs abruptly towards July (Figure 3.4). However, the average differences of the model SSS from EN4 ranged between 0.35 psu (ORAS) to 2.3 psu (GLORYS12). The EN4 data shows its minimum (maximum) SSS during autumn (spring), reaching its largest magnitude at 25.5 psu (29.71 psu). MIZMAS showed a wide range of seasonal SSS fluctuations, with its lowest salinity in autumn 2012 around 25.2 psu and highest salinity near 31.45 psu in 2016. MIZMAS salinity values were comparable to GLORYS12 during winter months, then abruptly decreased by summer, closer to *in situ* and satellite products. ECCO estimated intermediate ranges between 27.84 psu and 30.28 psu throughout the time range. GLORYS12 and ORAS5 showed earlier minimum SSS dates in September at 31 psu and 29.3 psu, respectively, whereas other models reached a minimum shortly after October. GLORYS12 reached consistently high SSS maximums near 31 psu.

The *in situ* data from BGP and SIZRS were not continuous. Therefore, we matched the products to the specific times and latitude of 126 SIZRS AXCTD, drops made between 2012 and 2017 along the 150°W transect. We collocated remote sensing and model estimates of SSS to the date and latitude of each AXCTD drop. SIZRS measurements began at shallow depths but showed near-surface transients. Consequently, we compared SIZRS measurements at 2m depth to satellites that measure salinity within the top few centimeters of the surface. The shallowest depth layer of many models begins at 5m and therefore was compared to SIZRS at 5 m. Product observations and estimates were available at each of the 126 SIZRS drops except for SMOS, SMAP, and BGP, which had 61, 27, and 32 samples at near-matching locations and times.

Figure 3.5 shows SSS comparisons between SIZRS and other products at each SIZRS drop (Figure 3.5). SIZRS salinity, at both a 2 m and 5 m, ranged from 23 psu to just below 31 psu. Satellites show a larger range of salinity compared to that of SIZRS at 2 m, from just below 21 psu to about 33 psu. The spread of SSS was greatest with satellite products compared to ocean models and other *in situ* observations. ECCO and HYCOM (Figure 3.5b) share higher salinity properties with values more than 2.1 psu higher than the *in situ* SSS on average as opposed to MIZMAS with SSS within 0.27 psu difference from SIZRS. Amongst all other products, EN4 and BGP averages were closest to SIZRS, with the exception of ORAS5 with a bias within 0.1 psu. BGP data had fewer distinct outliers than EN4 (Figure 3.5d). Due to the lack of similar data available at the same temporal range, BGP had a lower sample size (32 samples) than SIZRS but showed a higher correlation than EN4. We provide further quantitative information regarding the correlation

coefficients of SSS between products and their respective p–values at each SIZRS drop (Table 3.2).

The average salinity difference from *in situ* to satellites was higher in SMOS than in SMAP. SMAP had a stronger correlation to SIZRS at 2 m, but both satellites' salinity data had higher p–values, implying they are not statistically significant (p–values > 0.05). The ocean models, ECCO, HYCOM, and GLORYS12 similarly yielded higher salinities (greater than 2.2 higher average psu) and moderate correlations (correlation coefficients < 0.6) with *in situ* observations in the BG region. ORAS5 had the salinities closest to SIZRS, within 0.06 psu difference on average, and the strongest correlation with SIZRS at 0.612.

The distribution of SSS differences of products minus SIZRS measurements were further analyzed through histograms, illustrated in Figure 3.6, to observe the distribution of product salinities from SIZR salinities at each SIZRS drop. The frequency of samples was distributed in 0.2 psu bins.

Satellite products (Figure 3.6a,b) showed departures from SIZRS salinities that vary widely. SMOS SSS data distributions are similar to SMAP, but with the majority of departures from SIZRS salinity being positive and a few outliers of large negative salinity differences. Salinity differences of SMOS relative to SIZRS are generally 1 psu higher than those of SMAP (Table 3.3). However, SMAP's bias was overall negative, which can be linked to the few large negative outliers (Figure 3.6b). The satellite remotely sensing SSS had the largest standard deviations from SIZRS SSS compared to other products, specifically in SMOS (~2.33 psu). Their variability compared to SIZRS salinity would be a consequence of the larger overall variability of the remote sensing SSS (Figure 3.4).

BGP observations were similar to SIZRS, but like the satellite product, compared to SIZRS, BGP has fewer samples with which to make definitive conclusions. In contrast to other products, the majority of salinity values from EN4 are fresher than SIZRS, with an average bias of −0.27 psu. *In situ* products showed close relation to SIZRS in average salinity. However, EN4 had a relatively high standard deviation, and a greater root mean square deviation (RMSD) from SIZRS than BGP. The RMSD signifies the accuracy measurement between the observed salinity and the SIZRS, where an RMSD of 0 would indicate a perfect comparison fit. This helped to delineate difference extremes rather than solely focusing on the average of the estimations.

When comparing models to SIZRS, GLORYS12, HYCOM, and ECCO contain more saline values with average biases greater than 2 psu and have the largest RMSD of the ocean models at 2.89 psu, 2.73 psu, and 2.63 psu, respectively. ECCO salinity departures from SIZRS salinities have the highest standard deviation (1.47 psu) compared to the other models. HYCOM and GLORYS 12 showed the greatest average disagreement with SIZRS salinity compared to all products with a bias of about 2.50 psu and 2.44 psu, respectively. MIZMAS and ORAS5 salinity anomalies relative to SIZRS are more centered around 0 psu, with ORAS5 showing the closest comparison to SIZRS as the only ocean model indicating a fresher bias (−0.052) and a closer relation with an RMSD of 1.05.

Since the SIZRS drops differ spatially as well as temporally, we next average the data along the transect (150°W from 70.5°N–80.5°N) to show the monthly average sea surface salinities between products on a timeline basis in Figure 3.7.

Differences in product salinities from SIZRS SSS revealed monthly patterns between instruments and estimations (Figure 3.7). Satellite salinity differences from SIZRS

tended to become more saline in later months, perhaps because the initial advance of the ice edge obscured the lowest salinities near the center of the BG. This pattern also held true for the models, where early months showed lower and fresher SSS differences, as opposed to later months where the differences were heightened and typically more saline than SIZRS. Compared to ECCO and HYCOM, the salinities of MIZMAS were less than SIZRS through many of the monthly means, especially during 2014 and 2016 (Figure 3.7b). GLORYS12 and ORAS5 had common patterns of local salinity variations throughout time, but GLORYS12 consistently showed higher salinity values at about 2.3 psu on average compared to ORAS5 and 2.5 psu compared with SIZRS (Figure 3.7c). On the other hand, ORAS5 SSS fluctuated between more saline or fresher estimations than SIZRS measurements. Differences between EN4 and SIZRS monthly averages stayed between 1psu, except for June and July 2016 observations.

B. VERTICAL SALINITY STRUCTURE

The vertical structure of the upper ocean defines changes in mixed layer depth, FWC, and stratification in the BG. We analyzed salinity within the water column between 2012 and 2017 from EN4 and ocean models averaged along the 150°W BG transect between 70.5°N and 80.5°N (Figure 3.8).

We examined salinity from 5 m to 200 m to include the mixed layer, usually shallower than 55 m in the BG region, and the main part of the upper ocean halocline. Seasonality between the EN4 data and ocean models is illustrated by the declining salinities throughout the summer into autumn months. MIZMAS salinity differences be-tween the surface and 200 m were the greatest of all the models with surface salinities under 27 psu and nearly 34 psu at 200 m. ORAS5 showed the closest relationship in seasonal variations

to EN4. Contrarily, ECCO and GLORYS12 indicated the lowest vertical gradients in salinity. Also, their surface salinities during autumn, when the annual salinity is lowest, were continuously higher than other products.

To directly compare these models to SIZRS, we provide snapshots of the specific August dates of each year averaged along the 150°W transect with BGP, EN4, and model estimations to the closest temporal resolution possible, ranging from daily to monthly data (Figure 3.9). Depth profiles above 100 m show large salinity differences among the products.

The *in situ* observations from BGP (Figure 3.9a,b) and EN4 closely matched SIZRS drops, although the slope of EN4 is smoothed with depth, and the mixed layer was not as distinguishable in the ECCO salinity profiles. Of the models, ORAS5 had the closest relation to SIZRS throughout the depth profiles, whereas GLORYS12 and ECCO were consistently higher than SIZRS with depth. MIZMAS salinity difference from SIZRS salinity was greatest between depths of about 20 m to 50 m. The mixed layer depth appeared in most products around 16 m, separating the fresher waters and sea ice cover from the more saline waters below. ECCO salinity is just under 29 psu at depths less than 15–m, at which depth it increases logarithmically. GLORYS12 was similar to ECCO with higher SSS; however, its halocline is not as pronounced as other products that showed large increases in salinity around the bottom of the mixed layer depth (~20 m).

To further distinguish the salinity profile differences between products, we took the average of SIZRS, EN4, and ocean model simulations where individual SIZRS latitude measurements were taken along 150°W in the BG during each available month (Figure 3.10).

Salinity contours from SIZRS and EN4 (Figure 3.10a,b) illustrate the vertical salinity structure of monthly averages at all SIZRS drops. With small exceptions, these two *in situ* products are very similar, with low salinities (~26 psu) above 25 m and showing salinities reaching 31 psu by 60 m. ECCO and GLORYS12 showed relatively higher salinity (over 2 psu) in the surface layer, but their differences with respect to SIZRS and EN4 sharply decreased below 60 m. MIZMAS showed salinities close to *in situ* values at the surface, but higher biases occurred between the 10 m and 50 to 60 m depth layers. Unlike other models, MIZMAS simulates higher salinities with 0.5–1 psu differences below 100 m depth. ORAS5 depth-profiles are overall very similar to SIZRS and EN4 but are slightly (higher) lower in 2017 when compared to SIZRS (EN4).

Overall, the greatest differences among the products were in the upper region of the water column above a 50 m depth, a region most important when analyzing the freshwater budget in the BG region. Therefore, to inspect model comparisons between the vertical layers where we saw the highest and lowest differences, we separated comparisons between an upper region (5 m–55 m) and lower region (55 m–207 m) in Figure 3.11. Depths of products are integrated to a 207 m depth as it is the EN4 product's depth layer closest to 200 m, as distinguished in previous figures.

Statistical analyses are described in Table 3.4, including standard deviations, RMSD, and average differences (or bias) from SIZRS and EN4 products for the upper region compared to the lower region averages. Upper region averages have positive differences between the models and both SIZRS and EN4, except for ORAS5, which fluctuated between positive and negative salinity differences and had the smallest bias to

both *in situ* products. However, for salinity differences in the lower regions, GLORYS12 data was closest to SIZRS, and MIZMAS data were closest to EN4.

Table 3.4 also highlights that the discrepancy between products was more concentrated in the upper region than the lower. The largest RMSD, representing a higher magnitude of errors, occurs with GLORYS12 in the upper region for both SIZRS and EN4, and in MIZMAS when comparing the lower region of both *in situ* products. This stresses the importance of analyzing salinity features in the upper region of the BG and the Arctic Ocean when evaluating critical characteristics or changes in the halocline structure and its influences, and the oceans' vertical circulation dynamics.

C. Freshwater Content

FWC as a measure of depth-integrated salinity anomaly per unit area indicates where FW is accumulating or decreasing in the Arctic Ocean. Different assimilation techniques and forcing between models influence the salinity estimates and FWC in turn. We interpolated salinity anomaly relative to 34.8 psu of each model into 1° × 1° grided data and calculated the accumulated depth FWC (Equation (3.1)) across the Arctic Ocean between 5 m and 500 m, averaged from 2012–2017 as seen in Figure 3.12.

As expected, low FWC comprises the more saline regions on the Atlantic side of the Arctic Ocean, whereas the Canadian Basin and Canadian Archipelago contain more FW for all models, especially in the BG region and the Davis Strait. The peak FWC was lowest in ECCO, between 16 m and 17 m on average between 2012–2017 (Figure 3.13b). MIZMAS and GLORYS12 maximum FWC was slightly greater than 18 m in the BG, whereas EN4 and ORAS5 showed at least 20 m of FWC in the Arctic Ocean during that

period. EN4 showed between 11 m and 12 m of FWC in the Davis Strait region. ECCO and GLORYS12 showed moderate levels of FWC in the Davis Strait, whereas ORAS5 did not. ORAS5 agreed well with the SIZRS FWC of 22.09 m averaged along the 150°W and integrated from 5.02 m to 435.65 m, its minimum sampled depth.

We next compared the box–accumulated FWC (km^3) of the Arctic Ocean deep basin, which encompassed areas with depths greater than 500 m, and the BG region to analyze the seasonal and interannual oscillations between 2012–2017 for each model (Figure 3.13). The FWC from MIZMAS was restricted between 180°W–80°W in the Arctic Ocean due to the geographic limits of the model; therefore, we excluded it from the Arctic Basin FWC calculations.

FWC seasonality is induced by runoff, precipitation, sea ice melt, or growth combined with seasonal wind-driven circulation changes. The ocean models expressed a switch from mostly negative to mostly positive anomalies by 2015 in the Arctic Basin and 2016 in the BG. Overall trends of FWC were not statistically significant during 2012–2017. Seasonal variations of FWC from the models were relatively consistent. Averages and standard deviations of the FWC time series for the Arctic Basin and BG are given in Table 3.5.

From 2003–2009, during the transition to a more cyclonic mode, Morison et al. (Morison et al. 2021) SI–7 (Freshwater Content Rate–of–Change Comparisons) found the total freshwater of the deep Arctic Ocean increased to 804 $km^3\ year^{-1}$ or $0.0255 \times 10^4\ m^3\ s^{-1}$ = 0.0255 Sverdrup, almost equal to the rate of sea ice loss but much smaller than the difference between BG and Eurasian Basin freshwater change. The BG minimum FWC in 2013 from all products except for GLORYS12 coincides with Proshutinsky et al. (2019).

Perhaps the most interesting feature was the behavior of EN4 Beaufort Gyre FWC in 2016, during which it rose out of phase with the models in the first part of the year and then, still out of phase, dropped during the summer. At the same time, the EN4 Arctic Ocean FWC remained unusually constant over much of 2016, suggesting a redistribution of freshwater from outside the BG into the BG in the winter and spring of 2016. Overall, the products express a greater range of differences in average FWC, greater than the seasonal variations.

3.4 DISCUSSION

A. SEA SURFACE SALINITY

We used SMOS produced by BEC, which, as Xie et al. (2019) shows, has a lower bias relative to *in situ* data in the BG area than alternative SMOS products. Despite having a lower temporal and spatial resolution than SMOS, SMAP showed more promising outcomes than SMOS along the BG 150°W transect, where it has a lower salinity bias than SIZRS data (Fournier et al., 2019; Bao et al., 2019; Bingham et al., 2020). Bingham et al. (2020) found higher bias in SMOS BEC than in SMAP and EN4. Fournier et al. (2019) said that SMAP RSS and SMOS BEC had lower RMSD relative to *in situ* than other SMAP and SMOS products. Among the satellite products, SMOS BEC had the lowest positive bias of (0.08). When comparing missions between 60°S–60°N, Bao et al. (2019) found a higher bias in SMOS (−0.113) than SMAP (−0.078). Nonetheless, satellites show small SSS correlation values compared with SIZRS observations, most likely due to the small sample size and low spatial coverage obtained.

All ocean models, except for ORAS5 and MIZMAS, have transect averages SSS greater than EN4. Carton et al. (2019) compared ORAS5 and earlier versions of ECCO (version 4, release 3) and EN4 (version 1.1) on a global scale as well as parts of the Arctic Ocean. Their results confirm closer comparisons between salinity estimations from ORAS5 and EN4 compared to ECCO and EN4. Through the analysis of transect averaged SSS, MIZMAS demonstrated the largest range of seasonal salinity fluctuations with higher winter values comparable to GLORYS12 and near equivalent summer month salinities to *in situ* products. MIZMAS forcing also incorporated monthly climatology of freshwater from river discharge into the Arctic Ocean and Bering Strait, to which we can attribute the lower salinity values viewed in spatial maps near the mouth of the Mackenzie River, the Canadian Archipelago, and the Chukchi Sea (2010).

Compared to SIZRS data, ORAS5 had the highest correlation coefficient (0.612), suggesting a higher accuracy in salinity estimates in the BG despite having a lower temporal resolution than other models. ORAS5 and ECCO shared the same ERA-Interim surface forcing fields and surface flux bias correction (Carton et al., 2019). Yet, these two products showed differing distributions in histograms of salinity differences from SIZRS, where the direction of outliers for ORAS5 (ECCO) was negative (positive). ORAS5 and GLORYS12 share the same NEMO model component, but GLORYS12 produced correlations coefficients (0.406) and higher bias (2.437 psu) relative to SIZRS, signifying that ORAS5 is moderately correlated to *in situ* data and GLORYS12 is not. When analyzing the monthly averages of salinity differences between products and SIZRS along the BG transect, most models tend to overestimate salinity near the end of each year.

This study emphasizes the importance of SSS product comparisons between satellite data and ocean model estimations in an area where *in situ* observations are abundant compared to the observation-poor Arctic regions like the Russian shelf. While satellite observations are restricted by the extent of sea ice in the Arctic Ocean, their averaged annual coverage extends over the East Siberian shelf (Figure 3.2). The bias and regional discrepancies shown by these products help to discern their advantages and disadvantages when analyzed in other regions of the Arctic Ocean. The scarcity of *in situ* measurements in portions of the Arctic Ocean that contribute to the overall analysis of the Arctic Ocean revealed the significance of improved remote sensing techniques and ocean model development.

B. Vertical Salinity Structure

Depth profile analysis in this study highlights the variability at depths shallower than 55 m and between 55 and 207 m for deeper layer comparisons. Past research has commonly defined the mixed layer depth as the depth where the density increase above the mixed layer reaches 0.25 kg/m^3, which is consistently deeper than 10 m in the BG and can reach 30 m in the winter (Proshutinsky et al., 2019; Peralta-Ferriz et al., 2015; Cole et al., 2019). In contrast, Jackson et al. (2012) emphasize that the alteration of the upper 100 m of the Canadian Basin has been influenced by heightened temperatures and freshwater levels where the mixed layer depth during winter months shoaled from 50 m prior to the 1970s to around 24 m more recently.

Seasonality of salinity-in-depth profiles, where the melting of sea ice during the summer causes surface freshening and stronger salinity gradients, is seen best in EN4 and ORAS5 compared to GLORYS12. ECCO shows a similar structure to GLORYS12; how-

ever, ECCO retains slightly fresher surface waters longer each year. Except for ORAS5, comparisons among the other three models varied, but they all maintained slightly higher salinities with depth compared to SIZRS. GLORYS12 (MIZMAS) had the highest bias in the upper (lower) region compared to SIZRS and EN4.

C. Freshwater Content

FWC analysis is vital to the understanding of the distribution and key role of salinity in the Arctic Ocean. Serreze et al. (2006) analyzed Arctic FWC, finding less in the central Arctic and more accumulating in the Eurasian basin, such as the Kara and Laptev Seas. Wang et al. (2019b) found that the FWC in the Canadian basin increased upwards of 5 m between 2004 and 2009, with a less significant difference between 2009 and 2015. The BG region accounts for about a fourth of the total liquid FWC, with a current peak between ~17 m for ECCO to ~21 m shown in EN4.

FWC from model estimations in our study also agreed with Proshutinsky et al. (2009) in that the BG seasonal changes of total FWC accounted for about 5% of its total volume, even for the current period, which they attribute to atmospheric circulation. EN4 estimated the FWC of the BG to be slightly higher than 22×10^3 km^3 during 2017, whereas the other models except for ORAS5 (just shy of 20×10^3 km^3) estimated lower than 18×10^3 km^3 throughout the timeline. The largest seasonal change of FWC from the EN4 data occurred near the end of 2017, decreasing at least 4.1×10^3 km^3, attributing to a departure of more than 3×10^3 km^3 from its monthly BG climatologies. The 2012 FWC anomalies in Figure 3.13c,d for the BG are slightly smaller, but similar to estimates shown by Rabe et al. (2014). However, these slight differences from Rabe et al. (2014) can be credited to the use of a different model and their reference salinity of 35 psu instead of our 34.8 psu.

The products do not show as great a seasonal difference in FWC as in their annual averages in the Arctic basin. The overall trend of FWC for the Arctic Ocean had relatively stabilized in the decade following 2010, between the relative balance of the BG freshening and the reduction of FW in the rest of the Arctic Ocean, especially in the Eurasian Basin, which Morison et al. (2021) attributes over the long term to the changes in surface circulation governed by the positive shift of the Arctic Oscillation in recent decades (Solomon et al., 2021).

3.5 CONCLUSION

This study primarily focuses on salinity comparisons between numerous salinity products commonly used in the Arctic Ocean and sub-Arctic seas. Large-scale SSS characteristics between these products are similar. However, important regions like the BG that provide insight into the state of the changing Arctic Ocean in a warming climate, show concerning dissimilarities. Present research has shown that over the past three decades, the Arctic Ocean surface circulation has been dominated by a more dominant cyclonic mode associated with higher average vorticity, advection of more Eurasian runoff into the Canadian Basin, enhanced divergence and thinning of the ice cover, and in principle more FW release (Morison et al., 2021). The changes we see in the Beaufort Gyre in recent years are embedded in the larger and longer scale change. Therefore, we have conducted a model–observation analysis of surface and depth profiles of salinity variations from 2012 to 2017 in the BG area. The satellite missions of SMOS, SMAP, and OISSS, combined with the Arctic Ocean model simulations from ECCO, MIZMAS, HYCOM, ORAS5, and GLORYS12, show a range of biases when compared to the *in situ* products of SIZRS surveys, BGP CTD casts, and the EN4 data.

In the BG area, SMAP shows more promising SSS comparisons to *in situ* data than SMOS. Ocean models evaluated in this study, except for ORAS5, tend to overestimate *in situ* SSS, with the largest positive bias represented by HYCOM at about 2.5 psu. ORAS5 provides the strongest positive correlation coefficient (0.612) and lowest salinity bias relative to observations. GLORYS12 salinity depth profiles above 55 m differ most from *in situ* data but are closest to SIZRS when comparing salinities between the 55 m and 207 m region. From 55 m to 207 m, MIZMAS shows higher biases relative to observations. FWC trends in the Arctic basin and the BG were insignificant between 2012 and 2017. The seasonal FWC differences between ocean models and EN4 were not as great as when comparing their averaged annual FWC. Future sea ice melt will contribute even more to the accumulation of FW to the BG that can be eventually released to adjacent seas if it does not form back into sea ice the following winter.

Table 3.1 Summary of ocean model characteristics used in this study.

Product	ECCO	MIZMAS	HYCOM	ORAS5	GLORYS12
Version	Version 4 Release 4	Version 1	+CICE version 1	Version 5	Version 1 Level 4
Origin	NASA	APL/PSC	NRL Mississippi	ECMWF/ICDC	CMEMS
Horizontal Resolution	1° (mid latitudes) - 1/5° (high latitudes); LLC90 grid	1/5°; Arctic version	1/12° gridded	1/4° gridded	1/12° gridded
Temporal Resolution	Daily; Jan. 1992 – Dec. 2017	Daily; Jan. 2012 – Dec. 2017	Daily; Nov. 2011 – Present	Monthly; Jan. 1979 – Dec. 2018	Daily; Jan. 1993 – Dec. 2019
Vertical Layers	50; (first layer: 5m – 5.9km)	40; (first layer : .5m – 4.3km)	40; This study uses surface layer	75; (first layer: 0.5m – 5.9km)	50; (first layer: 0.5m – 5.7km)
Data Assimilated or constrained	SSS: Aquarius constrained; Salinity profiles: Argo floats, CTDs, APB gliders, ITP, moorings	Salinity: Polar Profiling Floats, Ice-Tethered Profilers, autonomous gliders	Performed using NCODA; Salinity: XBTs, Argo floats, moored buoys	NEMOv3.4 coupled with LIM2 sea ice model; 3DVar-FGAT	NEMO; ECMWF ERA-Interim atmospheric reanalysis
Atmospheric Forcing	high-frequency atmosphere pressure from ERA-Interim	NCEP/ NCAR reanalysis data	NAVGEM	ERA-Interim (1979 – 2015), ECMWF NWP (2015 – Present)	CMEMS high-res. Forecasting system PSY4V3

Table 3.2 Statistical analysis including the total drop average, the average difference, the correlation coefficient, and the p–value of sea surface salinity (psu) between SIZRS other salinity products at each SIZRS drop point.

Product	**Total Drop Avg. (psu)**	**Avg. Diff. (psu)**	**Correlation Coeff.**	**p-value**
SIZRS 2m/5m	26.552/26.706	-	-	-
SMOS	27.825	1.274 *	0.1283 *	0.3243 *
SMAP	26.095	–0.457 *	0.3615 *	0.0540 *
ECCO	28.973	2.267	0.3378	<.001
MIZMAS	26.959	0.261	0.5115	<.001
HYCOM	29.200	2.493	0.3808	<.001
ORAS5	26.646	–0.060	0.6120	<.001
GLORYS12	29.135	2.428	0.4055	<.001
EN4	26.426	–0.280	0.3816	<.001
BGP	26.310	–0.396	0.5060	0.0027

* Compared with SIZRS at 2 m.

Table 3.3 Median, mean, standard deviation (Std. Dev.), and Root Mean Square Deviation (RMSD) of SSS differences between products and SIZRS *in situ* data at each latitude SIZRS measurements were taken.

Product	**Median (psu)**	**Bias (psu)**	**Std. Dev. (psu)**	**RMSD**
SMOS	1.676	1.658	2.326	2.840
SMAP	0.681	–0.061	1.828	1.794
ECCO	1.998	2.183	1.474	2.630
MIZMAS	0.087	0.105	1.212	1.237
HYCOM	2.581	2.502	1.140	2.747
ORAS5	–0.046	-0.052	1.053	1.050
GLORYS12	2.443	2.437	1.132	2.685
EN4	–0.047	–0.271	1.262	1.276
BGP	0.114	0.039	0.638	0.630

Table 3.4 Standard deviation of salinity (psu) profile differences between model minus *in situ* (SIZRS and EN4) products for upper region (above 55 m depth) and lower region (below 55 m depth).

Product	**Upper SIZRS 5m–55m**			**Lower SIZRS 55m–207m**			**Upper EN4 5m–55m**			**Lower EN4 55m–207m**		
	Std. Dev.	**RMSD**	**Bias**	**Std. Dev.**	**RMSD**	**Bias**	**Std. Dev.**	**RMSD**	**Bias**	**Std. Dev.**	**RMSD**	**Bias**
ECCO	0.36	1.78	1.74	0.15	0.18	0.10	0.58	1.70	1.60	0.15	0.22	0.16
MIZMAS	0.43	0.94	0.84	0.29	0.51	0.43	0.56	0.84	0.64	0.24	0.44	0.38
ORAS5	0.28	0.28	0.05	0.12	0.15	–0.10	0.45	0.46	–0.10	0.17	0.20	–0.12
GLORYS12	0.42	2.01	1.97	0.13	0.15	–0.08	0.49	1.76	1.69	0.15	0.16	–0.06

Table 3.5 Statistical analysis of averages (avg.) and standard deviations for FWC in the Arctic Basin and the Beaufort Gyre depicted in Figure 3.13.

	2012–2017	Avg. (10^3 km^3)	Std. dev. (10^3 km^3)	Anomaly Std. dev. (10^3 km^3)
Arctic Basin	EN4	49.1	1.80	1.55
	ECCO	47.2	2.06	1.04
	ORAS5	45.5	1.34	0.658
	GLORYS12	48.8	1.24	0.418
Beaufort Gyre	EN4	19.6	0.974	0.936
	ECCO	16.1	0.834	0.588
	MIZMAS	15.0	0.651	0.423
	ORAS5	18.1	0.768	0.662
	GLORYS12	16.3	0.531	0.415

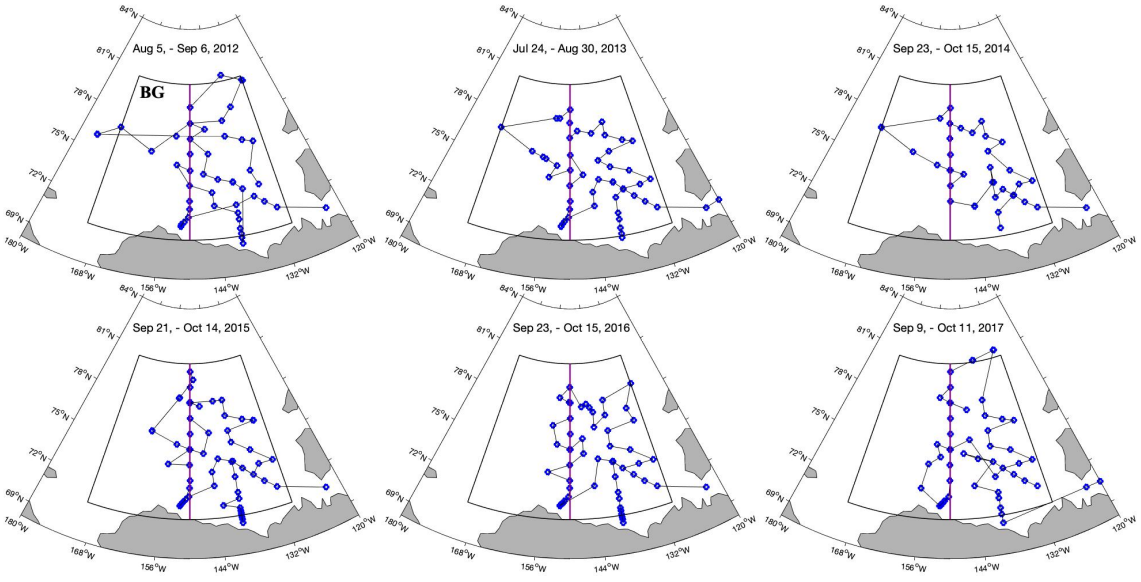

Figure 3.1 Map of the Beaufort Gyre Exploration Project (BGP) CTD casts (blue dots) from (a–f) 2012–2017 in the (black outline) Beaufort Gyre (BG). The line along 150°W delineates the transect between 70.5°N and 80.5°N.

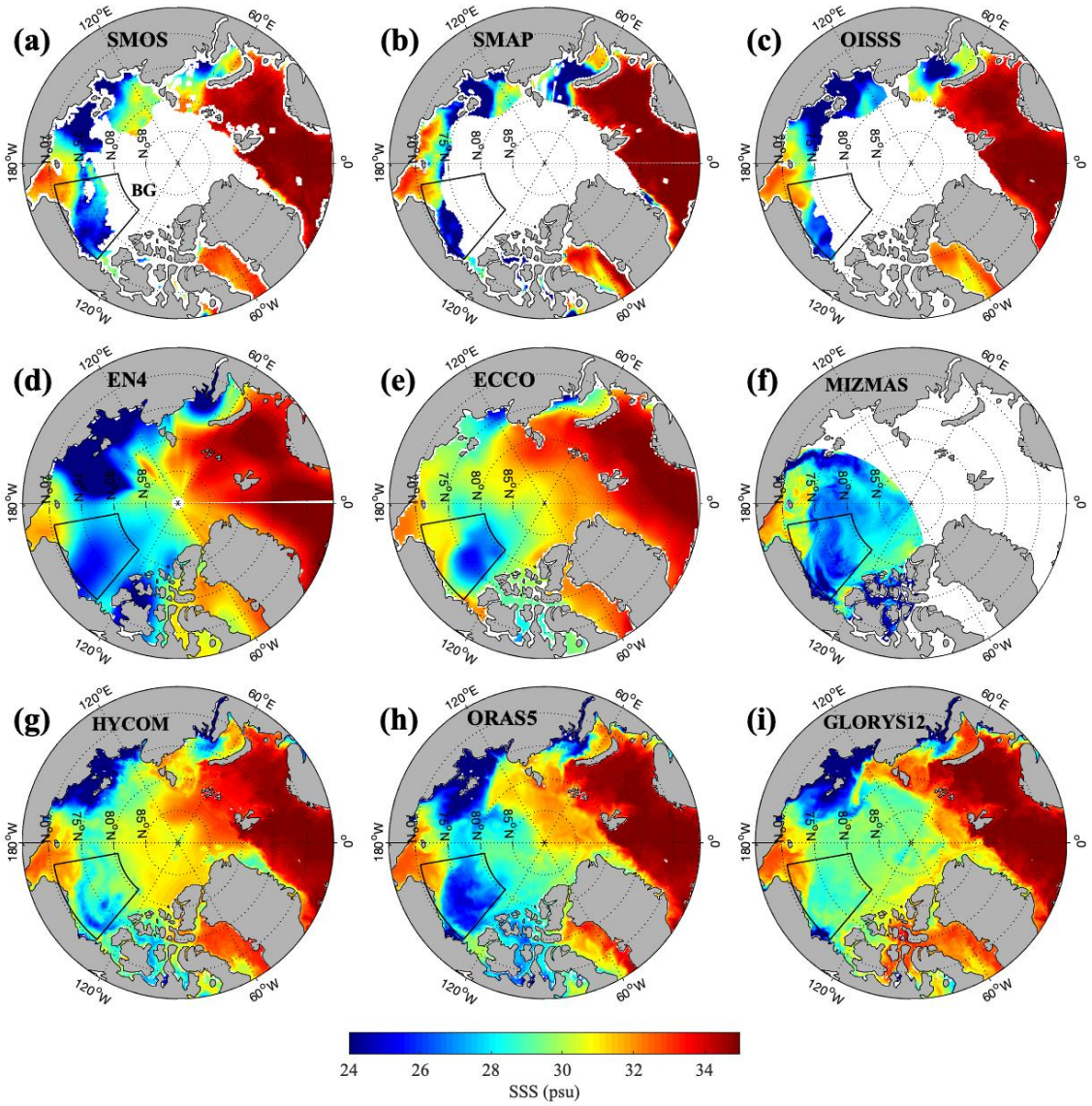

Figure 3.2 Arctic Ocean sea surface salinity (SSS) averaged over the month of September 2015 from satellites: (a) SMOS, (b) SMAP, (c) OISSS, objective analysis product: (d) EN4, and ocean model simulations: (e) ECCO, (f) MIZMAS, (g) HYCOM, (h) ORAS5, and (i) GLORYS12.

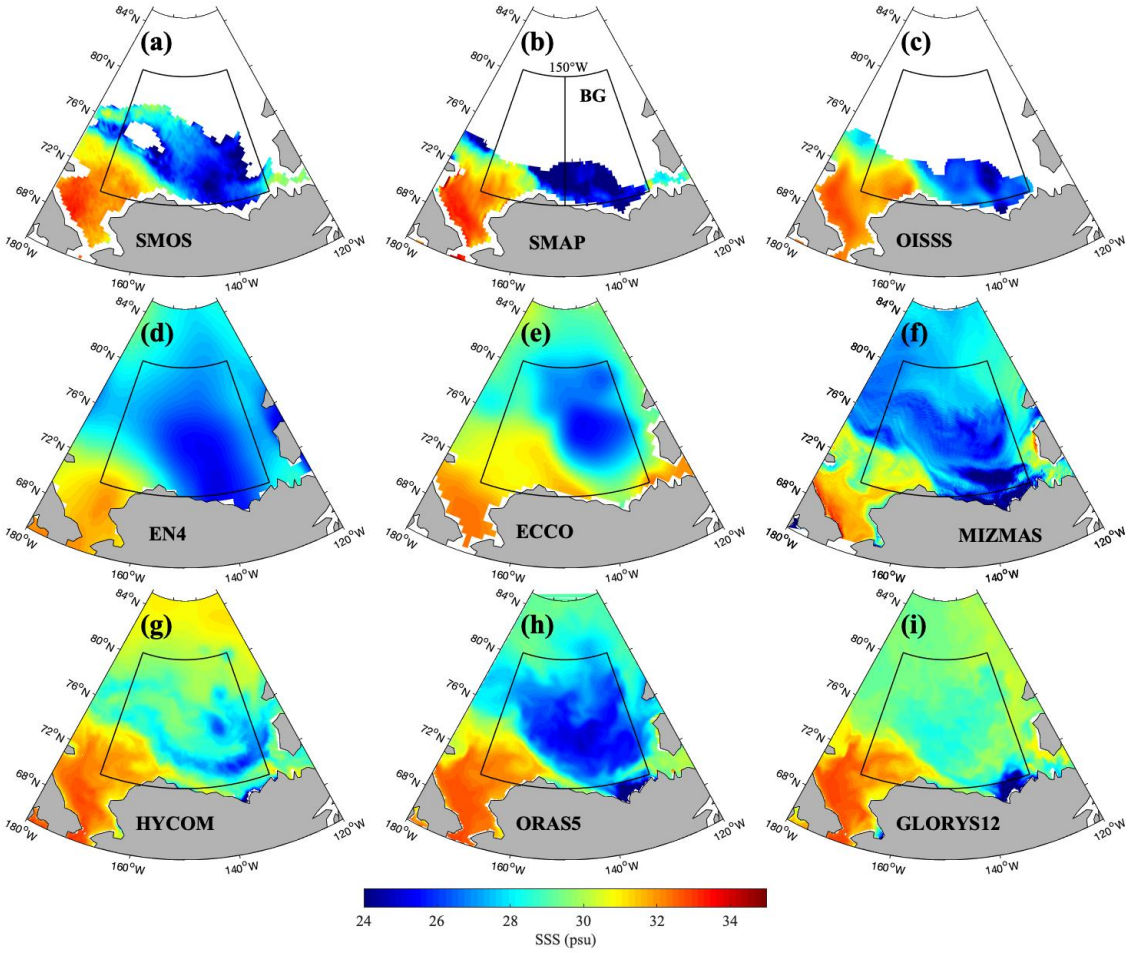

Figure 3.3 Arctic Ocean sea surface salinity (SSS) averaged over the month of September 2015 in the Beaufort Gyre (BG) region derived from satellites: (a) SMOS, (b) SMAP, (c) OISSS, objective analysis product: (d) EN4, and ocean model simulations: (e) ECCO, (f) MIZMAS, (g) HYCOM, (h) ORAS5 and (i) GLORYS12. 150°W transect is outlined for comparisons in this study.

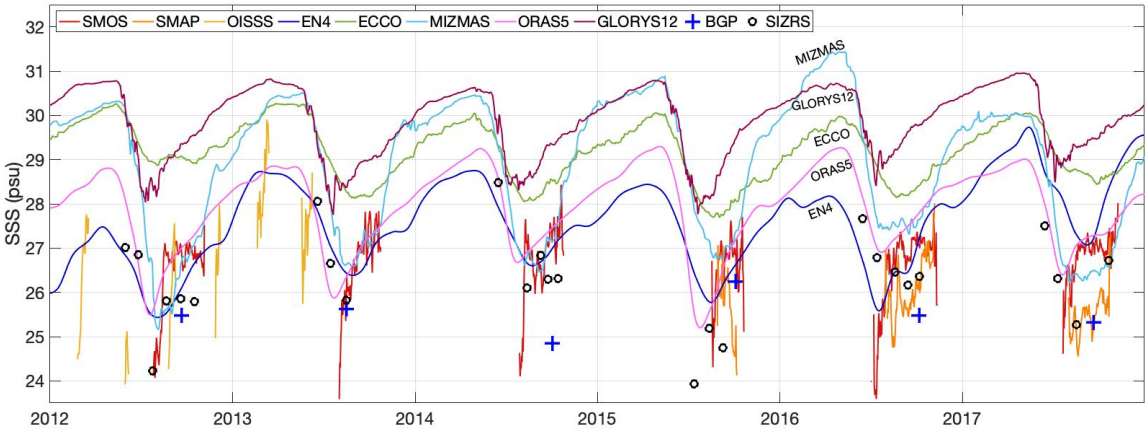

Figure 3.4 Averaged sea surface salinity (SSS) along a 150°W transect between 70.5°N–80.5°N as seen in Figure 3.1 among ocean products between January 2012–December 2017.

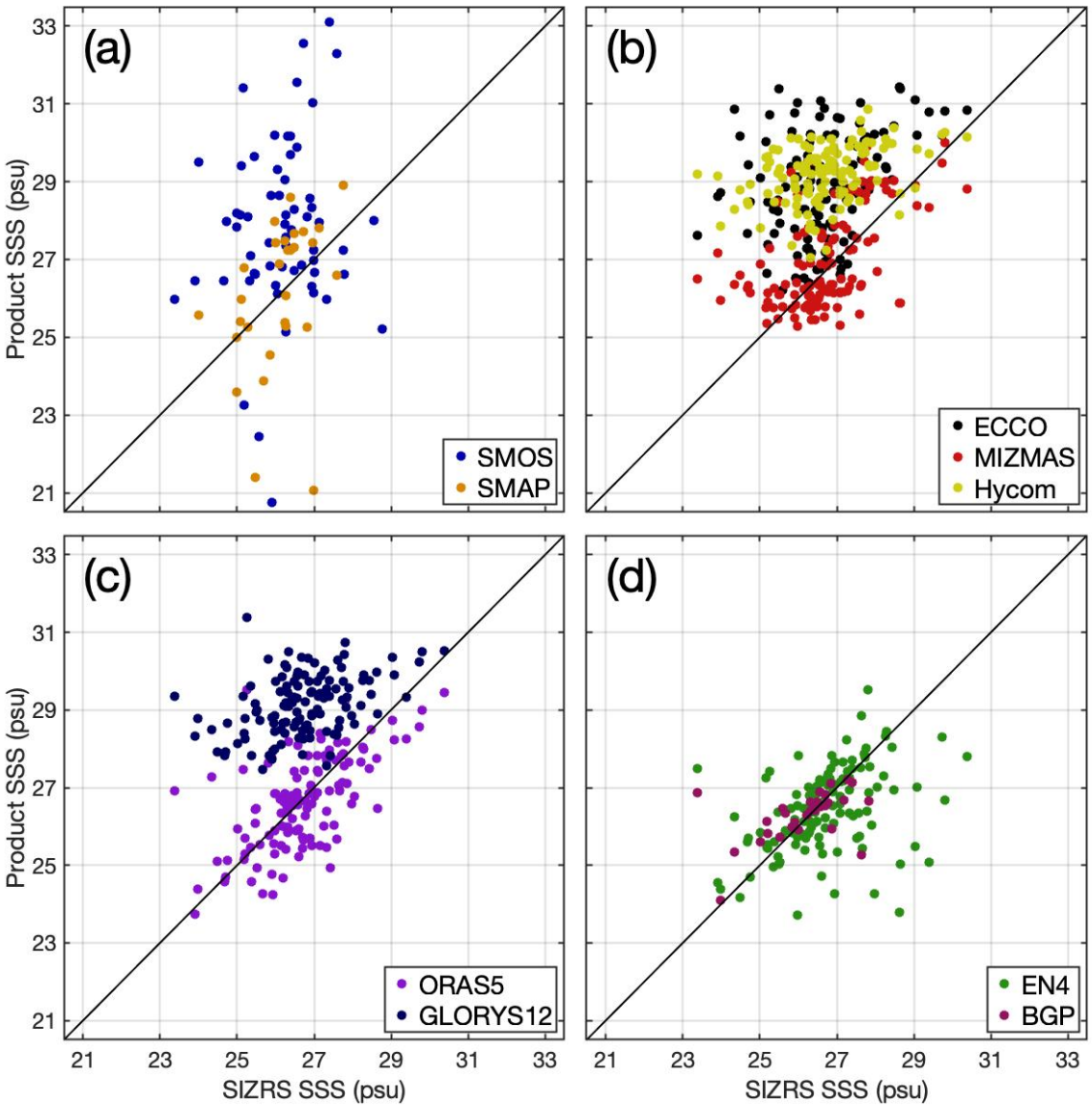

Figure 3.5 Scatter diagrams of sea surface salinity (SSS) of SIZRS (2 m) to (a) satellite missions, and of SIZRS (5 m) to (b,c) ocean model simulations, and (d) in–situ observations during SIZRS AXCTD drops. Black line signifies equivalent salinity values (psu).

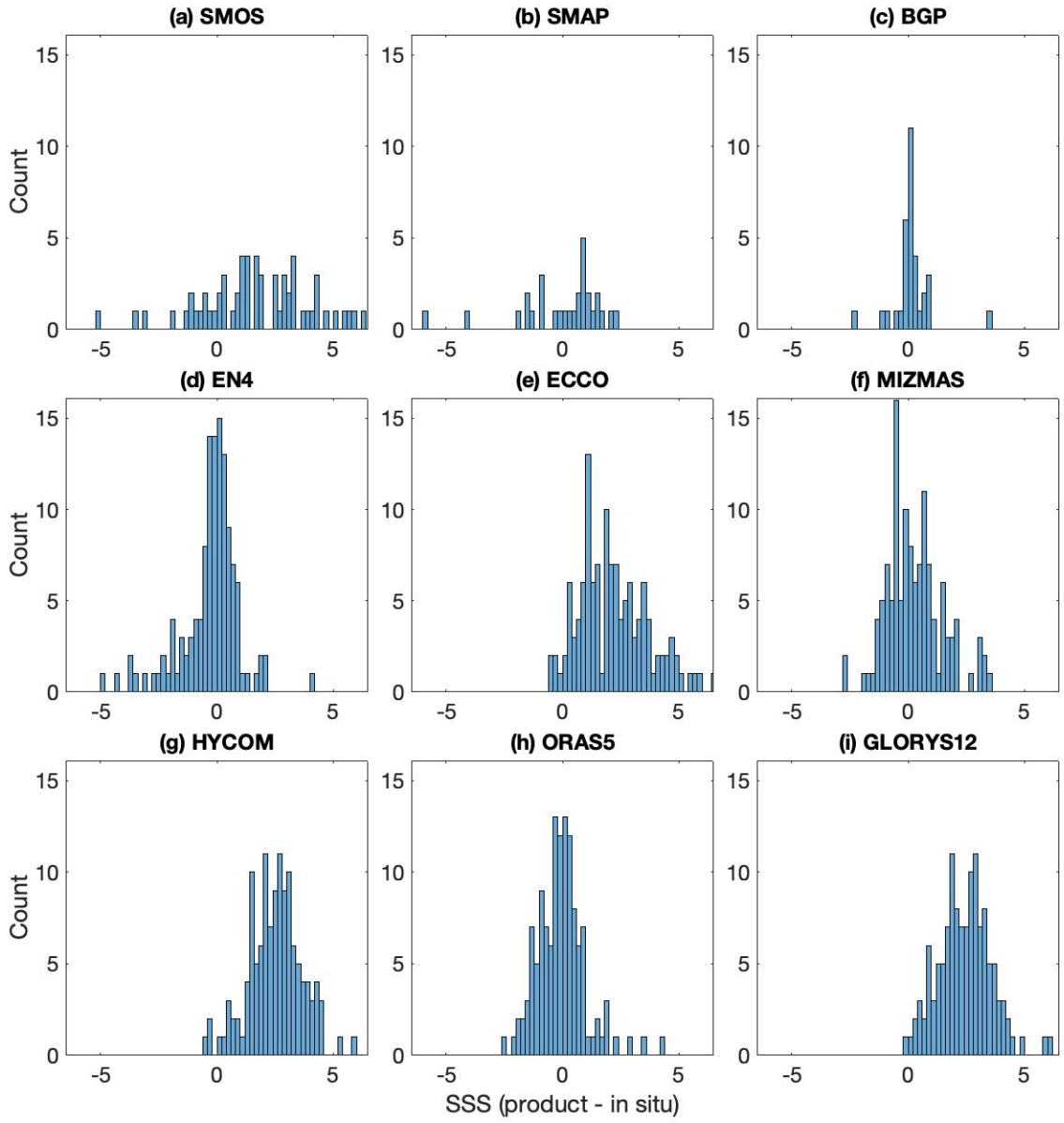

Figure 3.6 Histograms of sea surface salinity (SSS) differences (psu) of products minus *in situ* (SIZRS). SIZRS at 2 m is used for (a,b) Satellites, and 5 m for (c,d) *in situ* and (e–i) models. Bin widths are 0.2 psu.

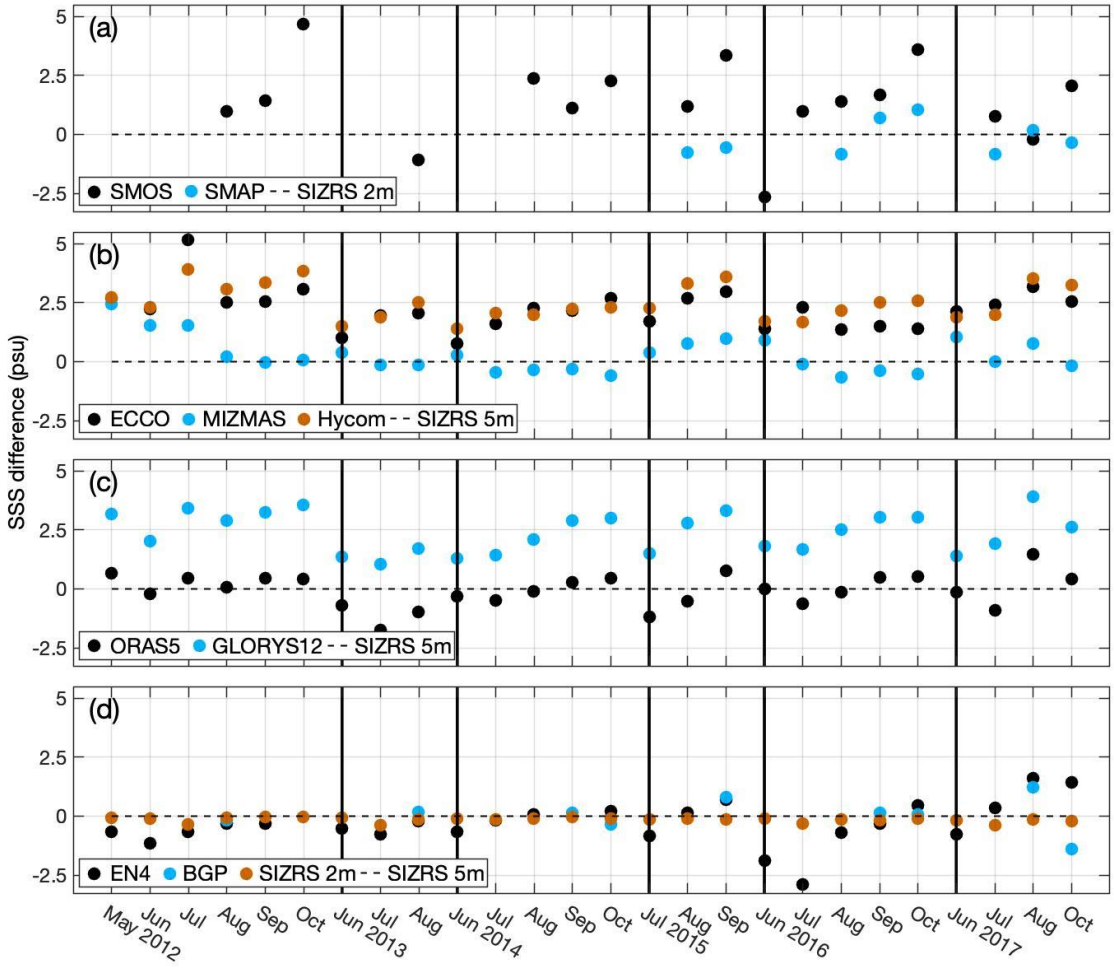

Figure 3.7 Sea surface salinity (SSS) differences (psu) from SIZRS (at 5 m) averaged along (150°W from 70.5°N–80.5°N) compared to (a) satellite missions, (b,c) ocean model simulations, and (d) in–situ observations. Grey, vertical lines separate years where months are not consecutive.

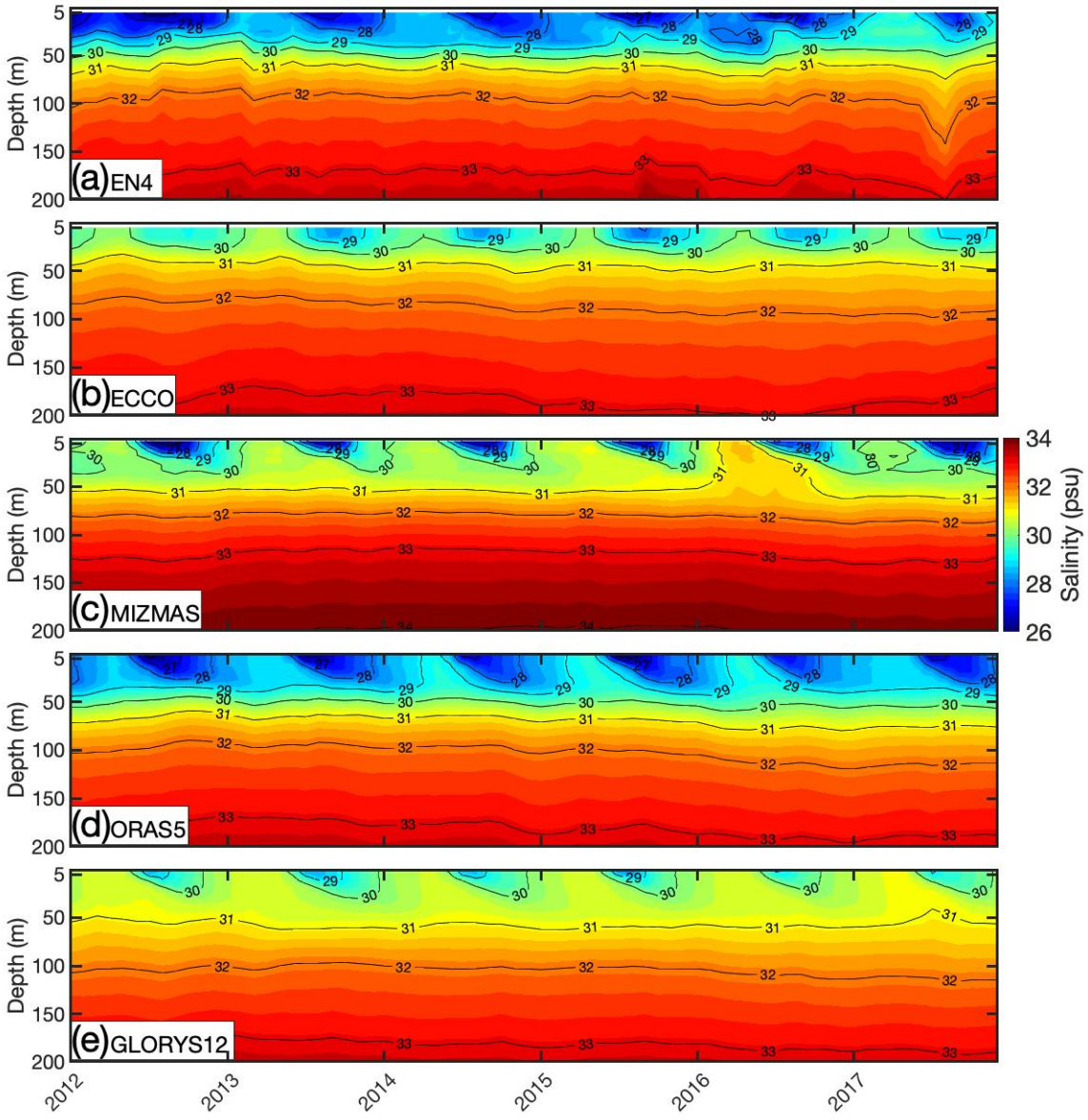

Figure 3.8 Contours of salinity (psu) averaged along 150°W between 70.5°N and 80.5°N, as a function of depth and time from 2012–2017.

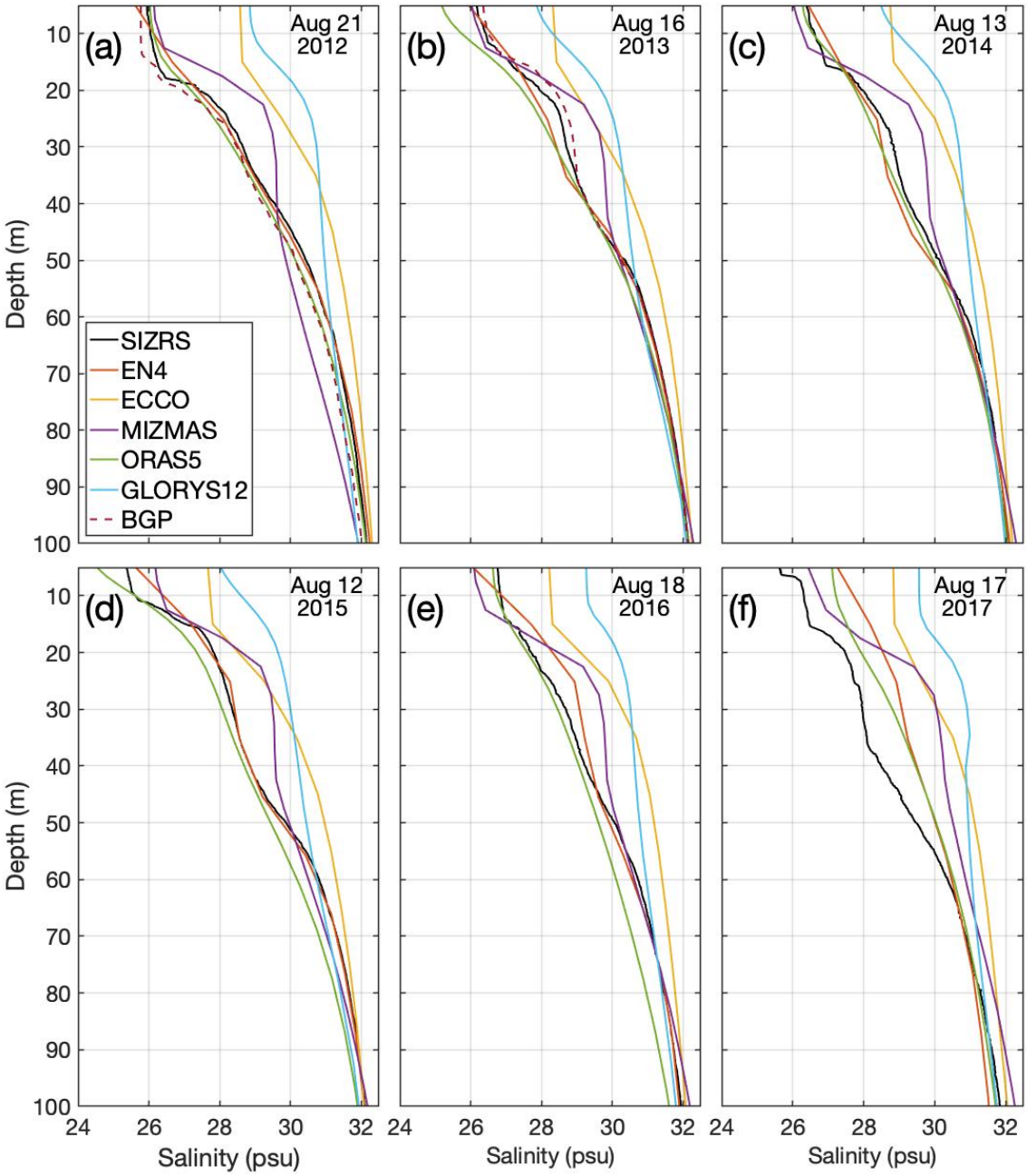

Figure 3.9 Salinity (psu) depth profile comparisons of SIZRS drops with other products over the transect average (150°W, 70.5°N–80.5°N) during (a) 21 August 2012, (b) 16 August 2013, (c) 13 August 2014, (d) 12 August 2015, (e) 18 August 2016, (f) 17 August 2017.

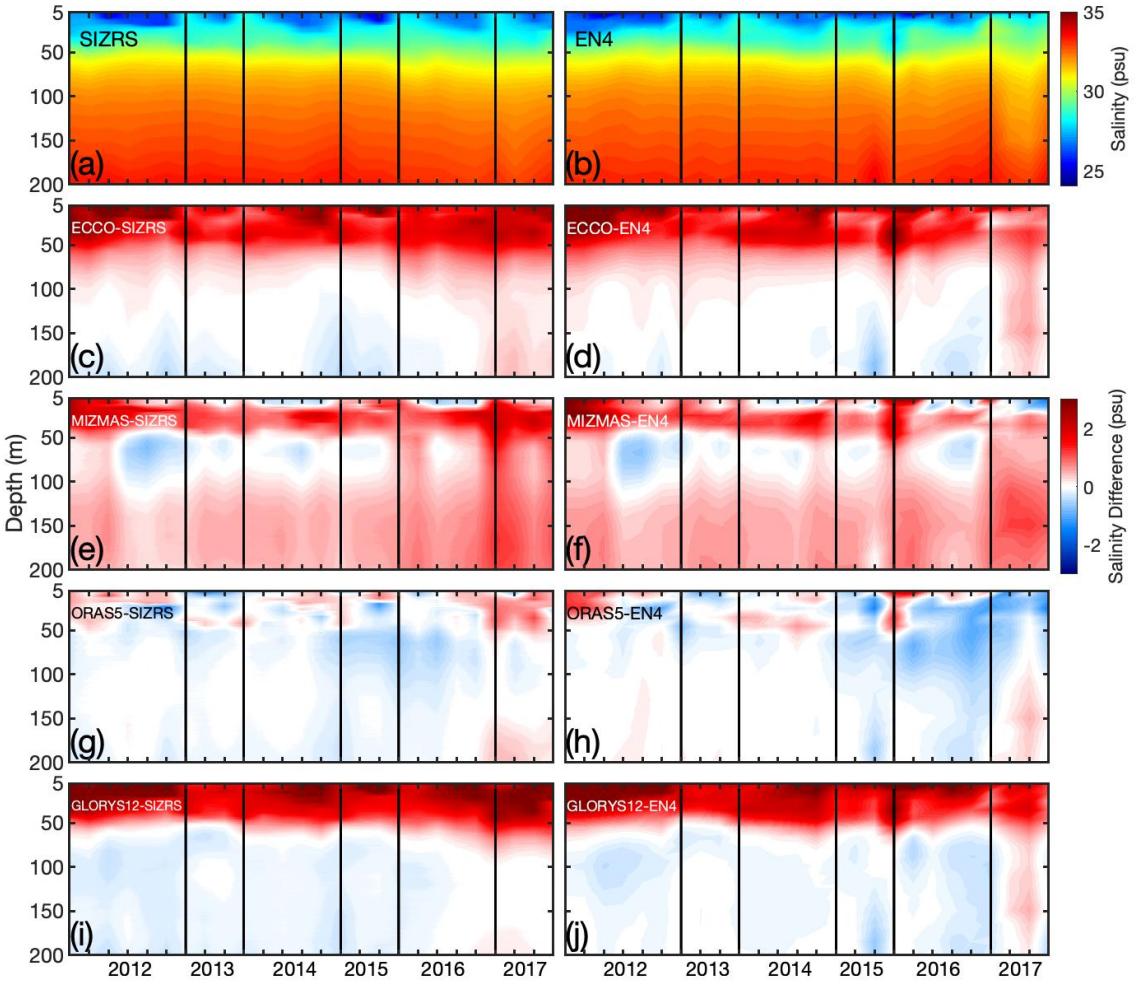

Figure 3.10 Salinity (psu) versus depth profiles averaged monthly over all SIZRS latitudes for (a) SIZRS and (b) EN4 from 2012–2017, and the departure of salinity from SIZRS (left column) and EN4 (right column) for the ocean models (c,d) ECCO, (e,f) MIZMAS, (g,h) ORAS5, and (i,j) GLORYS12. Grey, vertical lines separate years where months are not consecutive.

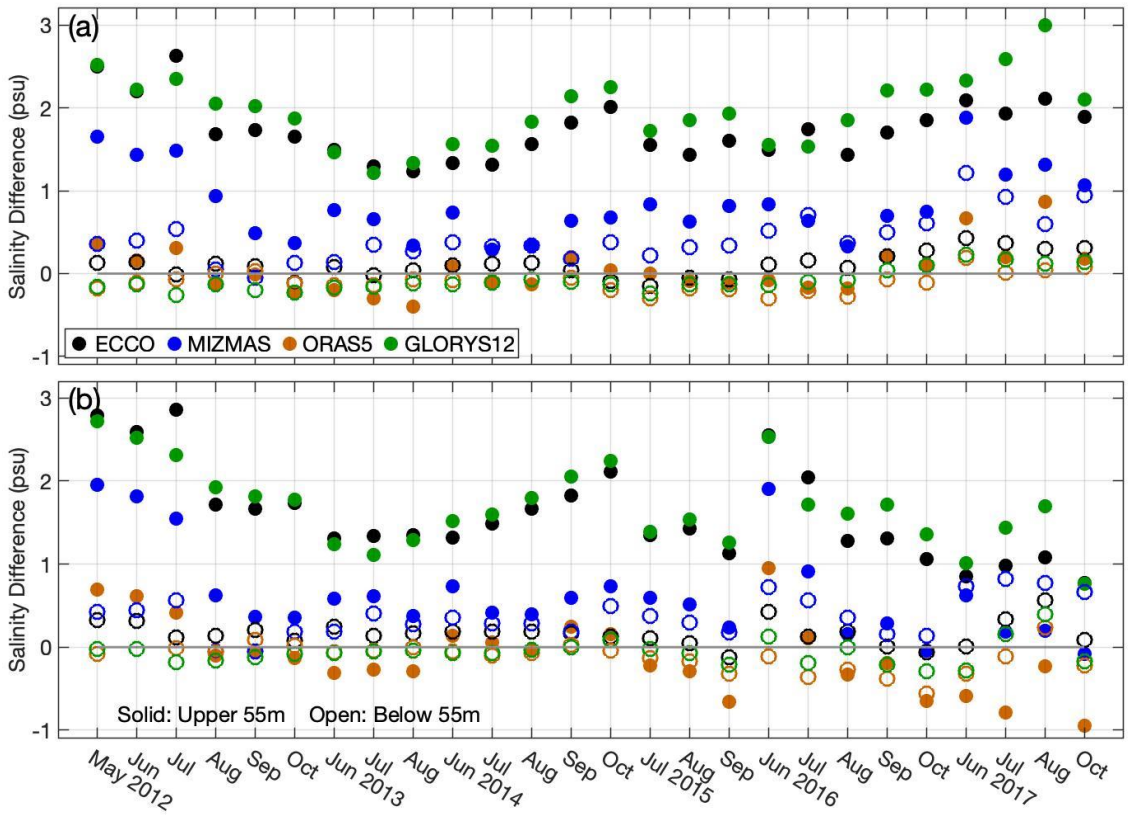

Figure 3.11 Differences in salinity (psu) depth profiles of each product at each SIZRS latitude averaged monthly from 2012–2017 separated by vertically-averaged (solid dot) upper 5 m to 55 m region and the (opened dot) lower 55 m to 207 m region for (a) model minus SIZRS, and (b) model minus EN4.

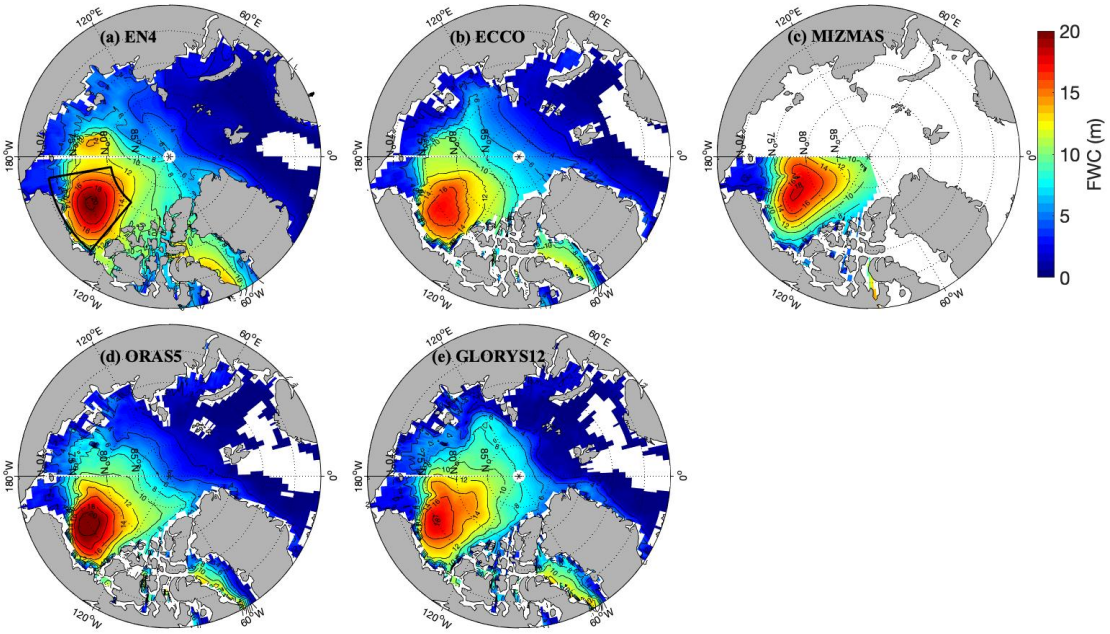

Figure 3.12 Freshwater content (FWC; m) from 5 m–500 m depth in the Arctic Ocean and averaged between 2012–2017 from the (a) EN4 data and five models: (b) ECCO, (c) MIZMAS, (d) ORAS5, and (e) GLORYS12. FWC is contoured every 2 m with a reference salinity of 34.8 psu. Beaufort Gyre region is outlined in a black box (Figure 12a).

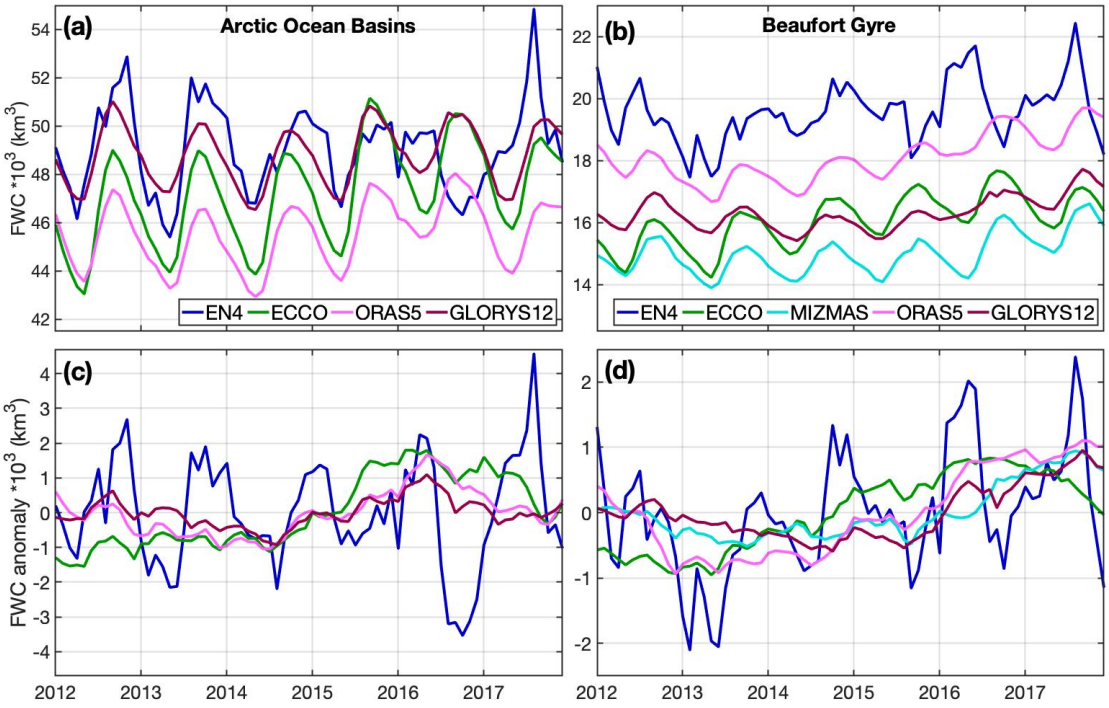

Figure 3.13 Timeseries of depth-integrated (5 m–500 m) and box–accumulated freshwater content (FWC; km^3) in the (a,c) Arctic Ocean Basins (180°W–180°E, 67°N–90°N) and the (b,d) Beaufort Gyre (170°W–130°W, 70.5°N–80.5°N) from (top panel) raw data and the (bottom panel) departure from the monthly climatology between 2012 and 2017.

CHAPTER 4

THE ROLE OF THE RUSSIAN SHELF IN SEASONAL AND INTERANNUAL VARIABILITY OF ARCTIC SEA SURFACE SALINITY AND FRESHWATER CONTENT[3]

[3]Hall, S.B., B. Subrahmanyam, and M. Steele (2022). The Role of the Russian Shelf in Seasonal and Interannual Variability of Arctic Sea Surface Salinity and Freshwater Content. Submitted to *Journal of Geophysical Research: Oceans.*

ABSTRACT

Freshwater plays a pivotal role in the Arctic Ocean's climate, as salinity governs upper ocean stratification, convection, and the promotion of seasonal sea ice growth or melt. The Beaufort Gyre contains a significant amount of freshwater; however, there is limited understanding of the role that the Russian Arctic Shelf plays in the Arctic Ocean's freshwater content (FWC). Here, we use salinity from the European Centre for Medium-Range Weather Forecasts' (ECMWF) Ocean Reanalysis System 5 (ORAS5) product to first compare with *in situ* and satellite observations. We then conduct analyses over the years 1979–2018 to examine FWC and salinity on the Russian Shelf (30°E–180°E; shallower than 200 m depth), in the Beaufort Gyre (130°W–170°W, 70.5°N–80.5°N), and over the Arctic Ocean as a whole (northward of 66°N). Our results indicate that the Russian Shelf consists of ~16% of the total freshwater volume (FWV) in the Arctic Ocean (80,7623 km^3) and has a negative trend (-15.63 km^3/year), primarily influenced by negative trends in the Kara and Laptev Seas. We also find a notable regime shift during the summer of 2007 for both the Beaufort Gyre (increased FWV) and Russian Shelf (decreased FWV). When computing Arctic FWV changes before and after this 2007 regime shift, there is up to a 14% error if the Russian Shelf's FWV is omitted.

4.1 INTRODUCTION

Freshwater plays a vital role in the Arctic Ocean as salinity variations determine the strength of stratification, ocean circulation, and biogeochemical cycles (Carmack et al., 2016; Cornish et al., 2020). Not only has there been a rapid depletion of perennial sea ice in the past two decades, but other freshwater sources such as major river discharge and Pacific Ocean import through the Bering Strait have contributed to an overall increase of freshwater in the Arctic Ocean (Serreze et al., 2006; Woodgate & Aagaard, 2005; Kelly et al., 2019). Wang et al. (2021c) showed that freshwater has increased in the Amerasian Basin (containing the Makarov and Canada Basins, see Figure 4.1a) and decreased in the Eurasian Basin (containing the Amundsen and Nansen Basins see Figure 4.1a).

Previous research has focused on the Beaufort Gyre (BG), since it contains 20-25% of the Arctic Ocean's total freshwater content (FWC) and has undergone significant freshwater accumulation in recent decades (Proshutinsky et al., 2019). FWC with units of meters is defined as:

$$FWC = \int_{z(S=S_{ref})}^{z_0} \frac{S_{ref}-S}{S_{ref}} \cdot dz \tag{4.1}$$

where z_0 indicates a data set's shallowest depth and z is the depth where salinity (S) is equal to the reference salinity (S_{ref}); we use the standard definition S_{ref} = 34.8 psu (Aagaard & Carmack, 1989; Serreze et al., 2006; Fuentes-Franco & Koenigk, 2019). Freshwater volume (FWV) is the longitude and latitude integration of FWC, as used by Cornish et al. (2020):

$$FWV = \int\int FWC \cdot dx \cdot dy \tag{4.2}$$

where dx and dy are the longitudinal and latitudinal expanse of the data grid cells, resulting in units of km^3 for the remainder of this study.

The Russian Shelf exhibits a wide range of salinity variability due to seasonal sea ice advance and retreat as well as discharge from major rivers. The largest three rivers are the Ob and Yenisei (flowing into the Kara Sea), and Lena (flowing into the Laptev Sea) that combined contribute ~2,300 km^3/yr which is roughly half of total discharge from all rivers flowing into the Arctic Ocean (Osadchiev et al., 2020). Ahmed et al. (2020) reported that the annual discharge over the years 1980-2009 from the Ob, Lena, and Yenisei Rivers increased by 10.3 km^3, 40.6 km^3, and 23.7 km^3 per decade respectively. Arctic shelves also tend to favor polynyas where ice grows and an excess of saline water is left behind (Spielhagen & Bauch, 2015). Both factors contribute greatly to seasonal and interannual variability.

Studies have shown that atmospheric circulation patterns as expressed by the Arctic Oscillation (AO) and the related North Atlantic Oscillation (NAO) have strong influence on the Arctic Ocean's sea ice motion, freshwater input and export pathways (Rigor et al., 2002; Jahn et al., 2010; Lique et al., 2010). For example, a positive NAO or AO (here referred to together as "N/AO" since they tend to co-vary) index is associated with enhanced outflow of sea ice and surface freshwater flux via Fram Strait, more westward Eurasian freshwater runoff pathways, and a reduction in the size of the BG (Morison et al., 2021; Wang, 2021). Steele and Ermold (2004) demonstrate salinity trends related to N/AO indices, which when positive, can broadly freshen the White and Kara seas while the East Siberian and Laptev seas experience freshening in the south and salinification in the north. More specifically, a positive (negative) N/AO index is associated with more westerly

(southerly) winds which guide freshwater along (across) the eastern shelves of the East Siberian and Laptev Seas. The Kara Sea however is primarily influenced by atmospheric moisture flux convergence that increases with higher N/AO indices that induce greater precipitation – evaporation (P-E) and river output (White et al., 2007; Peterson et al., 2002; Steele & Ermold, 2004).

Freshwater accumulation and release from the Arctic Ocean southward into the North Atlantic Ocean can have significant impacts. For example, "The Great Salinity Anomaly" event in the 1970's resulted in ~10% decrease in strength of the Atlantic Meridional Overturning Circulation current that is responsible for the deep-water formation source of the thermohaline circulation system and plays a vital role in the regulation of the global climate (Rahmstorf et al., 2015; Johnson et al., 2018). Rising surface air temperatures as a consequence of increased anthropogenic emissions have also instigated a changing regime of the Arctic Ocean, which can drastically alter the spatial distribution and magnitude of FWC (Serreze & Francis, 2006). Understanding the freshwater contribution from the Russian Shelf through quantitative analysis is pivotal to the interpretation of Arctic Ocean processes; especially as "ice-free" summers are anticipated to occur within the next two decades (Guarino et al., 2020).

Our study is focused on FWC changes and trends in the Arctic Ocean over the recent four decades, with emphasis on the Russian Shelf region where *in situ* observations are limited. This region has often been overlooked in terms of FWC. Here, we use *in situ* measurements, remote sensing observations, and the European Centre for Medium-Range Weather Forecasts' (ECMWF) Ocean Reanalysis System 5 (ORAS5) product to examine FWC and sea surface salinity (SSS) on the Russian Shelf, in the Beaufort Gyre, and over

the Arctic Ocean as a whole. Section 2 provides an overview of the data and methodology used in this study, while Section 3 presents the results and discusses the outcomes of this work. Section 4 provides a summary of our significant findings.

4.2 Data and Methods

A. Data

The Arctic Ocean is defined here as 66–90°N. The Russian Shelf region is defined as areas shallower than 200 m within longitudes 30–180°E, using the General Bathymetric Chart of the Oceans' (GEBCO) gridded bathymetry (GEBCO Compilation Group, 2020).

The European Centre for Medium-Range Weather Forecasts' (ECMWF) Ocean Reanalysis System 5 (ORAS5) product provides 40 years of monthly data between January 1979 and December 2018. This study utilizes the 3D fields of salinity, temperature, zonal and meridional current velocity, which are provided on a tripolar grid, with the poles of the grid located on the Antarctic continent, in Central Asia, and North Canada. The horizontal resolution is 1/4° (27.75 km) at the equator and increases to ~ 9 km in the Arctic (Zuo et al., 2019). ORAS5 consists of multiple ensemble members with a model component from the Nucleus for European Modelling of the Ocean (NEMO) version 3.4.1 coupled to the Louvain-la-Neuve Sea Ice Model for global configuration. Atmospheric forcing fields are derived from ERA-Interim prior to 2015 and from the ECMWF operational numerical weather prediction after 2015 (Dee et al., 2011; Zuo et al., 2018). The 3-Dimensional VARiational data assimilation system's First-Guess at the Appropriate Time configuration from NEMOVAR is used to assimilate temperature and salinity profiles for ORAS5. Observational data assimilated to construct ORAS5's temperature and salinity include Woods Hole Institution's Ice-Tethered Profilers, The Hadley Centre Global Sea Ice and

Sea Surface Temperature, Research African-Asian-Australian Monsoon Array moorings, Argo floats, and Autonomous Pinniped Bathythermographs (Zuo et al., 2019). Temperature and salinity profiles are also assimilated from the quality-controlled EN4 with depth corrections from the Expendable Bathy Thermograph and Mechanical bathythermograph before May 2015, and from Global Telecommunications System after (Good et al., 2013). The Integrated Climate Data Center provides ORAS5 output online at: https://icdc.cen.uni-hamburg.de/thredds/catalog/ftpthredds/EASYInit/oras5/ORCA025/catalog.html.

This study provides a comparison of SSS in the ORAS5 model (at its top layer depth of 0.5 m) to the following three satellite-derived SSS products. The first is SSS from the European Space Agency's Soil Moisture and Ocean Salinity (SMOS) Arctic product version 3.1 produced at the Barcelona Expert Center (BEC; Martínez et al., 2022). SMOS has a temporal resolution of a 3-day repeat and a spatial resolution of 25 km, using an Equal-Area Scalable Earth (EASE)-Grid 2.0 (http://bec.icm.csic.es/). The second satellite SSS data set is processed by Remote Sensing Systems (RSS) using NASA's SMAP level 3 version 5 product available online at: https://data.remss.com/smap/SSS/V05.0/FINAL/ (Meissner et al., 2022). The final satellite data set used here is level 4 version 1 Multi-Mission Optimal Interpolated Sea Surface Salinity (OISSS; Melnichenko et al., 2016). This is produced by the International Pacific Research Center of the University of Hawaii at Manoa in collaboration with RSS and combines salinity data from SMOS, SMAP, and Aquarius/SAC-D satellite missions (Melnichenko, 2021; Melnichenko et al., 2016) on a 0.25 × 0.25 grid, with data provided weekly from 24 August 2011 to 31 August 2021 through the Physical Oceanography Distributed Active Archive Center's (PODAAC)

(https://podaac.jpl.nasa.gov/dataset/OISSS_L4_multimission_7day_v1?provider=POCLOUD).

In situ ship CTD data from the Russian shelf taken during the Nansen and Amundsen Basins Observational System (NABOS) program are also analyzed (https://nabos.iarc.uaf.edu/NABOS2/data/registered/2018/index.php). We focus here on the 2018 NABOS cruise, specifically CTD station numbers 36–134 within 75.46°N–81.45°N latitude and 102.85°E–168.85°E longitude.

B. METHODS

To explore FWC and SSS trends without seasonal influence, such as sea ice growth and melt periods, we formed deseasonalized time series by dividing monthly means in each year by the long-term annual mean (this is well-defined for positive-definite quantities such as FWC and SSS). We then summed these normalized values for all like-months and divided by 40 years to get an average normalized monthly value also called the "seasonal index." For example, in winter the seasonal index for SSS will generally be greater (less) than 1 for SSS (FWC). The deseasonalized time series is then formed by dividing the raw monthly mean time series by the seasonal index for each corresponding month.

We describe the spatial and temporal patterns of FWC and SSS through Empirical Orthogonal Function (EOF) analysis with related principal component time series. EOF analyses highlight the different modes of variability to identify temporal trends and determine whether certain spatial areas are in or out of phase with one another. Techniques used to compute these analyses followed the Climate Data Toolbox by Greene et al. (2019).

4.3 Results and Discussion

A. Salinity in the Arctic Ocean

We begin by analyzing SSS spatial distributions averaged over 1979–2018 in the Arctic Ocean (Figure 4.1b). The Russian Arctic Shelf region (hereafter, Russian Shelf; Figure 4.1c) is further divided into subregions. The North Atlantic Ocean provides an inflow of saline water towards the Nordic Seas, while the lowest salinity waters are concentrated near river mouths, with less extreme low-salinity waters in the BG and the western Canadian Archipelago. Particularly low SSS is evident in the Kara Sea (influenced by the Ob and Yenisei Rivers) and the Laptev Sea (influenced by the Lena River). Low salinity water also spreads eastward from the Laptev into the East Siberian Sea, mostly governed by wind as well as local river discharge (Osadchiev et al., 2020). Highest SSS on the Russian Shelf is found in the Barents Sea as it is predominately subjected to the saline inflow of North Atlantic Ocean water.

B. Comparison Between Observations and ORAS5

Remote sensing observations are limited to ice-free regions and collect measurements of only the top few centimeters of the ocean's surface but provide greater spatial and temporal resolution observations of the Arctic Ocean compared to *in situ* measurements. Satellite data from SMOS, SMAP, and OISSS are shown in Figure 4.2a-c. The satellite data display similarities to each other in that saline water enters from the North Atlantic side and freshwater is mostly found in the East Siberian, Laptev, and Kara Seas and the BG.

The bias between the reanalysis and satellite data is shown in Figure 4.2d-f. Overall, less bias is seen between products on the North Atlantic side, where spatial and temporal variability of mean SSS is relatively small. On the other hand, biases are larger over the Russian Shelf and the Beaufort Sea, although mostly within +/- 3 g/kg. Compared to other ocean models commonly utilized to estimate Arctic Ocean salinity, Hall et al. (2022) found ORAS5 to have the largest positive correlation and smallest bias to satellite and *in situ* observations in the BG area, both at the surface and at depth.

To further investigate the effectiveness of ORAS5 in the Russian Shelf region, we compare the reanalysis salinity and temperature to CTD data from the September 2018 NABOS cruise (Figure 4.3). Absolute salinity and conservative temperature were computed from NABOS *in situ* measurements and ORAS5 estimations and are herein used for comparisons. The monthly mean ORAS5 data from September 2018 is spatially interpolated to the locations of each cast to for a "spatial match-up" comparison. The CTD casts were primarily taken within the Laptev Sea and the East Siberian Sea, within and outside of the Russian Shelf boundary. Despite the differences in spatial and temporal resolutions of each product, the average absolute salinity from ORAS5 is generally within 1 g/kg of the NABOS data between 2–500 m, reaching a maximum bias of 1.03 g/kg at 23 m depth (sea surface salinity at 1 m has a difference of 1.17 g/kg. The averaged NABOS (ORAS5) salinity had a minimum of 30.5 g/kg (30.1 g/kg) at 2 m depth and reached 34.8 psu (34.8 psu) at 133 m (138 m) depth. The average FWC computed from NABOS and ORAS5 averaged absolute salinity data were 4.2 m and 5.4 m respectively. The difference in FWC is due to the slightly lower salinity estimates from ORAS5 compared to NABOS throughout depth. The average conservative temperature for both NABOS and ORAS5 was

about 0.45°C at 10 m and -0.64°C at 100 m. However, the minimum temperature for NABOS reached -1.58°C while ORAS5 was significantly warmer at -0.9°C.

C. Freshwater Content

Maps of ORAS5-derived FWC and its corresponding trend between 1979–2018 are provided in Figure 4.4. The Russian Shelf has relatively high FWC owing to its low salinity, but its shallow bathymetry limits the vertical integral so that the highest FWC values are found in the BG and outflows areas to the south. FWC trends of statistical significance, as illustrated by stipple marks in Figure 4.4b, denotes the 95% confidence level. The BG has been freshening during this period as well as a large portion of these outflow areas, i.e., the Canadian Basin, Canadian Arctic Archipelago, north of Greenland, and in Baffin Bay (Kelly et al., 2019). These areas are also similar to the pathway highlighted by Zhang et al. (2021) where the BG-sourced freshwater potentially travels to the Labrador Sea rather than through the Fram Strait. Strong freshening observed in Baffin Bay is also attributed by Greenland's meltwater (Dukhovskoy et al., 2016). In contrast, there are negative FWC trends in the Kara, Laptev, and far northwest East Siberian Sea, as well as the basins to the north of these seas. Notably, the regions of the Russian shelf that contain major river discharge (i.e., the Laptev and Kara Seas) display negative or insignificant FWC trends. The negative FWC trend over the Russian Shelf can partly be explained by the progressive shoaling of the incoming warm, salty Atlantic-origin waters after 2007 along the East Siberian slope (Bertosio et al., 2022; Polyakov et al., 2017). The shoaling of the isohalines (by 50 m between 2007–2018) near the continental slope coincide with a weakened halocline layer (Bertosio et al., 2022).

ORAS5 also exhibits a less intense decline of FWC in the Makarov Basin region; however, Bertosio et al. (2022) suggests that after 2012 the northward transition of the BG center was responsible for increased FWC in the Makarov Basin. Overall, Figure 4.4b highlights the opposing FWC trends between the Eurasian Basin and the Canadian Basin as examined by Wang et al. (2021c) and Pnyushkov et al. (2022), but also demonstrates the extension of negative Eurasian Basin FWC trends onto the Russian Shelf, as also shown by Morison et al. (2012) with a shorter time series.

The Arctic Ocean has undergone considerable changes in FWV in the last four decades (Figure 4.5a), influenced by oceanic inflow to the region, atmospheric circulation, river discharge, and sea ice state (Carmack et al., 2016; Pnyushkov et al., 2022). While the Arctic's FWV decreased in the initial years to 71,220 km^3 in 1985, it has subsequently sustained an increase, reaching a maximum of 90,450 km^3 in 2018. On average, the Arctic Ocean's FWV has been reported to be roughly 84,000 km^3 (Serreze et al., 2006; Spielhagen et al., 2015). Here, ORAS5 shows a comparable FWV of 80,763 km^3 (Table 4.1), with the Russian Shelf contributing ~ 16% and the BG ~ 23%. The long-term mean amplitude of the Arctic Ocean's FWV seasonal cycle is 6,407 km^3 (±467 one standard deviation), while it is 1,990 km^3 (±142) for the Russian Shelf and 734 km^3 (±189) for the BG. Therefore, the Russian Shelf represents 31% of the Arctic Ocean's FWV seasonal variability.

In 2007 there was a step function increase in BG FWV amounting to ~ 2,390 km^3, while during the same year the Russian Shelf had a net FWV loss of about 864 km^3. The two months with the largest FWV change during 2007 were September and October for the BG, while this change was earlier for the Russian shelf, between June and July. During this year, the BG ocean circulation accelerated in response to surface wind forcing and

early sea ice retreat, resulting in a gyre spin up and accumulated freshwater via Ekman convergence (Armitage et al., 2017; Zhong et al., 2019). However, the identification and cause for the nearly simultaneous FWV decrease observed here for the Russian Shelf region has not previously been described. This 2007 "regime shift" on the Russian Shelf and the BG may have some correspondence to previously identified freshwater advection from the Eurasian Basin to the Canadian Basin in response to wind-driven processes (Morison et al., 2021).

To further investigate the 2007 transition, we analyze FWV during the 11 years leading up to and succeeding this year, herein referred to as Pre-2007 (1997–2007) and Post-2007 (2008–2018). Linear FWV trends of both the Pre-2007 and Post-2007 periods are illustrated by grey lines on Figure 4.5. The Arctic Ocean's FWV Pre-2007 trendline was greater compared to that of the Post-2007 period. In addition, we address the significant contribution of FWV from each of the different Russian Seas by examining the separate components of the Russian Shelf's (Figure 4.5d). The East Siberian Sea region contributes roughly half of the freshwater towards the Russian Shelf's freshwater, given its relatively large size and the incorporation of the Kolyma river discharge. However, in contrast to the East Siberian Sea's positive FWV trend during the Pre-2007 period, the Post-2007 period experienced a negative trend. The Laptev and Kara Sea's FWV are comparable to each other and contribute roughly 21% and 25% of the Russian Shelf. As the Barents and White Sea do not supply a sizeable amount of FWV to the Russian Shelf, their analyses are combined for the rest of this study.

The Russian Shelf reached a peak FWV during June 2007 before its decrease later in the year, losing about 8.2% until January 2008. Figure 4.5d aids in the understanding of

the different Russian seas' contribution to this loss. The Laptev Sea between June 2007 – January 2008 experienced a 12% FWV loss while the East Siberian Sea's decreased by 10%. The Kara Sea did not have as significant a decline of FWV (4%) while the Barents and White Sea's change was negligible (<1%). Therefore, we conclude that the Laptev and East Siberian Seas contributed the most to the loss of FWV over the Russian Shelf during its 2007 regime transition.

We now compare our ORAS5 FWV analysis with that of Rabe et al. (2011), who found an 8,400 km^3 FWV increase for the Arctic Basin from a 1992–1999 average to 2006–2008 average using *in situ* observations. This calculation excluded the Russian Shelf. For the Arctic Basin (defined as areas with depth greater than 500 m), ORAS5 gets a comparable increase of 7,531 km^3 for these two time periods. The reanalysis also provides a FWV increase of 2,450 km^3 in the BG and FWV decrease of 63 km^3 on the Russian Shelf. Thus, the neglect of the Russian Shelf in Rabe et al. (2011) seems justified by the ORAS5 analysis, which predicts an error of only 63/7,531 = 0.8%

However, this is not the case for the 2007 regime shift. In this case, the BG contributed a ~ 3,700 km^3/year FWV increase out of an Arctic Ocean total increase of ~ 5,300 km^3/yr . At the same time, the Russian Shelf provided a ~ 1,300 km^3/yr FWV *decrease* over this transition, with significant contributions from the East Siberian, Kara, and Laptev Seas. Thus, neglecting Russian Shelf FWV change in this case creates an error of 25% = 1300/5300. This means that omitting the Russian Shelf region can be a source of significant error when computing Arctic Ocean FWV change, depending on the time periods examined.

We examine long-term monthly mean FWV trends in Figure 4.6 over the four-decade period. We also investigate the monthly trends of Post-2007 period (blue) and Pre-2007 (red) to better understand the influence from the regime shift. While the Arctic Ocean experiences one peak and minimum per year, the BG region experiences two major FWV peaks that can be attributed to sea ice melt and advection further described by Proshutinsky et al. (2009). The long-term trend of the Arctic Ocean's FWV peaks in June, which is similar to the years leading up to the regime change.

However, after 2007, the FWV peak is dramatically earlier, i.e., in April, and the amplitude of the seasonal cycle is larger. Earlier onsets of increased inflow of freshwater sources can be related to the earlier shift in peak FWV trend for each region in Figure 4.6. Makarieva et al. (2019) describe a shift in the hydrological regime near major Arctic rivers, as precipitation is favoring rain rather than snow as a result of warmer air temperatures from climate change. The availability of liquid freshwater can quicken the rate of river discharge as it does not need the time to melt that snow does. Ahmed et al. (2020) emphasizes that snow melt is occurring earlier, having a 2.5% increase in the spring while there is a decrease of 5.8% in the summer between 1980–2009. Niederdrenk et al. (2016) described enhanced cyclone activity over land to be the cause of increased precipitation in late spring and summer, causing more runoff on the Russian Shelf region and being further responsible for the large variability in Arctic river runoff.

D. Analysis of Salinity and Freshwater Content

The long-term mean spatial variance of FWC and SSS is shown in Figure 4.7 where the maximum and mean values of these variances are provided in Table 4.2. The largest FWC variance occurs in the Makarov Basin north of the New Siberian Islands. This is

possibly due to the influence of adjacent waters that make up the Markarov Basin. Surface waters are sourced from the Canadian Basin while the Eurasian Basin waters make up the parts of the halocline and deeper waters (Swift et al., 1997). There are also implications from the East Siberian cold shelf water's offshore advection that supplies the transitional and upper halocline waters of the Makarov Basin (Wang et al., 2021d). Wang et al. (2021d) found that the East Siberian Sea contributes up to three kinds of the Makarov Basin's halocline waters. A change in the properties of these waters can result in the disturbance of dynamics and circulation that transport freshwater. The Eurasian Basin's boundary current takes two major pathways near the intersection of the Lomonosov Ridge and the Russian's continental margin north of the Laptev and East Siberian seas; one that flows northward on the west side Lomonosov Ridge and one that flows along the shelf break and crosses eastward into the Makarov Basin (Woodgate et al. 2001; Aagaard & Carmack, 1989). This pathway is in proximity to the East Siberian Sea which contains the maximum FWC variance (5.24 m^2) in the Russian Shelf region, close to the 200 m isobath. Woodgate et al. (2001) also highlight potential pathways of the Atlantic layer water and deep waters that flow across the Lomonosov Ridge and into the Makarov Basin where Figure 4.7a illustrates high FWC variability.

The largest variance of FWC in the BG region occurs in the northwest, where Regan et al. (2019) reports the center of the gyre expanded between 2003 and 2014. Baffin Bay also experiences moderate variance which could be associated to the changes in positive and negative NAO indices that strengthen and weaken the cyclonic circulation in the Baffin Bay (Münchow et al., 2015). Variations are also possibly due to varying input of freshwater from the Beaufort Gyre and runoff from the Greenland Ice Sheet (Zhang et al., 2021; Carr

et al., 2021). Tang et al. (2004) speculates that the interannual variations of salinity in the upper 400 m of the Baffin Bay have been caused by surface water flux from the combined precipitation, sea ice melt, and runoff that is then advected by the West Greenland Current, its strength and transport in which varies on interannual timescales (Rykova et al., 2015).

Substantial SSS variance is concentrated along the coastal and shelf regions (Figure 4.7b), likely influenced by river discharge (Lambert et al., 2019). A notable tongue of relatively high SSS variance extends from the Lena river mouth northeastward toward and beyond the shelf break and into the Makarov Basin. This tongue can be associated to the interannual variability of the propagation and distribution of the Lena River plume, the freshened water mass (thickness ~ 10 m) provided by river discharge into the ocean (Zhuk et al., 2021). The largest SSS variance occurs in the Russian Shelf region, particularly in the Kara Sea (~33 psu^2), likely forced by large interannual variations in the Ob and Yenisei rivers and at their mouths where, fresh river water meets the more saline Siberian shelf waters (Kuzin et al., 2010). Current circulation and changes in prevailing winds affect the buoyancy of river-sourced freshwater surface layers in this region (Umbert et al., 2021). Large SSS coastal variance in the East Siberian Sea could be attributed to the shallow Siberian Coastal Current (SCC). The SCC is a wind-driven eastward flowing current trapping and bringing freshwater from the Lena and Kolyma rivers alongshore until it connects with the Bering Strait inflow and veers northward (Weingartner et al., 1999).

To further understand the variance of FWC and SSS in the Arctic Ocean, we employ Empirical Orthogonal Function (EOF) analysis with particular focus on the first mode and its associated principal component timeseries. EOF analyses aid in the identification of spatial patterns associated with correlations between FWC and SSS. The

dominant (or first) EOF of FWC (Figure 4.8a) explains 36.7% of the total variance, with maximum positive EOF values (red) in the Canada Basin extending with generally lower amplitude into the regions north of Greenland and Baffin Bay. Negative EOFs (blue) are located in the deep basin north of the Laptev Sea and in the Laptev and Kara Seas, with a maximum amplitude along the 200 m isobath between the East Siberian Sea and Laptev Sea. The negative EOF values of FWC and SSS occur in the Laptev sea near the edge of the Russian shelf border (Figure 4.8a,b). Atlantic-source water, brought through the Barents Sea, is cooled by atmospheric heat loss and freshened by the melting of sea ice and mixing with Norwegian coastal current waters and flows to the Laptev sea after mixing with the Lena and Yenisei rivers in the Kara Sea (Anderson et al., 1994; Gascard et al., 2004).

The dominant EOF of SSS explains 16.6% of the total variance, with large negative amplitude in the Laptev and Kara Seas and positive amplitudes over a similar area as for FWC. Figure 4.8c shows how the amplitude of the leading principal component modes (PC1) of FWC and SSS vary over our study period. Overall, there is an inverse relationship in trends between the PC1 of FWC (upward) and SSS (downward) which is expected as freshwater is equivalent to low salinity values. This indicates a strong, negative correlation coefficient (-0.858) for the PC1 timeseries between the surface salinity and the depth integrated measure of salinity stratification (i.e., FWC). Strong negative (positive) trends of salinity (FWC) occur between the years of 1987–1991 and 2005–2008, while between 1991–2005 the PC1 experiences lower amplitudes. These positive trends combined with the total Arctic FWC (Figure 4.5) can be interpreted as a period of significant rise in FWC overall. Stroeve et al. (2008) indicate significant diminishing ice concentrations through

their PC analysis during 1987–1991 which can possibly be related to significant changes in the spatial distribution of freshwater. The standard deviation of the first PC for salinity was 108.7 psu and for FWC was 222 m. The time series also show that after 1985 a negative (positive) trend in salinity (FWC) are the dominate modes of variability of these two fields in the Arctic. During 2007 alone, the rate of change in PC1 for both components was particularly large, in line with the shift we see in total FWC in the BG and Russian Shelf regions. The strong variability in the PC1 timeseries occur during time periods leading up to the local maxima of wintertime AO, as seen in Figure 4.9, where a record high occurred in 1989 and a significant maximum in 2007. Increased index of N/AO influences FWC and SSS variance as it indicates increased export of upper ocean freshwater from the Arctic Ocean, changes in Eurasian River runoff pathways, and the accumulation of freshwater in the BG (Morison et al., 2012).

Figure 4.10 reveals the differences of Post-2007 minus Pre-2007 averaged ocean current vectors overlaid on changes in FWC, FWC linear trend, and SSS. Since FWC is the integration of the vertical component of freshwater, the vectors in Figure 4.10a are the Post-2007 minus Pre-2007 differences of average ocean currents from the surface to the depth at which FWC was calculated at each location (i.e., depth at which the salinity was equal to the reference salinity). The ocean current vectors, computed from Post-2007 minus Pre-2007 periods, indicate the anticyclonic circulation of the BG, with greater velocities near the continental shelf and toward the northwest. Ocean currents beginning in the Laptev Sea, show stronger velocities associated with the Transpolar Drift aligning with the Mendeleev Ridge rather than the Lomonosov Ridge after 2007 as suggested also by Bertosio et al. (2022). The enhanced rate at which freshwater is driven off the Russian

Shelf is highly influenced by the intensification and cyclonic shift of the Transpolar Drift under an increase in the AO phase (Mysak, 2001). Timmermans et al. (2011) suggest the Transpolar Drift and BG become weaker from 2007–2008 to 2009–2010 linked with a change in sea ice flow and sea level pressure. Figure 4.10a shows negative (positive) FWC differences between Pre-2007 and Post-2007 periods over the Russian Shelf (BG) region. There is a significant negative signal over the Russian Shelf leading into the Makarov Basin. Whereas an especially strong, positive signal is seen between the Makarov and Canadian basin, connected between the Mendeleev Ridge and Alpha Ridge.

Compared to Pre-2007, the Post-2007 average SSS anomalies are increased (reduced) nearly throughout the entire Russian Shelf (BG) region. Again, there is extension of positive anomalies into the Makarov Basin to the north of the New Siberian Islands. Surface current velocities (m/s) are overlaid in Figure 4.10b to compare with SSS differences between Pre-2007 and Post-2007. The direction and magnitude of surface current differences are similar to the currents averaged with depth (Figure 4.10a).

To further understand the changes in seasonality from the regime shift, we provide differences in FWC and SSS between Pre-2007 and Post-2007 averages of each season shown in Figure 4.11. For this analysis, only December 1979 – November 2018 is considered since we define winter as DJF. For both quantities, strong seasonal differences are apparent. FWC change across the 2007 threshold is relatively minor in the Amerasian Basin, while it is stronger in the Eurasian Basin and Nordic Seas, with opposite polarity anomalies in winter and spring versus summer and fall. This could indicate a change in the influence of surface freshwater inputs from ice growth/melt and/or meteoric inputs (i.e.,

river discharge and precipitation less evaporation); advective effects seem likely too slow to explain these seasonal changes.

SSS differences are also of opposing sign in winter and spring versus summer and fall and are of highest amplitude in coastal and shelf regions. This could indicate a change in river discharge, but it could also result from a change in the ocean circulation of such riverine-influenced waters and/or in ice melt/growth on the shelves. The amplitude of seasonal sea ice growth and melt has increased as multi-year ice fraction has declined, but this effect on ocean salinity will eventually abate in the long term, as the Arctic transitions to a perennially ice-free state (Brown et al., 2020). The average salinity anomalies of the Post-2007 period are significantly less (greater) at the mouth of the Ob, Yenisei, Lena, and Mackenzie rivers in the winter and spring (summer and autumn) relative to the 11 years prior. The northern Kara Sea also experiences a drastic increase (decrease) of average FWC anomalies during winter and spring (summer and autumn) seasons. Brown et al. (2020) remarks on the influence of seasonal timing for sea ice melt and freeze, where the Amerasian Basin is reliant on enhanced stratification due to the high FWC and increased freshening. In contrast, the Eurasian Basin is highly influenced by the import of warmer and more saline Atlantic waters.

4.4. CONCLUSION

This study assesses the role of the Russian Shelves in long-term trends and variability of the Arctic Ocean's FWC and SSS over the span of 4 decades, between 1979 and 2018, using the ECMWF's ORAS5 product. We show that the Russian Shelf experienced a large step change in FWV during the summer of 2007, similar to that previously noted for the BG (Zhong et al., 2019). In contrast to the increase of FWV

between Pre-2007 and Post-2007 in the BG (about 3,700 km^3), the Russian Shelf experienced a significant decrease of around 1,300 km^3. While the accumulation of freshwater in the BG in recent decades has been quantified by many studies (Proshutinsky et al., 2019; Armitage et al., 2020; Regan et al., 2019), the decreasing FWV in the Eurasian Basin including the Russian Shelf should not be overlooked as it may highlight the limitation of FWV increase towards the storage of the Arctic Ocean as a whole. While the Russian shelf contributes around 16% of the Arctic Ocean's FWV, its step change decrease in 2007 was about 25% of the total step change over the entire Arctic Ocean in this transition year.

Our study brings to light the significant regime shift over the Russian Shelf during 2007. There are many possible forcings at play that may contribute to the sharp decrease of the Russian Shelf's FWV at that time. It is interesting to note that 2007 experienced a minimum summer sea ice extent, which would promote increased freshwater from melt. In addition, there was anomalously high (~4,000 km^3/yr) Eurasian river outflow into the Arctic Ocean (Feng et al., 2021). Shiklomanov and Lammers (2009) reveal that this record-breaking Eurasian river discharge was due to the increased precipitation across the coastal region and that the Eurasian pan-Arctic experienced the highest air temperatures that caused permafrost to thaw. Despite the increased freshwater sources, the Russian Shelf experienced a large decrease in FWV. One possibility is the occurrence of a local maximum of the North Atlantic Oscillation or Arctic Oscillation (N/AO) index as seen in the winter (December through February) normalized AO index timeseries as seen in Figure 9 (Bourgain et al., 2013; Nakamura et al., 2015). Previous studies highlight the connection between decadal atmospheric variability in the AO to the Transpolar Drift's strength and

orientation with influence from the circulation patterns of the Beaufort Gyre and Eurasian Basin (Mysak, 2001; Timmermans & Marshall, 2020). The increased N/AO index between 2005–2008 led to a more cyclonic circulation over the Eurasian Basin which diverted river discharge eastward, driving freshwater into the Canadian Basin (Morison et al., 2021). The Russian shelf plays an important role on the communication between the Canadian and Eurasian basins partially determined by the route of the Transpolar Drift and other wind-driven processes (Woodgate et al., 2001). The positive N/AO index during 2007 suggests the White and Kara Seas broadly freshened while the East Siberian Sea and Laptev Sea redistributed the freshwater laterally, possibly causing salinification in these regions (Steele & Ermold, 2004). The loss of FWV on the Russian Shelf Post-2007 compared to Pre-2007, especially seen in the Kara Sea (-391 km^3), may also be explained by the progressive shoaling of the incoming warm, salty Atlantic-origin waters (Bertosio et al., 2022; Polyakov et al., 2017). The shoaling of the isohalines (by 50 m between 2007–2018) near the continental slope coincide with a weakened halocline layer (Bertosio et al., 2022).

We also find that the Russian Shelf's maximum SSS variance occurs in the Kara Sea (~33 psu^2) while its maximum FWC variance occurs along the 200 m isobath in the East Siberian Sea (~5 m^2). The variability of SSS in the Kara Sea is most likely due to the combination of spring to summer sea ice melting, surface wind-driven currents, and propagation of its river plume (Duan et al., 2019; Kubryakov et al., 2016). The Ob and Yenisei rivers discharge into the Kara Sea and are responsible for most of the fresh river water input compared to other major rivers that lead to the Arctic Ocean with strong seasonal and interannual variations (Stein et al. 2004). The large FWC variance in the East Siberian Sea is in proximity to the pathway that the Eurasian Basin's boundary current

flows when crossing the Lomonosov ridge into the Makarov Basin (Woodgate et al. 2001; Aagaard & Carmack, 1989).

The seasonal cycle of FWV also is important to consider when understanding the role that the Russian Shelf has in the Arctic Ocean. Monthly trends of FWV reveal a phenological shift of maximum FWV, suggesting that since 2007, freshwater is increasing sooner in the year (April) relative to before this transition year. This may be tied to earlier sea ice retreat and melting (Peng et al., 2021, Bliss et al., 2019) or increased precipitation in the Arctic (Vihma et al., 2016) that has been favoring rain rather than snow (Ahmed et al., 2020) which does not require melt time that snow needs to become liquid freshwater. Earlier freshening, particularly near coastal and shelf regions, also has a great ecological impact as it can determine the displacement of nutrient-rich waters, their dilution, and thus reduce the amount of production that would be pushed offshore, slowing the drawdown of nutrients as stratification strengthens, and causing smoother primary production gradients between on-shore and off-shore (McClelland et al., 2012). Seasonal anomaly differences of FWC between Pre-2007 and Post-2007 reveal strong contrasts along the continental shelf on either side of the 200 m isobath boundary of the Kara Sea; positive in the winter and spring and negative during summer and autumn seasons.

Changes in the Russian Shelf from increased freshwater import through river runoff and melting sea ice have been linked with a changing global climate (Carmack et al., 2006; Wang et al., 2021b). There is a need for a better understanding of the Arctic Ocean's FWC especially as it approaches a new stage of ice-free summers (Notz & SIMIP Community, 2020). Our results from this study, primarily based on output from the ORAS5 reanalysis, suggest that the FWC and SSS on the Russian Shelf needs to be considered when

understanding and predicting the changes in the Arctic on both spatial and temporal scales. The magnitude, trends, and variability presented in this research highlight the transient state of the Arctic Ocean and the possible transformations they could endure along with climate change.

Table 4.1 Freshwater volume (FWV) of Arctic Ocean regions between 1979–2018 using ORAS5 reanalysis; regions of the Russian shelf are separated into the East Siberian Sea (ESS), Laptev Sea (LS), Kara Sea (KS), and the Barents Sea (BS) and White Sea (WS) combined and bolded values emphasize the difference between Post-2007 (2008–2018) from the Pre-2007 (1997–2018) of the major regions.

Region		FWV (km^3)	% of Arctic FWV	FWV Trend 1979–2018 (km^3/year)	Post-2007 minus Pre-2007 FWV (km^3)
Arctic Ocean		80,763	100	263	**5,266**
Beaufort Gyre		18,407	23	166	**3,690**
Russian Shelf		12,574	16	-16	**-1,276**
	ESS	6,151	8	2	-461
	LS	2,657	3	-9	-337
	KS	3,105	4	-9	-455
	BS +WS	661	1	1	-22

Table 4.2 Average and max variance of deseasoned freshwater content (FWC; m^2) and sea surface salinity (SSS; psu^2) of Arctic Ocean regions between 1979–2018 using ORAS5 reanalysis following Figure 4.7; regions of the Russian shelf are separated into the East Siberian Sea (ESS), Laptev Sea (LS), Kara Sea (KS), and the Barents Sea (BS) and White Sea (WS) combined and bolded values indicate maximum variance from the Arctic subregions.

Region		FWC variance (m^2)		SSS variance (psu^2)	
		Mean	Maximum	Mean	Maximum
Arctic Ocean		0.58	**6.83**	0.43	**32.97**
Beaufort Gyre		1.63	4.73	0.57	6.01
Russian Shelf		0.27	**5.24**	0.79	**32.97**
	ESS	0.68	**5.24**	1.00	7.61
	LS	0.24	4.59	0.78	12.54
	KS	0.21	3.62	1.11	**32.97**
	BS +WS	0.04	2.26	0.14	6.24

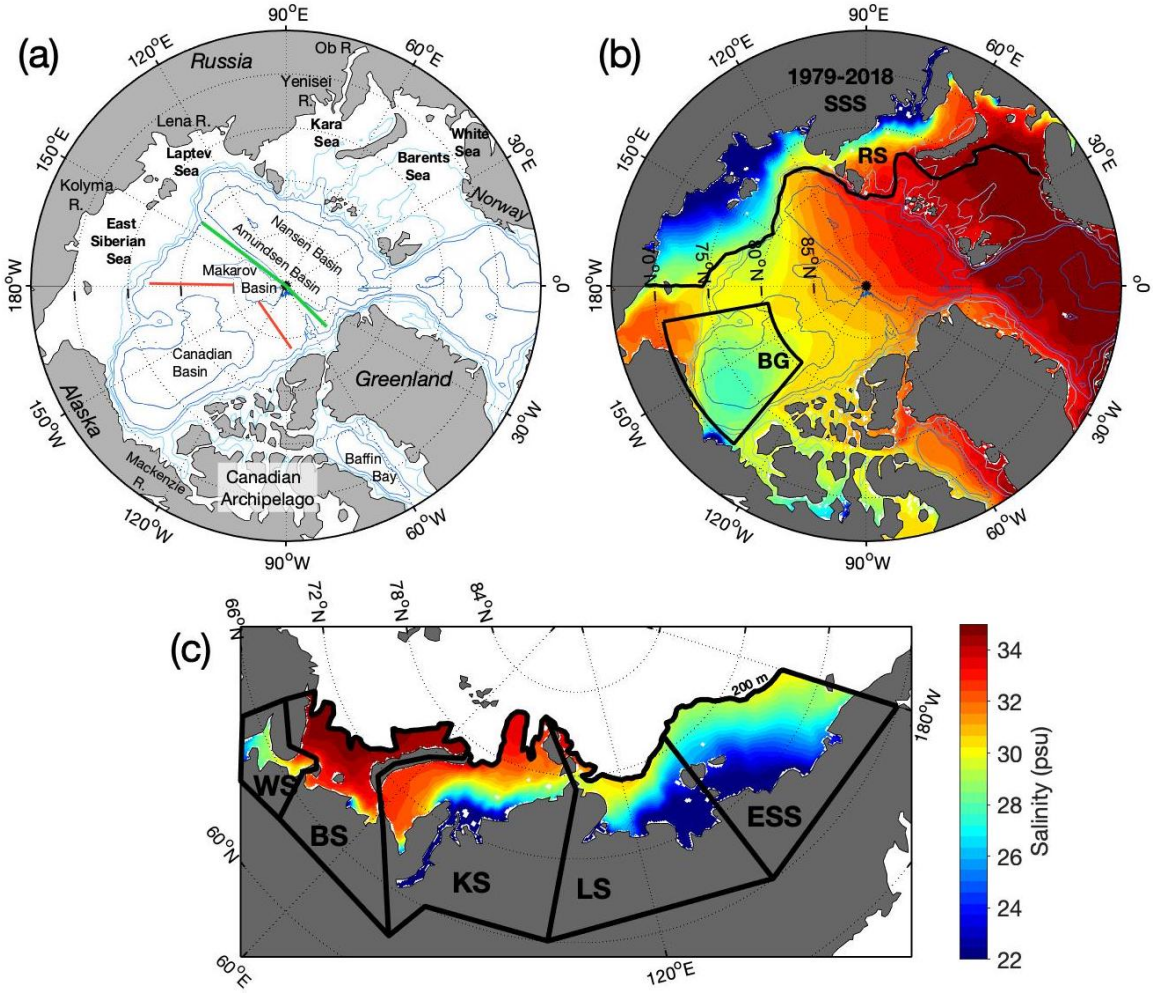

Figure 4.1 (a) Arctic Ocean schematic with geographical labels and bathymetric lines: 200 m (lightest blue), 500 m, 1000 m, 3000 m, 5000 m (darkest blue). Sea surface salinity (SSS; psu) from ORAS5 reanalysis averaged between 1979–2018 over the (b) Arctic Ocean (>66°N) and the (c) Russian shelf region indicated within the 200 m isobath north of Russia between 30°E and 180°E with the East Siberian Sea (ESS), the Laptev Sea (LS), the Kara Sea (KS), the Barents Sea (BS), and the White Sea (WS) regions defined. Major rivers (ending with 'R.') are labeled in near their respective discharge regions, the Lomonosov ridge (green) and the Mendeleev and Alpha ridge (red) are marked as lines in (a). The Russian Shelf (RS) and Beaufort Gyre (BG) regions are outlined in (b).

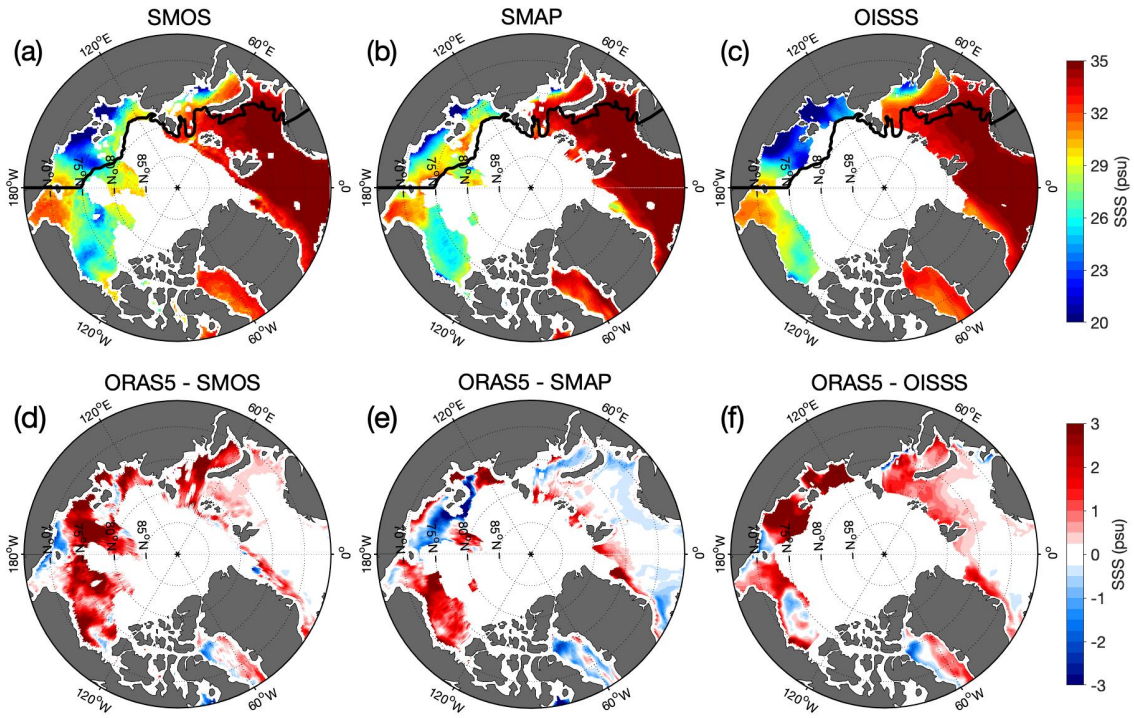

Figure 4.2 Sea surface salinity (SSS; psu) in the Arctic Ocean from (a) SMOS, (b) SMAP, and (c) OISSS satellite observations averaged over the year 2016. Black contour delimits the Russian Shelf region's (see Figure 4.1c). (d-f) Difference between ORAS5 at 0.5 m depth and satellite SSS.

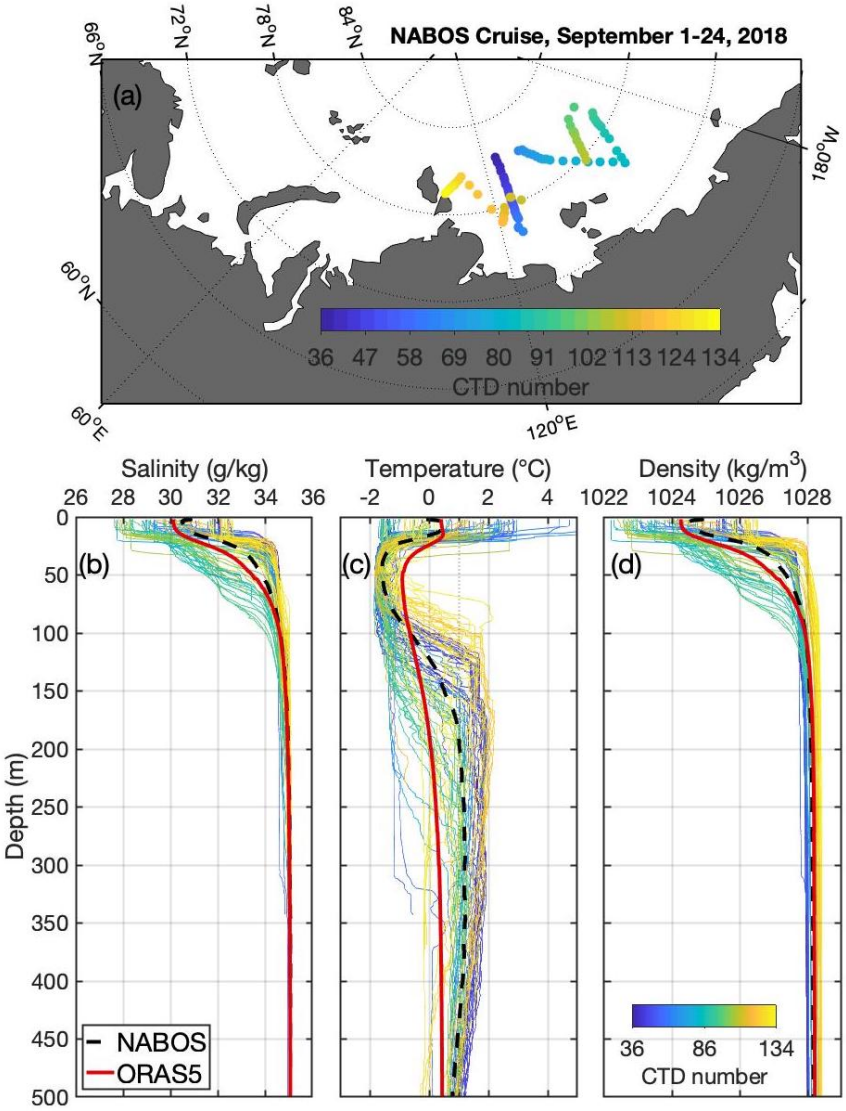

Figure 4.3 (Top) NABOS Cruise CTD data locations taken between September 1–24, 2018 with the respective cast numbers indicated in color. (Bottom) CTD (a) absolute salinity (g/kg) and (b) conservative temperature (°C) were computed from data and (c) density of each cast. Black dashed lines are the CTD averages for each parameter. ORAS5 September data were extracted at nearest latitude and longitude from CTD casts then averaged and absolute salinity and conservative temperature were computed (red line).

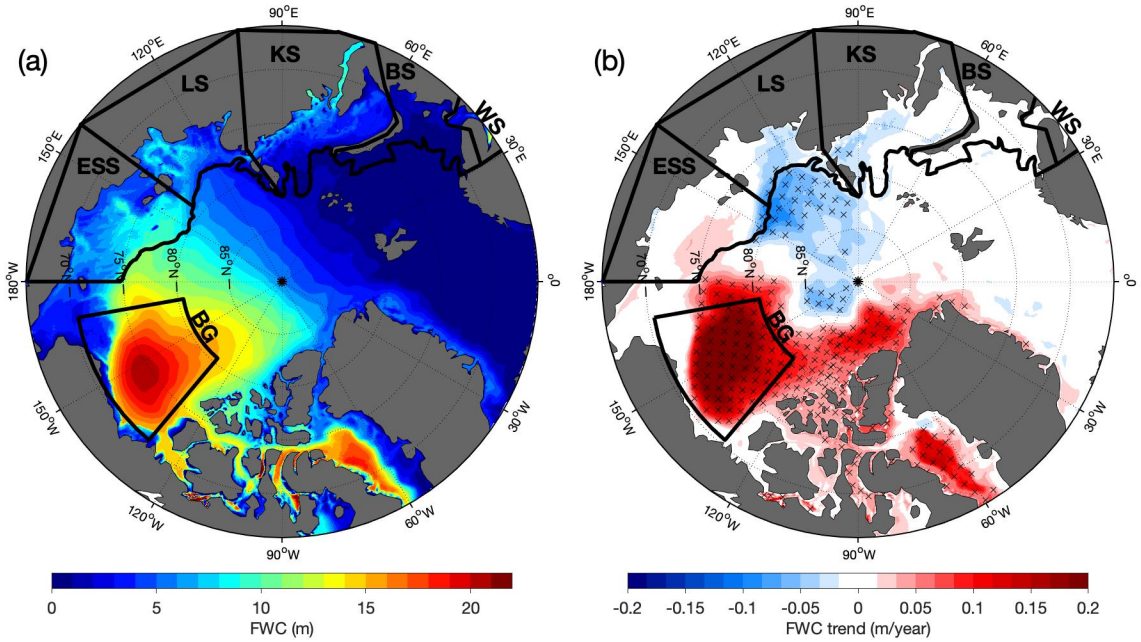

Figure 4.4 Spatial maps of the Arctic Ocean's (a) average Freshwater Content (FWC; m) and (b) FWC trend (m/year) between 1979–2018 with the 200 m (black line) and 2000 m (grey line) bathymetric contours between 30°E–180°E and Russian regions as described in Figure 4.1 and the Beaufort Gyre (BG; black box) region labeled. Stippling shows the statistically significant FWC trend at the 95% confidence level.

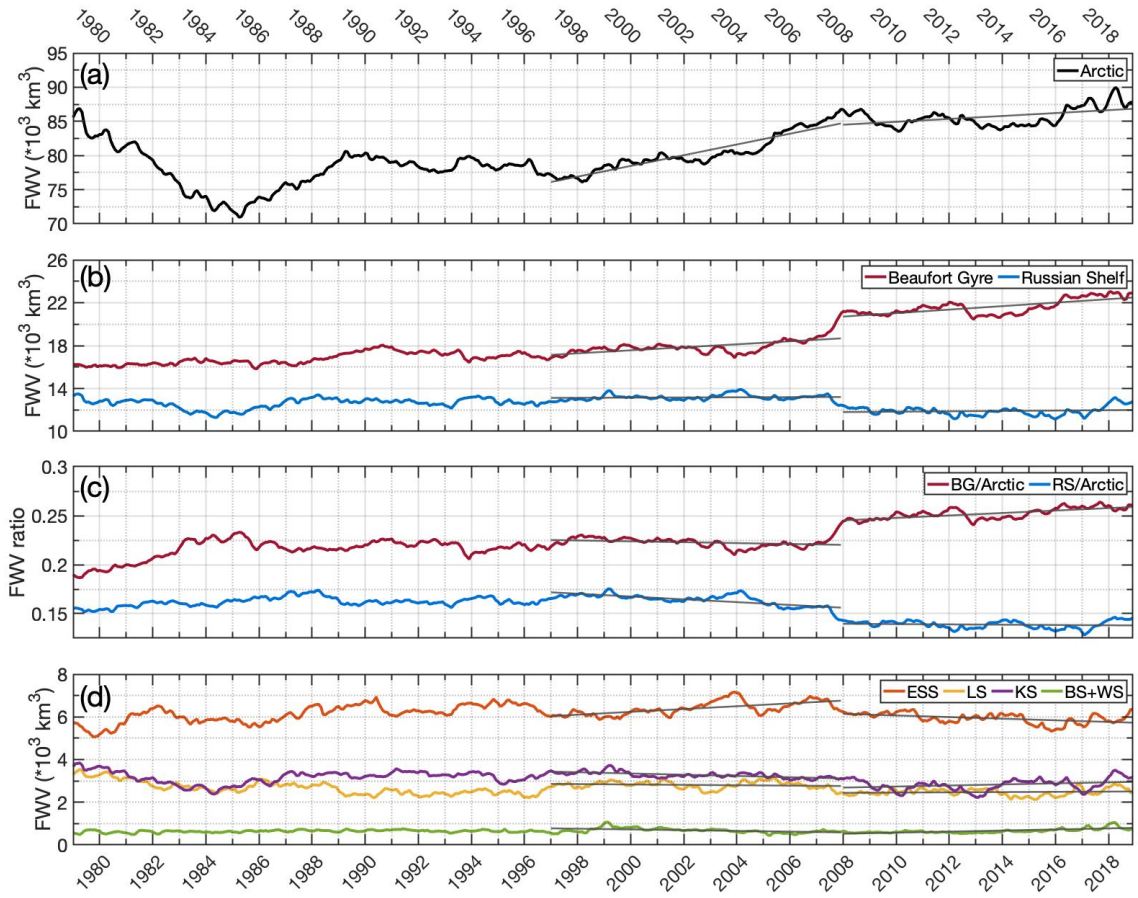

Figure 4.5 Timeseries of deseasoned Freshwater volume (FWV; km^3) between January 1979 – December 2018 for (a) Arctic Ocean above 66°N, (b) the Russian Shelf and the Beaufort Gyre regions, (c) total FWV ratio of the Russian Shelf region (RS) and the Beaufort Gyre region (BG) to the Arctic Ocean region, and the (d) FWV of the subset regions that make up the Russian Shelf including the East Siberian Sea (ESS), the Laptev Sea (LS), the Kara Sea (KS), the Barents Sea (BS), and the White Sea (WS).

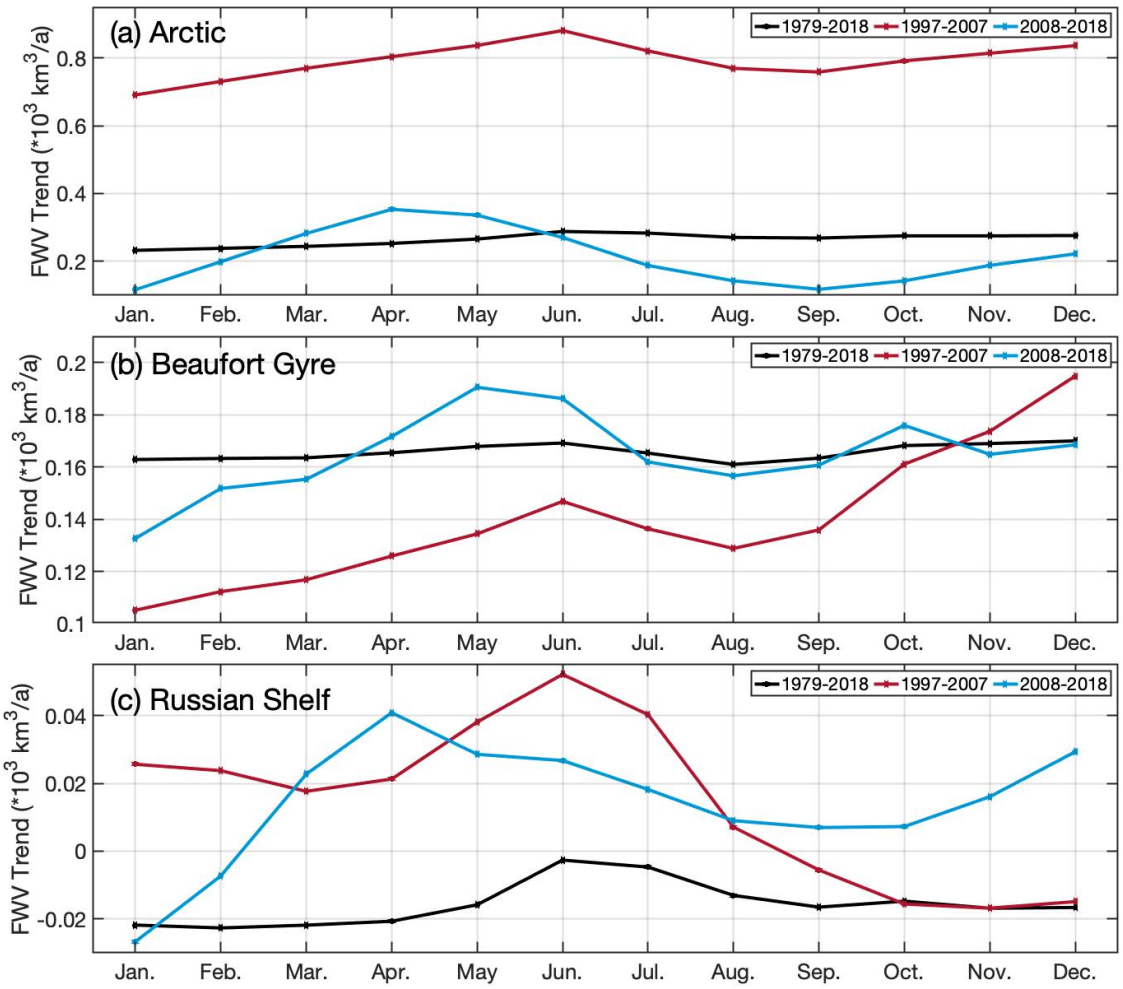

Figure 4.6 Freshwater volume (FWV) monthly trends (km^3/a) for the (a) Arctic Ocean, (b) Beaufort Gyre region, and the (c) Russian Shelf region for the full period: 1979–2018 (black line), Pre-2007 (1997–2007; red line) and the Post-2007 (2008–2018; blue).

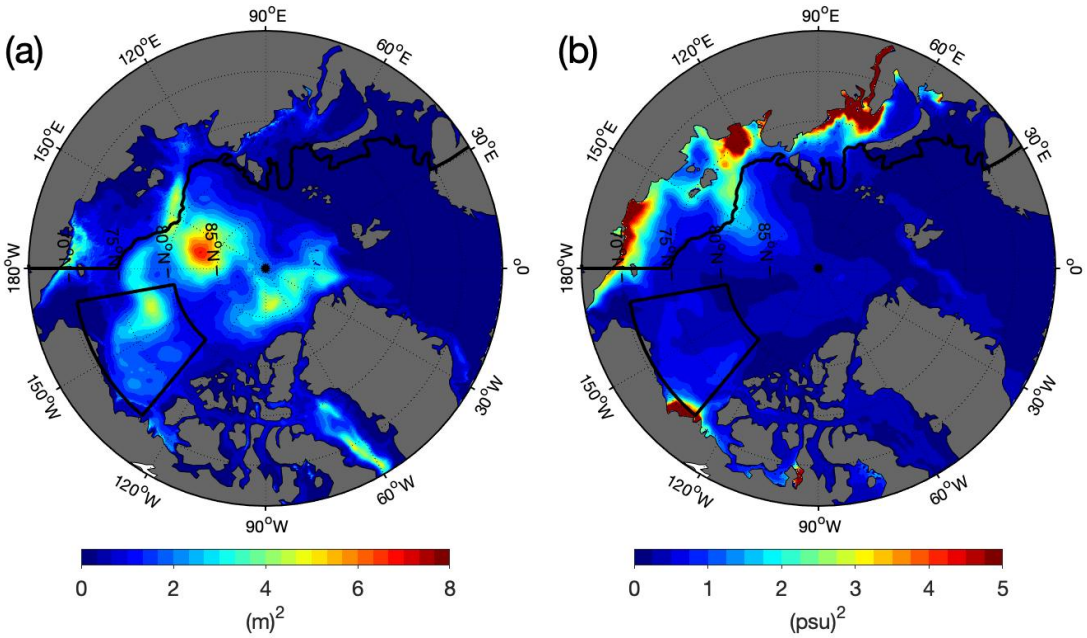

Figure 4.7 Variance of deseasoned and detrended (a) freshwater content (FWC; m^2), and (b) sea surface salinity (psu^2) between 1979–2018 from ORAS5. Boundaries of the Russian Shelf and Beaufort Gyre are outlined in black lines.

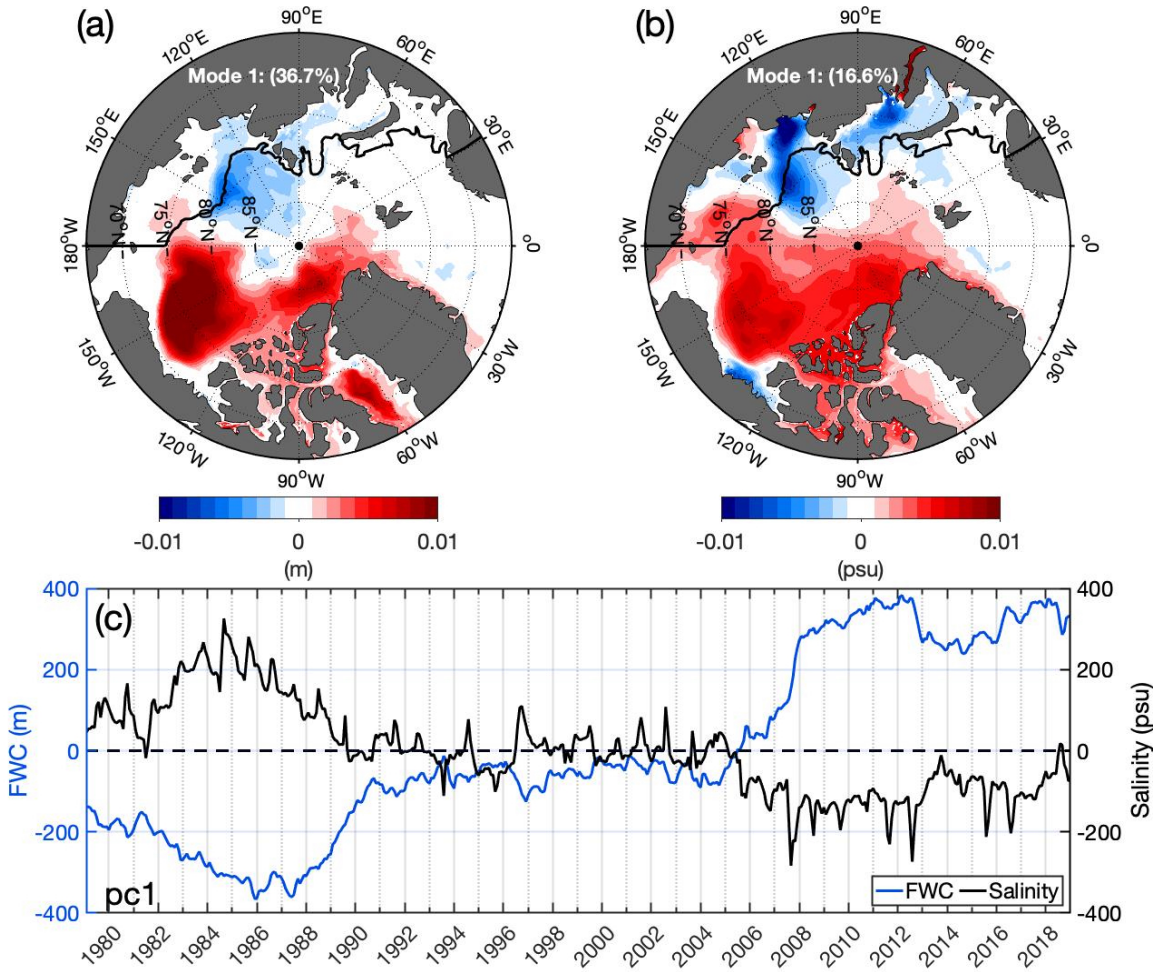

Figure 4.8 First empirical orthogonal function (EOF) of (a) freshwater (FWC; m) and (b) salinity (psu) of the Arctic Ocean (>66°N) between (1979–2018) derived from ORAS5 data. (c) Principal component (PC) time series for FWC (blue) and salinity (black).

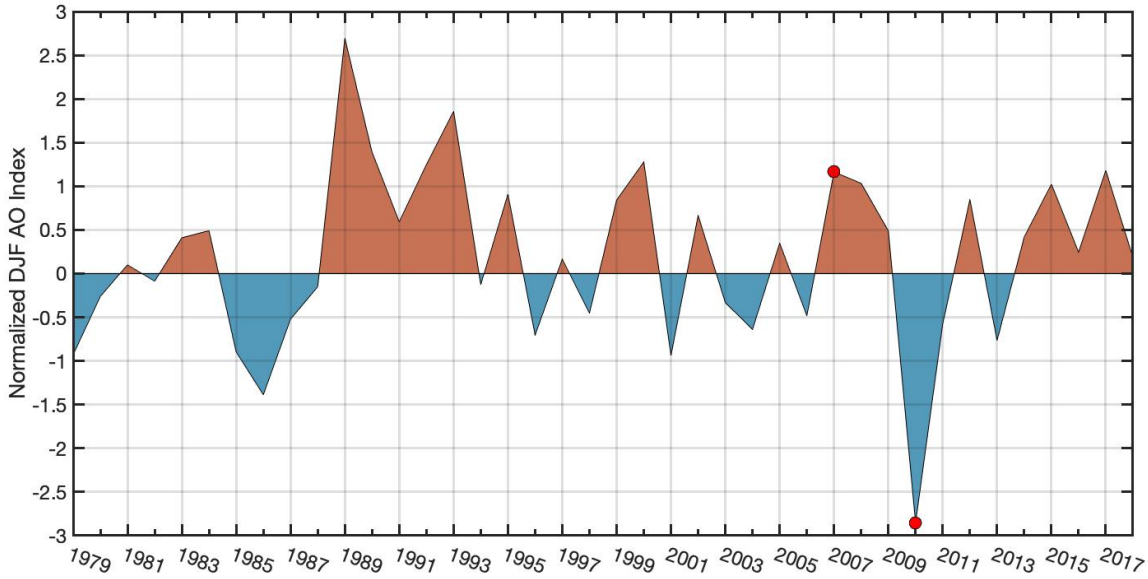

Figure 4.9 Timeseries of AO index averaged over December, January, and February and normalized for the period 1950–2021. Positive (red shading) and negative (blue shading) AO index where years of interest (2007 and 2010) are indicated by red circles. Data obtained from www.ncep.noaa.gov/.

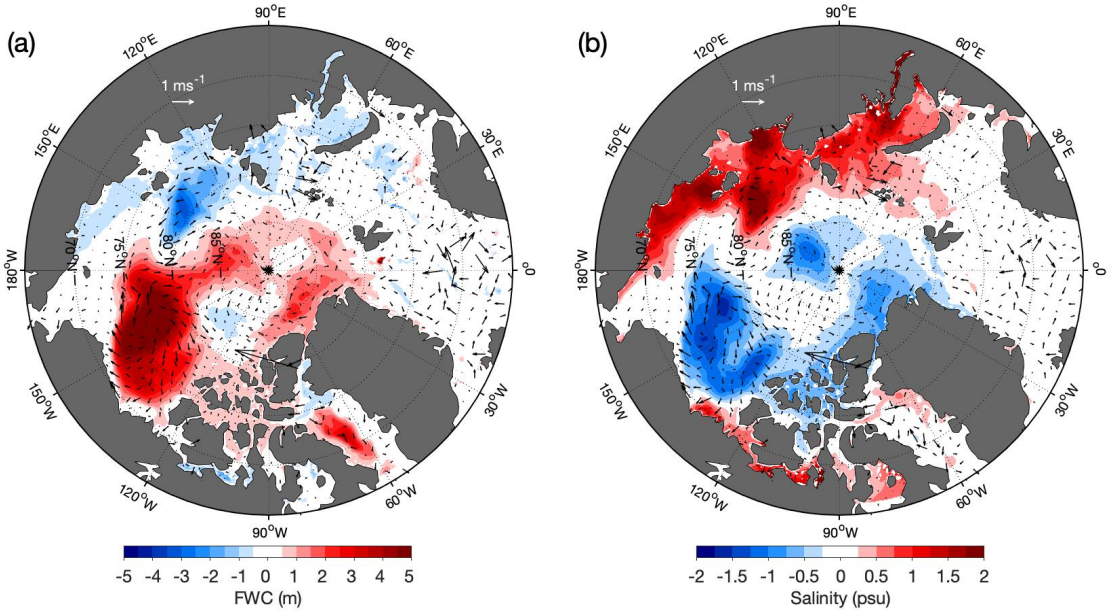

Figure 4.10 ORAS5 differences of new period (2008–2018) minus old period (1979–2007) averages of (a) freshwater content (FWC; m) and (b) sea surface salinity (psu). Black arrows indicate Post-2007 minus Pre-2007 anomalies of current velocities (m/s) averaged over depth of the FWC column and the surface for (c).

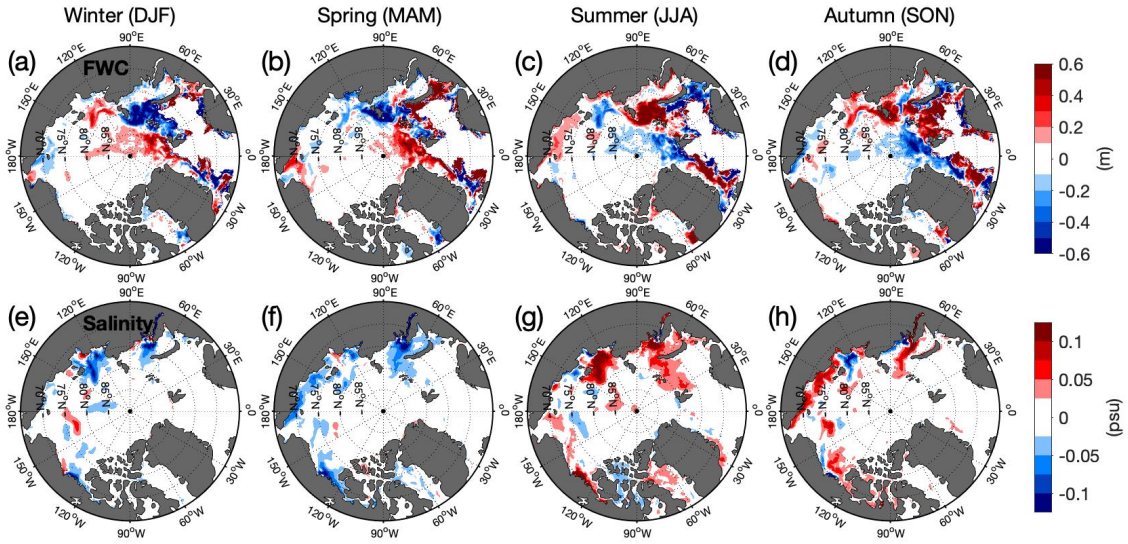

Figure 4.11 ORAS5 differences of Post-2007 (2008–2018) minus Pre-2007 (1997–2007) average anomalies of (first column) winter: December, January, February, (second column) spring: March, April, May, (third column) summer months: June, July, August, and (fourth column) autumn months: September, October, November for (a-d) freshwater content (FWC; m) and (e-h) sea surface salinity (SSS; psu).

CHAPTER 5

CONCLUSIONS

The Arctic Ocean has changed in unprecedented ways, where sea ice is rapidly declining, major river discharge is increasing, and heightened freshwater export to the North Atlantic Ocean may have detrimental effects on the AMOC system and thus consequences to the global climate (Yamamoto et al., 2012; Kacimi & Kwok, 2022; Peterson et al., 2002; Wang et al., 2018b). Therefore, studies such as those presented in this dissertation are necessary to advance the understanding of the Arctic Ocean and the changes in salinity as freshwater increases. However, because of the reasons previously examined, the lack of observations in the Arctic Ocean can lead to flawed models. A vast array of *in situ* observations, satellite measurements, and ocean model estimations were employed to determine the bias, validity, and analyze different parameters in the Arctic. This study highlights discrepancies between products and emphasizes the importance of advancements in ocean model estimates.

This dissertation focused on physical oceanographic processes that are influenced by salinity-driven density structure in the Arctic Ocean through recent climatic changes. While the focus of each chapter covered different facets of exploring freshwater in the Arctic Ocean, they all highlight the need for continued observations at high spatial and temporal resolutions to improve our models and better understand how the Arctic Ocean is changing. It is the hope of the author that the results of this dissertation aid in the

understanding of the upcoming changes to be expected of the Arctic and to grow awareness of the continued need for Arctic research.

The everchanging conditions of the Arctic Ocean also show direct and indirect impacts towards indigenous communities, national security of maritime advancement with the melting of sea ice, and the freshwater export to the AMOC that is responsible for the global circulation and the regulation of Earth's climate (Huntington et al., 2022).

Chapter 2 delineates freshwater flux between the Arctic Ocean region and adjacent seas. Particular interest was set on comparing years of high and low summer sea ice extent and how the freshwater flux, other oceanographic features (SST, SIC, surface current velocities) and atmospheric processes (wind velocities) differed. A commonality between the focused years was that the Kara Sea had the greatest SST anomalies during years of low sea ice extent while the Laptev Sea and the Bering Strait region had the lowest SST anomalies. Most importantly, increasing export of surface freshwater through the Fram Strait was found.

In Chapter 3, the validity of ocean models and reanalysis products were tested against observations, particularly in the BG region. L-band radiometry methods used by satellites are highly sensitive to measuring salinity in cold waters, and therefore the remote sensing-based data was restricted to ice-free regions and to surface measurements. Prevailingly, ORAS5 showed the smallest difference to *in situ* observations when compared to the other salinity products at the surface (-0.052 bias) and at depth. The spatial and total FWC between EN4 analysis product and the ocean models were calculated. Although ORAS5 had closer values in total FWC in the BG, ECCO and GLORY12 did better when FWC was considered for the Arctic Basin. While observations can be restricted

due to sea ice, ocean models will help fill this data gap; however, this study motivates improvement for model estimates to become more accurate.

The Russian Shelf, a region not as well observed and therefore has limitations in our understanding of its freshwater contributions to the Arctic Ocean, was examined in Chapter 4. This study investigated the role of sea surface salinity and freshwater content in the Russian Shelf over a four-decadal period between 1979–2018. Using ORAS5, it was found that the Russian Shelf makes up around 16% of the Arctic Ocean's total FWC. A negative FWC trend was computed for the Russian Shelf (-15.63 km^3/year), with the most influenced by the Kara and Laptev Seas. During the summer of 2007, the study discovered a notable regime shift in which the Russian Shelf and BG simultaneously experienced a decrease and increase in FWC. AO seems to take a large impact on this change as, during 2007, the positive, winter AO reached its peak. During a positive AO, the Transpolar Drift moves water along the shelf and into the Canadian Basin. Neglecting FWC on the Russian Shelf during an instance such as the 2007 regime transition could result in an error of ~25% from the total Arctic Ocean's FWC.

While this work was able to address many essential aspects of oceanography in the Arctic, many more unanswered questions or worthy of further study. Specifically, regions that lack the necessary data for interannual and decadal analysis will need to be examined. These implications will help improve our understanding of the air-sea dynamics on previous and future expectations for this important region. An updated report of freshwater volume transport through major straits through the use of high spatial and temporal resolution ocean models is needed. The focus should be on the freshwater export towards the AMOC; especially the role of interannual and decadal salinity variability in the Arctic

on the AMOC regime. Future analysis of salinity product comparisons should incorporate different models and delineate the components of each that contribute toward accurate salinity values in such high latitudes. Finally, identification should be made between the BG dynamics and characteristics that favor anomalous freshening (e.g. wind stress curl, gyre strength and size, Ekman pumping).

REFERENCES

Aagaard, K., & Carmack, E.C. (1989). The role of sea ice and fresh water in the Arctic circulation. *Journal of Geophysical Research: Oceans, 94*(C10), 14485–14498. https://doi.org/10.1029/JC094iC10p14485

Aagaard, K., & R. A. Woodgate (2001). Some Thoughts on the Freezing and Melting of Sea Ice and their Effects on the Ocean. *Ocean Modelling, 3*, 127–135. https://doi.org/10.1016/S1463-5003(01)00005-1

Ahmed, R., Prowse, T., Dibike, Y., Bonsal, B., & O'Neil, H. (2020). Recent trends in freshwater influx to the Arctic Ocean from four major Arctic-draining rivers. *Water, 12*, 1189. https://doi.org/10.3390/w12041189

Anderson, L. G., Bjork, G., Holby, O. Jones, E.P., Kattner, G., Koltermann, K.P., et al. (1994). Water masses and circulation in the Eurasian Basin_Results from the Oden 91 expedition. *Journal of Geophysical Research, 99*, 3273–3283, https://doi.org/10.1029/93JC02977

Anderson L. G., & Macdonald R. W. (2015). Observing the Arctic Ocean Carbon Cycle in a Changing Environment. *Polar Research, 34*. https://doi.org/10.3402/polar.v34.26891

Armitage, T. W. K., Bacon, S., Ridout, A. L., Petty, A. A., Wolbach, S., & Tsamados, M. (2017). Arctic Ocean surface geostrophic circulation 2003–2014. *The Cryosphere, 11*, 1767–1780. https://doi.org/10.5194/tc-11-1767-2017

Armitage, T. W. K., Manucharyan, G. E., Petty, A. A., Kwok R., & Thompson, A. F. (2020). Enhanced eddy activity in the Beaufort Gyre in response to sea ice loss. *Nature Communications, 11*, 761. https://doi.org/10.1038/s41467-020-14449-z

Aune, M., Aniceto, S., Biuw, M., Daase, M., Falk-Petersen, S., Leu, E., Ottesen, C., Sagerup, K., & Camus, L. (2018). Seasonal ecology in ice-covered Arctic seas-Considerations for spill response decision making. *Marine Environmental Research, 141*, 275-288. https://doi.org/10.1016/j.marenvres.2018.09.004

Bamber, J., van den Broeke, M., Ettema, J., Lenaerts, J., & Rignot, E. (2012). Recent Large Increases in Freshwater Fluxes from Greenland into the North Atlantic. *Geophysical Research Letters, 39*, L19501. https://doi.org/10.1029/2012GL052552

Bao, S., Wang, H., Zhang, R., Yan, H., & Chen, J. (2019). Comparison of Satellite-Derived Sea Surface Salinity Products from SMOS, Aquarius, and SMAP. *Journal of Geophysical Research*, *124*, 1932–1944. https://doi.org/10.1029/2019jc014937

Bertosio, C., Provost, C., Athanase, M., Sennéchael, N., Garric, G., Lellouche, J.-M., et al. (2022). Changes in Freshwater Distribution and Pathways in the Arctic Ocean Since 2007 in the Mercator Ocean Global Operational System. *Journal of Geophysical Research: Oceans, 127*(6), e2021JC017701. https://doi.org/10.1029/2021JC017701

Bingham, F., Brodnitz, S., & Yu, L. (2020). Sea Surface Salinity Seasonal Variability in the Tropics from Satellites, Gridded In Situ Products and Mooring Observations. *Remote Sensing, 13*, 110. https://doi.org/10.3390/rs13010110

Bliss, A. C., Steele, M. S., Peng, G., Meier, W. N., & Dickinson, S. (2019). Regional Variability of Arctic Sea Ice Seasonal Change Climate Indicators from a Passive Microwave Climate Data Record. *Environmental Research Letters, 14*(4), 045003. https://doi. org/10.1088/1748-9326/aafb84

Boé, J., Hall, A., & Qu, X. (2009). September Sea-Ice Cover in the Arctic Ocean Projected to Vanish by 2100. *Nature Geoscience, 2*, 341–343. https://doi.org/10.1038/ngeo467

Bourgain, P., Gascard, J., Shi, J., & Zhao, J. (2013). Large-scale temperature and salinity changes in the upper Canadian Basin of the Arctic Ocean at a time of a drastic Arctic Oscillation inversion. *Ocean Science Discussions, 9*, 447-460. https://doi.org/10.5194/os-9-447-2013

Boutin, J., Vergely, J. L., Marchand, S., D'Amico, F., Hasson, A., Kolodziejczyk, N., Reul, N., Reverdin, G., & Vialard, J. (2018). New SMOS Sea Surface Salinity with Reduced Systematic Errors and Improved Variability. *Remote Sensing of Environment, 214*,115-134. https://doi.org/10.1016/j.rse.2018.05.022

Breivik, Ø., Mogensen, K., Bidlot, J.-R., Balmaseda, M. A., & Janssen, P. A. E. M. (2015). Surface wave effects in the NEMO ocean model: Forced and coupled experiments. *Journal of Geophysical Research: Oceans, 120*, 2973–2992. https://doi.org/10.1002/2014jc010565

Brown, N. J., Nilsson, J., & Pemberton, P. (2019). Arctic Ocean Freshwater Dynamics: Transient Response to Increasing River Runoff and Precipitation. *Journal of Geophysical Research: Oceans, 124*. https://doi.org/10.1029/2018JC014923

Brown K. A., Holding J. M., & Carmack E. C. (2020). Understanding regional and seasonal variability is key to gaining a pan-Arctic perspective on Arctic Ocean freshening. *Frontiers in Marine Science, 7*. https://doi.org/10.3389/fmars.2020.00606

Carmack, E., McLaughlin, F., Yamamoto-Kawai, M., Itoh, M., Shimada, K., Krishfield, R., & Proshutinsky, A. (2008). Freshwater Storage in the Northern Ocean and the Special Role of the Beaufort Gyre. In: Dickson, R. R., Meincke, J., Rhines, P. (eds)

Arctic–Subarctic Ocean Fluxes, Springer, Dordrecht, 145-170. https://doi.org/10.1007/978-1-4020-6774-7_8

Carmack, E., Barber, D., Christensen, J., Macdonald, R., Rudels, B., & Sakshaug, E. (2006). Climate variability and physical forcing of the food webs and the carbon budget of panArctic shelves. *Progress in Oceanography, 71*, 145–181. https://doi.org/10.1016/j.pocean.2006.10.005

Carmack, E. C., Yamamoto-Kawai, M., Haine, T. W. N., Bacon, S., Bluhm, B. A., Lique, C., et al. (2016). Freshwater and its role in the Arctic Marine System: Sources, Disposition, Storage, Export, and Physical and Biogeochemical Consequences in the Arctic and Global Oceans. *Journal of Geophysical Research: Biogeoscience, 121*(3), 675–717. https://doi.org/10.1002/2015JG003140

Carr, G. , Crosbie, J., Lundgren, P., Peissel, N., Pett, P., Turner, W., et al. (2021). The 2017 Mission Arctic Citizen Science Sailing Expedition Conductivity, Temperature, and Depth Profiles in Western Greenland and Baffin Bay. *Frontiers in Marine Science, 8*, 665582. https://doi.org/10.3389/fmars.2021.665582

Carton, J. A., Penny, S., & Kalnay, E. (2019) Temperature and Salinity Variability in the SODA3, ECCO4r3, and ORAS5 Ocean Reanalyses, 1993–2015. *Journal of Climatology, 32*, 2277–2293. https://doi.org/10.1175/jcli-d-18-0605.1

Carvalho, K.S., & Wang, S. (2020). Sea Surface Temperature Variability in the Arctic Ocean and Its Marginal Seas in a Changing Climate: Patterns and Mechanisms. Global and Planetary Change, 193, 103265. https://doi.org/10.1016/j.gloplacha.2020.103265

Caesar, L., McCarthy, G. D., Thornalley, D. J. R., Cahill, N., & Rahmstorf, S. (2021). Current Atlantic Meridional Overturning Circulation Weakest in Last Millennium. *Nature Geoscience, 14*, 118–120. https://doi.org/10.1038/s41561-021-00699-z

Chassignet, E. P., Hurlburt, H. E., Metzger, E. J., Smedstad, O. M., Cummings, J. A., Halliwell, et al. (2009). US GODAE: Global Ocean Prediction with the HYbrid Coordinate Ocean Model (HYCOM). *Oceanography, 22*, 64–75. https://doi.org/10.5670/oceanog.2009.39

Chao, Y., Li, Z., Farrara, J. D., & Hung, P. (2009). Blending Sea Surface Temperatures from Multiple Satellites and In Situ Observations for Coastal Oceans. *Journal of Atmospheric and Oceanic Technology, 26*(7), 1415-1426. https://doi.org/10.1175/2009JTECHO592.1

Cole, S. T., & Stadler, J. (2019). Deepening of the Winter Mixed Layer in the Canada Basin, Arctic Ocean Over 2006–2017. *Journal of Geophysical Research: Oceans*, *124*, 4618–4630. https://doi.org/10.1029/2019jc014940

Comiso, J. C., Parkinson, C.L., Gersten, R., & Stock, L. (2008). Accelerated Decline in the Arctic Sea Ice Cover. *Geophysical Research Letters, 35*, L01703. https://10.1029/2007GL031972

Cornish, S. B., Kostov, Y., Johnson, H. L., & Lique, C. (2020). Response of Arctic Freshwater to the Arctic Oscillation in Coupled Climate Models. *Journal of Climate, 33*(7), 2533-2555. https://doi.org/10.1175/JCLI-D-19-0685.1

de Steur, L., Peralta-Ferriz, C., Pavlova, O. (2018). Freshwater Export in the East Greenland Current Freshens the North Atlantic. *Geophysical Research Letters, 45*(24), 13359–13366. https://doi.org/10.1029/2018GL080207

de Steur, L., Pickart, R. S., Macrander, A., Våge, K., Harden, B., Jónsson, S., Østerhus, S., & Valdimarsson, H. (2017). Liquid Freshwater Transport Estimates from the East Greenland Current Based on Continuous Measurements North of Denmark Strait. *Journal of Geophysical Research: Oceans. 122*(1), 93-109. https://doi.org/10.1002/2016JC012106

de Steur, L., Steele, M., Hansen, E., Morison, J., Polyakov, I., Olsen, S.M., et al. (2013). Hydrographic Changes in the Lincoln Sea in the Arctic Ocean with Focus on an Upper Ocean Freshwater Anomaly Between 2007 and 2010. *Journal of Geophysical Research: Oceans, 118*, 4699–4715. https://doi.org/10.1002/jgrc.20341

di Lorenzo, E., & Mantua, N. (2016). Multi-Year Persistence of the 2014/15 North Pacific Marine Heatwave. *Nature Climate Change, 6*, 1042–1047, https://doi.org/10.1038/nclimate3082

Davis, P. E. D., Lique, C., Johnson, H. L., & Guthrie, J. D. (2016). Competing Effects of Elevated Vertical Mixing and Increased Freshwater Input on the Stratification and Sea Ice Cover in a Changing Arctic Ocean. *Journal of Physical Oceanography, 46,* 1531–1553. https://doi.org/10.1175/JPO-D-15-0174.1

Dee, D. P., Uppala, S. M., Simmons, A. J., Berrisford, P., Poli, P., Kobayashi, et al. (2011). The ERA-Interim Reanalysis: Configuration and Performance of the Data Assimilation System. Quarterly *Journal of the Royal Meteorological Society, 137*(656), 553–597. https://doi.org/10.1002/qj.828

Dewey, S.R., Morison, J.H., & Zhang, J. (2017). An Edge-Referenced Surface Fresh Layer in the Beaufort Sea Seasonal Ice Zone. *Journal of Physical Oceanography, 47*, 1125–1144. https://doi.org/10.1175/jpo-d-16-0158.1

Docquier, D., & Koenigk, T. (2021). Observation-based Selection of Climate Models Projects Arctic Ice-free Summers Around 2035. *Communications Earth & Environment, 2*, 144. https://doi.org/10.1038/s43247-021-00214-7

Dodd, P. A., Heywood, K .J., Meredith, M. P., Naveira-Garabato, A. C., Marca, A. D., & Falkner, K. K. (2009). Sources and Fate of Freshwater Exported in the East Greenland Current. *Geophysical Research Letters, 36*(19), https://doi.org/10.1029/2009GL039663

Duan, C., Dong, S., Xie, Z., & Wang, Z. (2019). Temporal Variability and Trends of Sea Ice in the Kara Sea and their Relationship with Atmospheric Factors. *Polar Science, 20*, 136-147. https://doi.org/10.1016/j.polar.2019.03.002

Dukhovskoy, D. S., Myers, P.G., Platov, G., Timmermans, M.-L. et al. (2016), Greenland Freshwater Pathways in the Sub-Arctic Seas from Model Experiments with Passive Tracers. *Journal of Geophysical Research: Oceans, 121*, 877– 907. https://doi.org/10.1002/2015JC011290

ECCO Consortium, Fukumori, I., Wang, O., Fenty, I., Forget, G., Heimbach, P., Ponte, R.M. ECCO Central Estimate (Version 4 Release 4). Retrieved from https://ecco.jpl.nasa.gov/drive/files/Version4/Release4/nctiles_daily (accessed on 22 Februrary 2021)

Feng, D., Gleason, C.J., Lin, P., Yang, X., Pan, M., & Ishitsuka, Y. (2021). Recent Changes to Arctic River Discharge. *Nature Communications, 12*, 6917. https://doi.org/10.1038/s41467-021-27228-1

Fetterer, F., Knowles, K., Meier, W. N., Savoie, M., & Windnagel, A.K. (2017). Sea Ice Index, Version 3. Boulder, Colorado USA. NSIDC: National Snow and Ice Data Center https://doi.org/10.7265/N5K072F8

Forget, G., Campin, J.-M., Heimbach, P., Hill, C. N., Ponte, R.M., & Wunsch, C. (2015). ECCO version 4: An Integrated Framework for Non-Linear Inverse Modeling and Global Ocean State Estimation. *Geoscientific Model Development, 8*, 3071–3104. https://doi.org/10.5194/gmd-8-3071-2015.

Fournier, S., Lee, T., Wang, X., Armitage, T. W. K., Wang, O., Fukumori, I., & Kwok, R. (2020). Sea Surface Salinity as a Proxy for Arctic Ocean Freshwater Changes. *Journal of Geophysical Research: Oceans*, *125*, e2020JC016110. https://doi.org/10.1029/2020jc016110

Fournier, S., Lee, T., Tang, W., Steele, M., & Olmedo, E. (2019) Evaluation and Intercomparison of SMOS, Aquarius, and SMAP Sea Surface Salinity Products in the Arctic Ocean. *Remote Sensing, 11*, 3043. https://doi.org/10.3390/rs11243043

Fore, A. G., Yueh, S. H., Tang, W., Stiles, B. W., & Hayashi, A.K. (2016). Combined Active/Passive Retrievals of Ocean Vector Wind and Sea Surface Salinity With SMAP. *IEEE Transactions on Geoscience and Remote Sensing, 54*(12), 7396-7404. https://doi.org/10.1109/TGRS.2016.2601486

Francis, J. A., & Wu, B. (2020). Why Has No New Record-Minimum Arctic Sea-Ice Extent Occurred since September 2012? *Environmental Research Letters, 15* 114034. https://doi.org/10.1088/1748-9326/abc047

Francis, J. A., Chan, W., Leathers, D. J., Miller, J. R., & Veron, D.E. (2009) Winter Northern Hemisphere Weather Patterns Remember Summer Arctic Sea-Ice Extent. *Geophysical Research Letters, 36*(7) L07503. https://doi.org/10.1029/2009GL037274

Fuentes-Franco, R. & Koenigk, T. (2019). Sensitivity of the Arctic Freshwater Content and Transport to Model Resolution. *Climate Dynamics, 53,* 1765–1781. https://doi.org/10.1007/s00382-019-04735-y

Fukumori, I., Wang, O., Fenty, I., Forget, G., Heimbach, P., & Ponte, R.M. (2021). Synopsis of the ECCO Central Production Global Ocean and Sea-Ice State Estimate, Version 4 Release 4 (Version 4 Release 4). *Zenodo*. Available online: https://ecco.jpl.nasa.gov/drive/files/Version4/Release4/nctiles_daily (accessed on 22 Februrary 2021)

Gascard, J. C., G. Raisbeck, S. Sequeira, F. Yiou, & K. A. Mork (2004). The Norwegian Atlantic Current in the Lofoten Basin Inferred from Hydrological and Tracer Data (I-129) and its Interaction with the Norwegian Coastal Current. *Geophysical Research Letters, 31*, L01308. https://doi.org/10.1029/2003GL018303.

GEBCO Compilation Group. (2022). GEBCO_2022 Grid. https://doi.org/10.5285/e0f0bb80-ab44-2739-e053-6c86abc0289c

Giles, K. A., Laxon, S. W., Ridout, A. L., Wingham, D. J., & Bacon, S. (2012). Western Arctic Ocean Freshwater Storage Increased by Wind-Driven Spin-up of the Beaufort Gyre. *Nature Geoscience, 5*(3), 194-197. https://doi.org/10.1038/ngeo1379

Good, S.A., Martin, M. J., & Rayner, N. A. (2013). EN4: Quality Controlled Ocean Temperature and Salinity Profiles and Monthly Objective Analyses with Uncertainty Estimates. *Journal of Geophysical Research: Oceans, 118*(12), 6704–6716. https://doi.org/10.1002/2013JC009067.

Greene, C. A., Thirumalai, K., Kearney, K. A., Delgado, J. M., Schwanghart, W., Wolfenbarger, N. S., et al. (2019). The Climate Data Toolbox for MATLAB. *Geochemistry, Geophysics, Geosystems, 20*(7), 3774-3781. https://doi.org/10.1029/2019GC008392

Guarino, M. V., Sime, L. C., Schröeder, D., Malmierca-Vallet, I., Rosenblum, E., Ringer, M., et al. (2020). Sea-ice-free Arctic During the Last Interglacial Supports Fast Future Loss. *Nature Climate Change, 10*, 928–932. https://doi.org/10.1038/s41558-020-0865-2

Haine, T. W. N., Curry, B., Gerdes, R., Hansen, E., Karcher, M., Lee, C., et al. (2015). Arctic Freshwater Export: Status, Mechanisms, and Prospects. *Global and Planetary Change, 125*, 13–35. https://doi.org/10.1016/j.gloplacha.2014.11.013

Hall, S. B., Subrahmanyam, B., & Morison, J. H. (2022). Intercomparison of Salinity Products in the Beaufort Gyre and Arctic Ocean. *Remote Sensing, 14*(1), 71. https://doi.org/10.3390/rs14010071

Harms, I. H., & Karcher, M. J. (2005). Kara Sea Freshwater Dispersion and Export in the Late 1990s. *Journal of Geophysical Research, 110*, C08007. https://doi.org/10.1029/2004JC002744

Hartmann, D. L. (2015). Pacific Sea Surface Temperature and the Winter of 2014. *Geophysical Research Letters, 42*(6), 1894-1902. https://doi.org/10.1002/2015GL063083

Houpert, L., Inall, M., Dumont, E., Gary, S., Johnson, C., Porter, M., Johns, W., & Cunningham, S. (2018). Structure and Transport of the North Atlantic Current in the Eastern Subpolar Gyre From Sustained Glider Observations. *Journal of Geophysical Research: Oceans, 123*(8), 6019-6038. https://doi.org/10.1029/2018JC014162

Hu, Z. Z., Kumar, A., Jha, B., Zhu, J., & Huang, B. (2017). Persistence and Predictions of the Remarkable Warm Anomaly in the Northeastern Pacific Ocean during 2014–2016. *Journal of Climate, 30*(2), 689-702. https://doi.org/10.1175/JCLI-D-16-0348.1

Hunke, E.C., & Lipscomb, W. (2008). CICE: The Los Alamos Sea Ice Model, Documentation and Software User's Manual, Version 4.0; Tech. rep. LA-CC-06-012; Los Alamos National Laboratory: Los Alamos, NM, USA.

Huntington, H. P., Zagorsky, A., Kaltenborn, B.P., Shin, H. C., Dawson, J, Lukin, M. (2022) Societal Implications of a Changing Arctic Ocean. *Ambio, 51*, 298–306. https://doi.org/10.1007/s13280-021-01601-2

Jackson, J., Williams, W. J., & Carmack, E. C. (2012). Winter Sea-Ice Melt in the Canada Basin, Arctic Ocean. *Geophysical Research Letters, 39*, L03603. https://doi.org/10.1029/2011gl050219

Jahn, A., Aksenov, Y., de Cuevas, B. A., de Steur, L., Häkkinen, S., Hansen, E., et al. (2012). Arctic Ocean Freshwater: How Robust Are Model Simulations? *Journal of Geophysical Research: Oceans, 117*(C8), C00D16. https://doi.org/10.1029/2012JC007907

Jahn, A., Tremblay, B., Mysak, L., & Newton, R. (2010). Effect of the Large-scale Atmospheric Circulation on the Variability of the Arctic Ocean Freshwater Export. Climate Dynamics, 34. 201–222. https://doi.org/10.1007/s00382-009-0558-z

Johnson, H. L., Cornish, S. B., Kostov, Y., Beer, E., & Lique, C. (2018). Arctic Ocean Freshwater Content and its Decadal Memory of Sea-level Pressure. Geophysical Research Letters, 45, 4991–5001. https://doi.org/10.1029/2017GL076870

Josey, S. A., & Marsh, R. (2005). Surface Freshwater Flux Variability and Recent Freshening of the North Atlantic in the Eastern Subpolar Gyre. *Journal of Geophysical Research: Oceans, 110*, 1–17, C05008. https://doi.org/10.1029/2004JC002521

Jung, O., Sung, M. K., Sato, K., Lim, Y. K., Kim, S. J., Baek, E. H., Jeong, J. H., & Kim, B. M. (2017). How Does the SST Variability over the Western North Atlantic Ocean Control Arctic Warming over the Barents–Kara Seas? *Environmental Research Letters, 12*(3), 034021. https://doi.org/10.1088/1748-9326/aa5f3b

Kalnay, E., Kanamitsu, M., Kistler, R., Collins, W., Deaven, D., Gandin, L., et al. (1996). The NCEP/NCAR 40-Year Reanalysis Project. Bull. *American Meteorological Society, 77*, 437–472. https://doi.org/10.1175/1520-0477(1996)0772.0.CO;2

Kacimi, S., & Kwok, R. (2022). Arctic Snow Depth, Ice Thickness, and Volume from ICESat-2 and CryoSat-2: 2018–2021. *Geophysical Research Letters, 49*, e2021GL097448. https://doi.org/10.1029/2021GL097448

Kawai, Y., Osafune, S., Masuda, S., & Komuro, Y. (2018). Relations between Salinity in the Northwestern Bering Sea, the Bering Strait Throughflow and Sea Surface Height in the Arctic Ocean. *Journal of Oceanography, 74*, 239–261. https://doi.org/10.1007/s10872-017-0453-x

Kelly, S. J., Proshutinsky, A., Popova, E. K., Aksenov, Y. K., & Yool, A. (2019). On the Origin of Water Masses in the Beaufort Gyre. *Journal of Geophysical Research: Oceans, 124*, 4696–4709. https://doi.org/10.1029/2019JC015022

Kędra, M., Moritz, C., Choy, E. S., David, C., Degen, R., Duerksen, S., et al. (2015). Status and Trends in the Structure of Arctic Benthic Food Webs. *Polar Research, 34*(1). https://doi.org/10.3402/polar.v34.23775

Kim, K. Y., Hamlington, B. D., Na, H., & Kim, J. (2016). Mechanism of Seasonal Arctic Sea Ice Evolution and Arctic Amplification. *Cryosphere, 10*(5), 2191–2202. https://doi.org/10.5194/tc-10-2191-2016

Kodaira, T., Waseda, T., Nose, T., & Inoue, J. (2020). Record High Pacific Arctic Seawater Temperatures and Delayed Sea Ice Advance in Response to Episodic Atmospheric Blocking. *Scientific Reports, 10*, 20830. https://doi.org/10.1038/s41598-020-77488-y

Krishfield, R. A., Proshutinsky, A., Tateyama, K., Williams, W. J., Carmack, E. C., McLaughlin, F. A., Timmermans, M.-L. (2014). Deterioration of Perennial Sea Ice in the Beaufort Gyre from 2003 to 2012 and its Impact on the Oceanic Freshwater Cycle. *Journal of Geophysical Research: Oceans, 119*, 1271–1305. https://doi.org/10.1002/2013jc008999

Kubryakov, A., Stanichny, S., & Zatsepin, A. (2016). River Plume Dynamics in the Kara Sea from Altimetry-based Lagrangian Model, Satellite Salinity and Chlorophyll Data. *Remote Sensing of Environment, 176*, 177-187. https://doi.org/10.1016/j.rse.2016.01.020

Kuzin, V.I., Platov, G.A. & Golubeva, E.N. (2010). Influence that Interannual Variations in Siberian River Discharge have on Redistribution of Freshwater Fluxes in Arctic Ocean and North Atlantic. *Izvestiya, Atmospheric and Oceanic Physics, 46,* 770–783. https://doi.org/10.1134/S0001433810060083

Kwok, R., Spreen, G., & Pang, S. (2013). Arctic Sea Ice Circulation and Drift Speed: Decadal Trends and Ocean Currents. *Journal of Geophysical Research: Oceans, 118*, 2408–2425. https://doi.org/10.1002/jgrc.20191

Lambert, E., Nummelin, A., Pemberton, P., & Ilıcak, M. (2019). Tracing the Imprint of River Runoff Variability on Arctic Water Mass Transformation. *Journal of Geophysical Research: Oceans, 124*, 302–319. https://doi.org/10.1029/2017JC013704

Large, W. G., & Yeager, S. G. (2009). The Global Climatology of an Interannually Varying Air–Sea Flux Data Set. *Climate Dynamics, 33*, 341–364. https://doi.org/10.1007/s00382-008-0441-3

Lang, R., Zhou, Y., Utku, C., & le Vine, D. (2016). Accurate Measurements of the Dielectric Constant of Seawater at L Band. *Radio Science, 51*, 2–24. https://doi.org/10.1002/2015RS005776

Lind, S., Ingvaldsen, R. B., & Furevik, T. (2018). Arctic Warming Hotspot in the Northern Barents Sea Linked to Declining Sea-Ice Import. *Nature Climate Change, 8*, 634–639. https://doi.org/10.1038/s41558-018-0205-y

Lique, C., Treguier, A. M., Blanke, B., & Grima, N. (2010). On the Origins of Water Masses Exported Along Both Sides of Greenland: A Lagrangian Model Analysis. *Journal of Geophysical Research, 115*, C05019. https://doi.org/10.1029/2009JC005316

Liu, Y., & Key, J. R. (2014). Less Winter Cloud Aids Summer 2013 Arctic Sea Ice Return from 2012 Minimum. *Environmental Research Letters, 9*, https://doi.org/10.1088/1748-9326/9/4/044002

Madhusoodanan, M.S., & Thompson, B. (2011). Decadal Variability of the Arctic Ocean Thermal Structure. *Ocean Dynamics, 61*. https://doi.org/10.1007/s10236-011-0386-7

Makarieva, O., Nesterova, N., Post, D. A., Sherstyukov, A., & Lebedeva, L. (2019). Warming Temperatures are Impacting the Hydrometeorological Regime of Russian Rivers in the Zone of Continuous Permafrost. *The Cryosphere, 13*, 1635–1659. https://doi.org/10.5194/tc-13-1635-2019

Martínez, J., Gabarró, C., Turiel, A., González-Gambau, V., Umbert, M., Hoareau, N., et al. (2022). Improved BEC SMOS Arctic Sea Surface Salinity Product v3.1, Earth System Science. *Data, 14*, 307–323. https://doi.org/10.5194/essd-14-307-2022

Matthews, J. L., Peng, G., Meier, W. N., & Brown, O. (2020). Sensitivity of Arctic Sea Ice Extent to Sea Ice Concentration Threshold Choice and Its Implication to Ice Coverage Decadal Trends and Statistical Projections. *Remote Sensing,, 12*, 807. https://doi.org/10.3390/rs12050807

Mazloff, M. R., Heimbach, P., & Wunsch, C. (2010). An Eddy-Permitting Southern Ocean State Estimate. *Journal of Physical Oceanography, 40*(5), 880–899. https://doi.org/10.1175/2009JPO4236.1

McClelland, J. W., Holmes, R. M., Dunton, K. H., & Macdonald, R. W. (2012). The Arctic Ocean Estuary. *Estuaries and Coasts, 35*, 353–368. https://doi.org/10.1007/s12237-010-9357-3

Meissner, T., Wentz, F.J ., & Le Vine, D. M. (2018). The Salinity Retrieval Algorithms for the NASA Aquarius Version 5 and SMAP Version 3 Releases. *Remote Sensing, 10*, 1121. https://doi.org/10.3390/rs10071121.

Meissner, T., Wentz, F. J., Manaster, A., & Lindsley, R. Remote Sensing Systems SMAP Ocean Surface Salinities Level 3 Running 8-Day, Version 4.0 Validated Release. Remote Sensing Systems. Santa Rosa, CA, USA. Available online: www.remss.com/missions/smap/salinity/ (accessed on 3 April 2021).

Meissner, T., Wentz, F. J., Manaster, A., Lindsley, R., Brewer, M., & Densberger, M. (2022). Remote Sensing Systems SMAP Ocean Surface Salinities [Level 2C, Level 3 Running 8-day, Level 3 Monthly], Version 5.0 validated release. Remote Sensing Systems, Santa Rosa, CA, USA. Available online at www.remss.com/missions/smap (accessed on 20 May 2021).

Melnichenko, O. (2021). Multi-mission L4 Optimally Interpolated Sea Surface Salinity. Ver. 1.0. PO.DAAC, CA, USA. Dataset accessed 2021-11-22 at https://doi.org/10.5067/SMP10-4U7CS

Melnichenko, O., Hacker, P., Maximenko, N., Lagerloef, G., & Potemra, J. (2016). Optimum Interpolation Analysis of Aquarius Sea Surface Salinity. *Journal of Geophysical Research: Oceans, 121*, 602–616. https://doi.org/10.1002/2015jc011343.

Melnichenko, O., Hacker, P., Maximenko, N., Lagerloef, G., & Potemra, J. (2014). Spatial Optimal Interpolation of Aquarius Sea Surface Salinity: Algorithms and Implementation in the North Atlantic. *Journal of Atmospheric and Oceanic Technology, 31*(7), 1583-1600. https://doi.org/10.1175/jtech-d-13-00241.1

Melnichenko, O., Hacker, P., Potemra, J., Meissner, T., & Wentz, F. (2021). Aquarius/SMAP Sea Surface Salinity Optimum Interpolation Analysis. *IPRC Technical Note No. 7.* Available online: https://podaac-tools.jpl.nasa.gov/drive/files/allData/smap/docs/OISSS_V1/L4OISSS_MultimissionProductGuide_V1.pdf (accessed on 10 September 2021).

Michon, S. (2020). Arctic Sea Ice Minimum Second Lowest on Record|NOAA Climate.gov. Available online: https://www.climate.gov/news-features/featured-images/2020-arctic-sea-ice-minimum-second-lowest-record (accessed on 19 February 2021).

Morison, J., Kwok, R., Dickinson, S., Andersen, R., Peralta-Ferriz, C., Morison, D., et al. (2021). The Cyclonic Mode of Arctic Ocean Circulation. *Journal of Physical Oceanography, 51*(4), 1053-1075. https://doi.org/10.1175/JPO-D-20-0190.1

Morison, J., Kwok, R., Peralta–Ferriz, C., Alkire, M., Rigor, I., Andersen, R., & Steele, M. (2012). Changing Arctic Ocean Freshwater Pathways. *Nature, 481*, 66–70. https://doi.org/10.1038/nature10705

Münchow, A., Falkner, K.K., & Melling, H. (2015). Baffin Island and West Greenland Current Systems in Northern Baffin Bay. *Progress in Oceanography, 132*, 305-317. https://doi.org/10.1016/j.pocean.2014.04.001

Mysak, L. A. (2001). Patterns of Arctic circulation. *Science, 293*, 1269–1270. https://doi.org/10.1126/science.1064217

Nakamura, T., Yamazaki, K., Iwamoto, K., Honda, M., Miyoshi, Y., Ogawa, Y., & Ukita, J. (2015). A Negative Phase Shift of the Winter AO/NAO Due to the Recent Arctic Sea-ice Reduction in Late Autumn. *Journal of Geophysical Research: Atmospheres. 120*(8), 3209-3227. https://doi.org/10.1002/2014JD022848

Nghiem, S. V., Hall, D. K., Mote, T. L., Tedesco, M., Albert, M. R., Keegan, K., Shuman, C. A., DiGirolamo, N. E., & Neumann, G. (2012). The Extreme Melt Across the Greenland Ice Sheet in 2012. *Geophysical Research Letters, 39*(20), L20502. https://doi.org/10.1029/2012GL053611

Nichols, R. E., & Subrahmanyam, B. (2019). Estimation of Surface Freshwater Fluxes in the Arctic Ocean Using Satellite-Derived Salinity. *Remote Sensing in Earth Systems Sciences, 2*, 247–259. https://doi.org/10.1007/s41976-019-00027-5

Niederdrenk, A.L., Sein, D.V. & Mikolajewicz, U. (2016). Interannual Variability of the Arctic Freshwater Cycle in the Second Half of the Twentieth Century in a Regionally Coupled Climate Model. *Climate Dynamics, 47*, 3883–3900. https://doi.org/10.1007/s00382-016-3047-1

Notz, D., & SIMIP Community (2020). Arctic Sea Ice in CMIP6. *Geophysical Research Letters, 47*(10), e2019GL086749. https://doi.org/10.1029/2019GL086749

Olmedo, E., Gabarró, C., González-Gambau, V., Martínez, J., Ballabrera-Poy, J., Turiel, A., et al. (2018). Seven Years of SMOS Sea Surface Salinity at High Latitudes: Variability in Arctic and Sub-Arctic Regions. *Remote Sensing, 10*(11), 1772. https://doi.org/10.3390/rs10111772

Osadchiev, A. A., Pisareva, M. N., Spivak, E. A., Shchuka, S. A., & Semiletov, I. P. (2020). Freshwater Transport Between the Kara, Laptev, and East-Siberian seas. *Scientific Reports, 10*, 13041. https://doi.org/10.1038/s41598-020-70096-w

Overland, J. E, &; Wang, M. (2016). Recent Extreme Arctic Temperatures Are Due to a Split Polar Vortex. *Journal of Climate, 29*(15), 5609–5616. https://doi.org/10.1175/JCLI-D-16-0320.1

Parkinson, C. L., & Cavalieri, D. J. (2008). Arctic Sea Ice Variability and Trends, 1979–2006. *Journal of Geophysical Research*, *113*, C07003. https://doi.org/10.1029/2007JC004558

Peng, L., Zhang, X., Kim, J. H., Cho, K. H., Kim, B. M., Wang, Z., & Tang, H. (2021). Role of Intense Arctic Storm in Accelerating Summer Sea Ice Melt: An In Situ Observational Study. *Geophysical Research Letters, 48*, e2021GL092714. https://doi.org/10.1029/2021GL092714

Peralta-Ferriz, C., & Woodgate, R.A. (2015). Seasonal and Interannual Variability of Pan-Arctic Surface Mixed Layer Properties from 1979 to 2012 from Hydrographic Data, and the Dominance of Stratification for Multiyear Mixed Layer Depth Shoaling. *Progress in Oceanography, 134*, 19–53. https://doi.org/10.1016/j.pocean.2014.12.005

Perovich, D., Meier, W., Tschudi, M., Farrell, S., Gerland, S., Hendricks, S., Krumpen, T., & Haas, C. (2016). Sea Ice. Available online: https://www.arctic.noaa.gov/Report-Card/Report-Card-2016/ArtMID/5022/ArticleID/286/Sea-Ice (accessed on 19 February 2021).

Perovich, D. K., & Richter-Menge, J.A. (2009). Loss of Sea Ice in the Arctic. *Annual Review of Marine Science, 1*, 417-441. https://doi.org/10.1146/annurev.marine.010908.163805

Peterson, B. J., Holmes, R. M., McClelland, J. W., Vörösmarty, C. J., Lammers, R. B., Shiklomanov, A. I., et al. (2002). Increasing River Discharge to the Arctic Ocean. *Science, 298*(5601), 2171-2173. https://doi.org/10.1126/science.1077445

Peterson, B.J. (2006). Trajectory Shifts in the Arctic and Subarctic Freshwater Cycle. *Science, 313*(5790), 1061-1066. https://doi.org/10.1126/science.1122593

Petty, A. A., Stroeve, J. C., Holland, P. R., Boisvert, L. N., Bliss, A. C., Kimura, N., & Meier, W.N. (2018). The Arctic Sea Ice Cover of 2016: A Year of Record-Low Highs and Higher-Than-Expected Lows. *Cryosphere, 12*, 433–452, https://doi.org/10.5194/tc-12-433-2018

Pnyushkov, A.V., Alekseev, G.V., & Smirnov, A.V. (2022). On the Interplay between Freshwater Content and Hydrographic Conditions in the Arctic Ocean in the 1990s–2010s. *Journal of Marine Science and Engineering, 10*(3), 401. https://doi.org/10.3390/jmse10030401

Polyakov, I. V., Pnyushkov, A. V., & Carmack, E. C. (2018). Stability of the Arctic Halocline: A New Indicator of Arctic Climate Change. *Environemental Research Letters, 13*, 125008. https://doi.org/10.1088/1748-9326/aaec1e

Polyakov, I. V., Pnyushkov, A. V., Alkire, M. B., Ashik, I. M., Baumann, T. M., Carmack, E. C., et al. (2017). Greater Role for Atlantic Inflows on Sea-Ice Loss in the Eurasian Basin of the Arctic Ocean. *Science, 356*(6335), 285–291. https://doi.org/10.1126/science.aai8204

Praetorius, S., Rugenstein, M., Persad, G., & Caldeira, K. (2018). Global and Arctic Climate Sensitivity Enhanced by Changes in North Pacific Heat Flux. *Nature Communications, 9*, 3124. https://doi.org/10.1038/s41467-018-05337-8

Prange, M., & Gerdes, R. (2006). The Role of Surface Freshwater Flux Boundary Conditions in Arctic Ocean Modelling. *Ocean Modelling, 13*(1), 25-43. https://doi.org/10.1016/j.ocemod.2005.09.003

Proshutinsky, A., Krishfield, R., Timmermans, M.-L., Toole, J., Carmack, E., McLaughlin, F., et al. (2009). Beaufort Gyre Freshwater Reservoir: State and Variability from Observations. *Journal of Geophysical Research, 114*, C00A10, doi:10.1029/2008JC005104

Proshutinsky, A., Krishfield, R., Toole, J. M., Timmermans, M.-L., Williams, W., Zimmermann, S., et al. (2019). Analysis of the Beaufort Gyre Freshwater Content in 2003–2018. *Journal of Geophysical Research: Oceans, 124*(12), 9658– 9689. https://doi.org/10.1029/2019JC015281

Proshutinsky, A. Y., & Johnson, M. A. (1997). Two Circulation Regimes of the Wind-Driven Arctic Ocean. *Journal of Geophysical Research: Oceans, 102*(C6), 12493–12514, doi:10.1029/97JC00738.

Rabe, B., Karcher, M., Schauer, U., Toole, J.M., Krishfield, R.A., Pisarev, S., et al. (2011). An Assessment of Arctic Ocean Freshwater Content Changes from the 1990s to the 2006–2008 Period. *Deep Sea Research Part 1: Oceanographic Research Papers, 58*(2), 173–185. https://doi.org/10.1016/j.dsr.2010.12.002

Rabe, B., Karcher, M., Kauker, F., Schauer, U., Toole, J. M., Krishfield, R. A., Pisarev, S., Kikuchi, T., & Su, J. (2014). Arctic Ocean Basin Liquid Freshwater Storage Trend 1992–2012. *Geophysical Research Letters, 41*(3), 961–968. https://doi.org/10.1002/2013GL058121

Rahmstorf, S., Box, J., Feulner, G., Mann, M. E., Robinson, A., Rutherford, S., & Schaffernicht, E. J. (2015). Exceptional Twentieth-Century Slowdown in Atlantic Ocean Overturning Circulation. *Nature Climate Change, 5*, 475–480. https://doi.org/10.1038/nclimate2554

Rantanen, M., Karpechko, A.Y., Lipponen, A., Nordling, K., Hyvärinen, O., Ruosteenoja, K., Vihma, T. & Laaksonen, A. (2022). The Arctic has Warmed Nearly Four Times Faster than the Globe since 1979. *Communications Earth & Environment, 3*, 168. https://doi.org/10.1038/s43247-022-00498-3

Regan, H. C., Lique, C., & Armitage, T. W. K. (2019). The Beaufort Gyre Extent, Shape, and Location Between 2003 and 2014 from Satellite Observations. *Journal of Geophysical Research: Oceans, 124*(2), 844–862. https://doi.org/10.1029/2018JC014379

Ricker, R., Hendricks, S., Girard-Ardhuin, F., Kaleschke, L., Lique, C., Tian-Kunze, X., Nicolaus, M., & Krumpen, T. (2017). Satellite-Observed Drop of Arctic Sea Ice Growth in Winter 2015–2016. *Geophysical Research Letters, 44*, 3236–3245. https://doi.org/10.1002/2016GL072244

Rigor, I. G., J. M. Wallace & R. L. Colony. (2002). Response of Sea Ice to the Arctic Oscillation. *Journal of Climate, 15*(18), 2648–2663. https://doi.org/10.1175/1520-0442(2002)015<2648:ROSITT>2.0.CO;2

Rudels, B., Jones, E. P., Anderson, L. G., & Kattner, G. (1994). On the Intermediate Depth Waters of the Arctic Ocean. *Washington DC American Geophysical Union Geophysical Monograph Series, 85*, 33-46. https://doi.org/10.1029/GM085p0033

Rykova, T., Straneo, F., & Bower, A.S. (2015). Seasonal and Interannual Variability of the West Greenland Current System in the Labrador Sea in 1993–2008. *Journal of Geophysical Research: Oceans, 12*0, 1318–1332. https://doi.org/10.1002/2014JC010386

Serreze, M. & Francis, J. (2006). The Arctic Amplification Debate. *Climatic Change, 76*, 241-264. https://doi.org/10.1007/s10584-005-9017-y

Serreze, M. C., Barrett, A. P., Slater, A. G., Woodgate, R. A., Aagaard, K., Lammers, R. B., et al. (2006). The Large-scale Freshwater Cycle of the Arctic. *Journal of Geophysical Research: Oceans, 111*(C11). https://doi.org/10.1029/2005JC003424

Serreze, M.C., Barrett, A.P., Stroeve, J.C., Kindig, D.N., & Holland, M.M. (2009). The Emergence of Surface-Based Arctic Amplification. *Cryosphere, 3*, 11–19. https://doi.org/10.5194/tc-3-11-2009

Serreze, M.C., & Barry, R.G. (2011). Processes and Impacts of Arctic Amplification: A Research Synthesis. *Global and Planetary Change, 77*, https://doi.org/10.1016/j.gloplacha.2011.03.004

Serreze, M.C., Stroeve, J., Barrett, A. P., & Boisvert, L. N. (2016). Summer Atmospheric Circulation Anomalies over the Arctic Ocean and Their Influences on September Sea Ice Extent: A Cautionary Tale. *Journal of Geophysical Research, 121*, 11463–11485. https://doi.org/10.1002/2016JD025161

Shiklomanov, A. & Lammers, R. (2009). Record Russian River Discharge in 2007 and the Limits of Analysis. *Environmental Research Letters, 4*, 045015. https://doi.org/10.1088/1748-9326/4/4/045015

Skliris, N., Marsh, R., Mecking, J. V., Zika, J. D. (2020). Changing Water Cycle and Freshwater Transports in the Atlantic Ocean in Observations and CMIP5 Models. *Climate Dynamics, 54*, 4971–4989. https://doi.org/10.1007/s00382-020-05261-y

Solomon, A., Heuzé, C., Rabe, B., Bacon, S., Bertino, L., Heimbach, P., et al. (2021). Freshwater in the Arctic Ocean 2010–2019. *Ocean Science Discussion, 17*, 1081–1102. https://doi.org/10.5194/os-2020-113

Spielhagen, R.F., & Bauch, H.A. (2015). The Role of Arctic Ocean Freshwater During the Past 200 ky. *arktos, 1*, 18. https://doi.org/10.1007/s41063-015-0013-9

Steele, M., & Ermold, W. (2004). Salinity Trends on the Siberian Shelves. *Geophysical Research Letters, 31*, L24308, https://doi.org/10.1029/2004GL021302

Stein, R., Dittmers, K., Fahl, K., Kraus, M., Matthiessen, J., Niessen, F., et al. (2004). Arctic (Palaeo) River Discharge and Environmental Change: Evidence from the Holocene Kara Sea Sedimentary Record. *Quaternary Science Reviews, 23*(11–13), 1485-1511. https://doi.org/10.1016/j.quascirev.2003.12.004

Stroeve, J., Frei, A., McCreight, J., & Ghatak, D. (2008). Arctic Sea-Ice Variability Revisited. *Annals of Glaciology, 48*, 71-81. https://doi.org/10.3189/172756408784700699

Stroh, J. N., Panteleev, G., Kirillov, S., Makhotin, M., & Shakhova, N. (2015). Sea-Surface Temperature and Salinity Product Comparison against External In Situ Data in the Arctic Ocean. *Journal of Geophysical Research: Oceans, 120,* 7223–7236. https://doi.org/10.1002/2015JC011005

Supply, A., Boutin, J., Vergely, J. L., Kolodziejczyk, N., Reverdin, G., Reul, N., Tarasenko, A. (2020). A New Methodology to Derive SMOS Sea Surface Salinity in the Arctic Ocean. *Remote Sensing of Environment, 249*, 112027. https://doi.org/10.1016/j.rse.2020.112027

Swift, J. H., Jones, E. P., Aagaard, K., Carmack, E. C., Hingston, M., MacDonald, R.W., McLaughlin, F. A., & Perkin, R. G. (1997). Waters of the Makarov and Canada Basins. *Deep Sea Research Part II: Topical Studies in Oceanography, 44*(8), 1503-1529. https://doi.org/10.1016/S0967-0645(97)00055-6

Tang, W., Yueh, S., Yang, D., Fore, A., Hayashi, A., Lee, T., Fournier, S., & Holt, B. (2018). The Potential and Challenges of Using Soil Moisture Active Passive (SMAP) Sea Surface Salinity to Monitor Arctic Ocean Freshwater Changes. *Remote Sensing, 10*, 869. https://doi.org/10.3390/rs10060869

Tang, C., Ross, C., Yao, T., Petrie, B., DeTracey, B., & Dunlap, E. (2004). The Circulation, Water Masses and Sea-Ice of Baffin Bay. *Progress In Oceanography, 63*, 183-228. https://doi.org/10.1016/j.pocean.2004.09.005

Tilling, R. L., Ridout, A., Shepherd, A., & Wingham, D. J. (2015). Increased Arctic Sea Ice Volume after Anomalously Low Melting in 2013. *Nature Geoscience, 8*, 643–646. https://doi.org/10.1038/ngeo2489

Timmermans, M.–L., Proshutinsky, A., Krishfield, R. A., Perovich, D. K., Richter–Menge, J. A., Stanton, T. P., & Toole, J. M. (2011). Surface Freshening in the Arctic Ocean's Eurasian Basin: An Apparent Consequence of Recent Change in the Wind–Driven Circulation. *Journal of Geophysical Research, 116*, C00D03. https://doi.org/10.1029/2011JC006975

Timmermans, M.-L., & Marshall, J. (2020). Understanding Arctic Ocean Circulation: A Review of Ocean Dynamics in a Changing Climate. *Journal of Geophysical Research: Oceans, 125*(4), e2018JC014378. https://doi.org/10.1029/2018JC014378

Tsubouchi, T., Bacon, S., Aksenov, Y., Naveira Garabato, A.C., Beszczynska-Möller, A., Hansen, E., de Steur, L., Curry, B., & Lee, C.M. (2018). The Arctic Ocean Seasonal Cycles of Heat and Freshwater Fluxes: Observation-Based Inverse Estimates. *Journal of Physical Oceanography, 48*, https://doi.org/10.1175/JPO-D-17-0239.s1

Umbert, M., Gabarro, C.,Olmedo, E., Gonçalves-Araujo, R., Guimbard, S., & Martinez, J. (2021). Using Remotely Sensed Sea Surface Salinity and Colored Detrital Matter to Characterize Freshened Surface Layers in the Kara and Laptev Seas during the Ice-Free Season. *Remote Sensing, 13*, 3828. https://doi.org/ 10.3390/rs13193828

Verezemskaya, P., Barnier, B., Gulev, S.K., Gladyshev, S., Molines, J., Gladyshev, V., Lellouche, J., & Gavrikov, A. (2021). Assessing Eddying (1/12°) Ocean Reanalysis GLORYS12 Using the 14-yr Instrumental Record From 59.5° N Section in the Atlantic. *Journal of Geophysical Research: Oceans, 126*, e2020JC016317. https://doi.org/10.1029/2020jc016317

Vihma, T., Screen, J., Tjernström, M., Newton, B., Zhang, X., Popova, V., et al. (2016). The Atmospheric Role in the Arctic Water Cycle: A Review on Processes, Past and Future Changes, and their Impacts. *Journal of Geophysical Research: Biogeosciences, 121*(3), 586–620, https://doi.org/10.1002/2015JG003132

Vihma, T. (2014). Effects of Arctic Sea Ice Decline on Weather and Climate: A Review. *Surveys in Geophysics, 35*, 1175–1214. https://doi.org/10.1007/s10712-014-9284-0

Walsh, J. E. (2014). Intensified Warming of the Arctic: Causes and Impacts on Middle Latitudes. *Global and Planetary Change, 117*, 52-63. https://doi.org/10.1016/j.gloplacha.2014.03.003

Walsh, J. E., Overland, J. E., Groisman, P. Y., Rudolf, B. (2011). Ongoing Climate Change in the Arctic. *Ambio, 40* (Suppl 1), 6–16. https://doi.org/10.1007/s13280-011-0211-z

Wang, Z., Hamilton, J., & Su, J. (2017). Variations in Freshwater Pathways from the Arctic Ocean into the North Atlantic Ocean. *Progress in Oceanography, 155*, 54–73. https://doi.org/10.1016/j.pocean.2017.05.012

Wang, Q., Wekerle, C., Danilov, S., Koldunov, N., Sidorenko, D., Sein, D., Rabe, B., & Jung, T. (2018a). Arctic Sea Ice Decline Significantly Contributed to the Unprecedented Liquid Freshwater Accumulation in the Beaufort Gyre of the Arctic Ocean. *Geophysical Research Letters, 45*, 4956–4964. https://doi.org/10.1029/2018GL077901

Wang, H., Legg, S., & Hallberg, R. (2018b). The Effect of Arctic Freshwater Pathways on North Atlantic Convection and the Atlantic Meridional Overturning Circulation. *Journal of Climate, 31*(13), 5165-5188. https://doi.org/10.1175/JCLI-D-17-0629.1

Wang, Q., Marshall, J., Scott, J., Meneghello, G., Danilov, S., & Jung, T. (2019a). On the Feedback of Ice-Ocean Stress Coupling from Geostrophic Currents in an

Anticyclonic Wind Regime over the Beaufort Gyre. *Journal of Physical Oceanography, 49*(2), 369–383. https://doi.org/10.1175/JPO-D-18-0185.1

Wang, Q., Wekerle, C., Danilov, S., Sidorenko, D., Koldunov, N., Sein, D., et al. (2019b). Recent Sea Ice Decline Did Not Significantly Increase the Total Liquid Freshwater Content of the Arctic Ocean. *Journal of Climate, 32*(1), 15-32. https://doi.org/10.1175/JCLI-D-18-0237.1

Wang, Q. (2021). Stronger Variability in the Arctic Ocean Induced by Sea Ice Decline in a Warming Climate: Freshwater Storage, Dynamic Sea Level and Surface Circulation. *Journal of Geophysical Research: Oceans, 126*(3), e2020JC016886. https://doi.org/10.1029/2020JC016886

Wang, Q., Ricker, R., & Mu, L. (2021a). Arctic Sea Ice Decline Preconditions Events of Anomalously Low Sea Ice Volume Export through Fram Strait in the Early 21st Century. *Journal of Geophysical Research: Oceans, 126*, e2020JC016607. https://doi.org/10.1029/2020jc016607

Wang Q., Danilov S., Sidorenko D., & Wang X. (2021b). Circulation Pathways and Exports of Arctic River Runoff Influenced by Atmospheric Circulation Regimes. *Frontiers in Marine Science, 8*(707593). https://doi.org/10.3389/fmars.2021.707593

Wang, S., Wang, Q., Shu, Q., Song, Z., Lohmann, G., Danilov, S., & Qiao, F. (2021c). Nonmonotonic Change of the Arctic Ocean Freshwater Storage Capability in a Warming Climate. *Geophysical Research Letters, 48*(10), e2020GL090951. https://doi.org/10.1029/2020GL090951

Wang, X., Zhao, J., Lobanov, V. B., Kaplunenko, D., Rudykh, Y. N., He, Y., & Chen, X. (2021d). Distribution and Transport of Water Masses in the East Siberian Sea and their Impacts on the Arctic Halocline. *Journal of Geophysical Research: Oceans, 126*, e2020JC016523. https://doi.org/10.1029/2020JC016523

Weatherly, J. W., & Walsh, J .E. (1996). The Effects of Precipitation and River Runoff in a Coupled Ice-Ocean Model of the Arctic. *Climate Dynamics, 12*. https://doi.org/10.1007/s003820050143

Weingartner, T. J., Danielson, S., Sasaki, Y., Pavlov, V., & Kulakov, M. (1999). The Siberian Coastal Current: A Wind- and Buoyancy-Forced Arctic Coastal Current, *Journal of Geophysical Research, 104*(C12), 29697–29713. https://doi.org/10.1029/1999JC900161

Wentz, F. J., Scott, J., Hoffman, R., Leidner, M., Atlas, R., & Ardizzone, J. (2015). Remote Sensing Systems Cross-Calibrated Multi-Platform (CCMP) 6-Hourly Ocean Vector Wind Analysis Product on 0.25 Deg Grid, Version 2.0. Remote Sensing Systems, Santa Rosa, CA. Available online: www.remss.com/measurements/ccmp (accessed on 30 March 2021).

White, D., Hinzman, L., Alessa, L., Cassano, J., Chambers, M., Falkner, K., et al. (2007). The Arctic Freshwater System: Changes and Impacts. *Journal of Geophysical Research: Biogeosciences, 112*(G4), https://doi.org/10.1029/2006JG000353

Woodgate, R. A., Aagaard, K., Muench, R. D., Gunn, J., Bjork, G., Rudels, B., et al. (2001). The Arctic Ocean Boundary Current Along the Eurasian Slope and the Adjacent Lomonosov Ridge: Water Mass Properties, Transports and Transformations from Moored Instruments. *Deep Sea Research Part 1: Oceanographic Research Papers, 48*(8), 1757–1792. https://doi.org/10.1016/S0967-0637(00)00091-1

Woodgate, R., & Aagaard, K. (2005). Revising the Bering Strait Freshwater Flux into the Arctic Ocean. *Geophysical Research Letters, 32*(2), L02602. https://doi.org/10.1029/2004GL021747

Xie, J., Raj, R. P., Bertino, L., Samuelsen, A., & Wakamatsu, T. (2019). Evaluation of Arctic Ocean Surface Salinities from the Soil Moisture and Ocean Salinity (SMOS) Mission Against a Regional Reanalysis and In Situ Data. *Ocean Science, 15*, 1191–1206. https://doi.org/10.5194/os-15-1191-2019

Yadav, J., Kumar, A., & Mohan, R. (2020). Dramatic Decline of Arctic Sea Ice Linked to Global Warming. *Natural Hazards, 103*, 2617–2621. https://doi.org/10.1007/s11069-020-04064-y

Yamamoto, A., Kawamiya, M., Ishida, A., Yamanaka, Y., & Watanabe, S. (2012) Impact of Rapid Sea-Ice Reduction in the Arctic Ocean on the Rate of Ocean Acidification, *Biogeosciences, 9*, 2365–2375. https://doi.org/10.5194/bg-9-2365-2012

Yang, Q., Dixon, T. H., Myers, P. G., Bonin, J., Chambers, D., & van den Broeke, M.R. (2016). Recent Increases in Arctic Freshwater Flux Affects Labrador Sea Convection and Atlantic Overturning Circulation. *Nature Communications, 7*. https://doi.org/10.1038/ncomms10525

Zhang, J., Weijer, W., Steele, M., Cheng, W., Verma, T., & Veneziani, M. (2021). Labrador Sea Freshening Linked to Beaufort Gyre Freshwater Release. *Nature Communications, 12*, 1229. https://doi.org/10.1038/s41467-021-21470-3

Zhang, J., Steele, M., Runciman, K., Dewey, S., Morison, J., Lee, C., et al. (2016). The Beaufort Gyre Intensification and Stabilization: A Model-Observation Synthesis. *Journal of Geophysical Research: Oceans*, *121*, 7933–7952. https://doi.org/10.1002/2016jc012196

Zhang, J.; Schweiger, A.; Steele, M. (2013). MIZMAS: Modeling the Evolution of Ice Thickness and Floe Size Distributions in the Marginal Ice Zone of the Chukchi and Beaufort Seas; Distribution Statement A; US Dept of the Navy: Arlington, VA, USA.

Zhang, J., Woodgate, R., & Moritz, R. (2010). Sea Ice Response to Atmospheric and Oceanic Forcing in the Bering Sea. *Journal of Physical Oceanography, 40*, 1729–1747. https://doi.org/10.1175/2010jpo4323.1

Zhang, J., & Rothrock, D.A. (2003). Modeling Global Sea Ice with a Thickness and Enthalpy Distribution Model in Generalized Curvilinear Coordinates. *Monthly Weather Review, 131*, 681–697. https://doi.org/10.1175/1520-0493(2003)1312.0.CO;2

Zhong, W., Zhang, J., Steele, M., Zhao, J., & Wang, T. (2019). Episodic Extrema of Surface Stress Energy Input to the Western Arctic Ocean Contributed to Step Changes of freshwater Content in the Beaufort Gyre. *Geophysical Research Letters, 46*, 12173–12182. https://doi.org/10.1029/2019GL084652

Zuo, H., Balmaseda, M. A., Tietsche, S., Mogensen, K., & Mayer, M. (2019). The ECMWF Operational Ensemble Reanalysis – Analysis System for Ocean and Sea Ice: a Description of the System and Assessment. *Ocean Science, 15*(3), 779–808. https://doi.org/10.5194/os-15-779-2019

Zuo, H., Balmaseda, M. A., Mogensen, K., & Tietsche, S. (2018). OCEAN5: the ECMWF Ocean Reanalysis System and its Real-Time Analysis Component. *European Centre for Medium-Range Weather Forecasts*. Report no. 823, https://doi.org/10.21957/la2v0442

APPENDIX A

COPYRIGHT PERMISSIONS

A.1 CHAPTER 2 COPYRIGHT PERMISSIONS

Open Access Article

Surface Freshwater Fluxes in the Arctic and Subarctic Seas during Contrasting Years of High and Low Summer Sea Ice Extent

by Sarah B. Hall [1,*], Bulusu Subrahmanyam [1], Ebenezer S. Nyadjro [2] and Annette Samuelsen [3]

[1] School of the Earth, Ocean and Environment, University of South Carolina, Columbia, SC 29208, USA
[2] Northern Gulf Institute, Mississippi State University, Stennis Space Center, MS 39529, USA
[3] Nansen Environmental and Remote Sensing Center, and Bjerknes Centre for Climate Research, N-5006 Bergen, Norway
[*] Author to whom correspondence should be addressed.

Academic Editors: Yi Luo and Viviane V. Menezes

Remote Sens. **2021**, *13*(8), 1570; **https://doi.org/10.3390/rs13081570**

Received: 5 March 2021 / Revised: 30 March 2021 / Accepted: 15 April 2021 / Published: 18 April 2021

(This article belongs to the Special Issue **Moving Forward on Remote Sensing of Sea Surface Salinity**)

View Full-Text | Download PDF | Browse Figures | Citation Export

Abstract

Freshwater (FW) flux between the Arctic Ocean and adjacent waterways, predominantly driven by wind and oceanic currents, influences halocline stability and annual sea ice variability which further impacts global circulation and climate. The Arctic recently experienced anomalous years of high and low sea ice extent in the summers of 2013/2014 and 2012/2016, respectively. Here we investigate the interannual variability of oceanic surface FW flux in relation to spatial and temporal variability in sea ice concentration (SIC), sea surface salinity (SSS), and sea surface temperature (SST), focusing on years with summer sea–ice extremes. Our analysis between 2010–2018 illustrate high parameter variability, especially within the Laptev, Kara, and Barents seas, as well as an overall decreasing trend of FW flux through the Fram Strait. We find that in 2012, a maximum average FW flux of 0.32 × 10^3 ms^{-1} in October passed over a large portion of the Northeast Atlantic Ocean at 53°N. This study highlights recent changes in the Arctic and Subarctic Seas and the importance of continued monitoring of key variables through remote sensing to understand the dynamics behind these ongoing changes. Observations of FW fluxes through major Arctic routes will be increasingly important as the polar regions become more susceptible to warming, with major impacts on global climate. **View Full-Text**

Keywords: **arctic**; **subarctic seas**; **freshwater flux**; **sea ice concentration**; **sea surface salinity**; **sea surface temperature**; **SMOS**; **SMAP**

▼ Show Figures

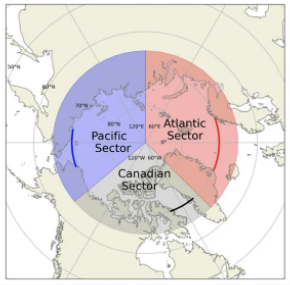

Figure 1

A.2 CHAPTER 3 COPYRIGHT PERMISSIONS

Open Access Article

Intercomparison of Salinity Products in the Beaufort Gyre and Arctic Ocean

by Sarah B. Hall [1,*], Bulusu Subrahmanyam [1] and James H. Morison [2]

[1] School of the Earth, Ocean and Environment, University of South Carolina, Columbia, SC 29208, USA
[2] Polar Science Center, Applied Physics Laboratory, University of Washington, Seattle, WA 98105, USA
* Author to whom correspondence should be addressed.

Academic Editors: Viviane V. Menezes, Emmanuel P. Dinnat and Jorge Vazquez

Remote Sens. **2022**, *14*(1), 71; **https://doi.org/10.3390/rs14010071**

Received: 1 November 2021 / Revised: 9 December 2021 / Accepted: 21 December 2021 / Published: 24 December 2021

(This article belongs to the Special Issue **Moving Forward on Remote Sensing of Sea Surface Salinity**)

View Full-Text | Download PDF | Browse Figures | Citation Export

Abstract

Salinity is the primary determinant of the Arctic Ocean's density structure. Freshwater accumulation and distribution in the Arctic Ocean have varied significantly in recent decades and certainly in the Beaufort Gyre (BG). In this study, we analyze salinity variations in the BG region between 2012 and 2017. We use in situ salinity observations from the Seasonal Ice Zone Reconnaissance Surveys (SIZRS), CTD casts from the Beaufort Gyre Exploration Project (BGP), and the EN4 data to validate and compare with satellite observations from Soil Moisture Active Passive (SMAP), Soil Moisture and Ocean Salinity (SMOS), and Aquarius Optimally Interpolated Sea Surface Salinity (OISSS), and Arctic Ocean models: ECCO, MIZMAS, HYCOM, ORAS5, and GLORYS12. Overall, satellite observations are restricted to ice-free regions in the BG area, and models tend to overestimate sea surface salinity (SSS). Freshwater Content (FWC), an important component of the BG, is computed for EN4 and most models. ORAS5 provides the strongest positive SSS correlation coefficient (0.612) and lowest bias to in situ observations compared to the other products. ORAS5 subsurface salinity and FWC compare well with the EN4 data. Discrepancies between models and SIZRS data are highest in GLORYS12 and ECCO. These comparisons identify dissimilarities between salinity products and extend challenges to observations applicable to other areas of the Arctic Ocean. View Full-Text

Keywords: **Beaufort Gyre**; **Arctic Ocean**; **sea surface salinity**; **freshwater content**

▼ Show Figures

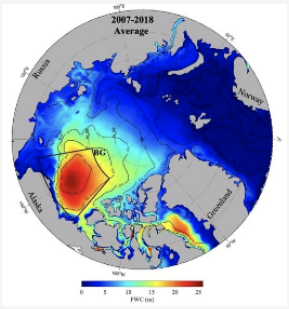

Graphical abstract